Published for SISSA by Springer

Received: May 19, 2025
Accepted: July 14, 2025
Published: August 19, 2025

Measurements of W^+W^- production cross-sections in pp collisions at $\sqrt{s} = 13$ TeV with the ATLAS detector

The ATLAS collaboration

E-mail: atlas.publications@cern.ch

Abstract: Measurements of $W^+W^- \to e^\pm\nu\mu^\mp\nu$ production cross-sections are presented, providing a test of the predictions of perturbative quantum chromodynamics and the electroweak theory. The measurements are based on data from pp collisions at $\sqrt{s} = 13$ TeV recorded by the ATLAS detector at the Large Hadron Collider in 2015–2018, corresponding to an integrated luminosity of 140 fb^{-1}. The number of events due to top-quark pair production, the largest background, is reduced by rejecting events containing jets with b-hadron decays. An improved methodology for estimating the remaining top-quark background enables a precise measurement of W^+W^- cross-sections with no additional requirements on jets. The fiducial W^+W^- cross-section is determined in a maximum-likelihood fit with an uncertainty of 3.1%. The measurement is extrapolated to the full phase space, resulting in a total W^+W^- cross-section of 127 ± 4 pb. Differential cross-sections are measured as a function of twelve observables that comprehensively describe the kinematics of W^+W^- events. The measurements are compared with state-of-the-art theory calculations and excellent agreement with predictions is observed. A charge asymmetry in the lepton rapidity is observed as a function of the dilepton invariant mass, in agreement with the Standard Model expectation. A CP-odd observable is measured to be consistent with no CP violation. Limits on Standard Model effective field theory Wilson coefficients in the Warsaw basis are obtained from the differential cross-sections.

Keywords: Electroweak Interaction, Hadron-Hadron Scattering, QCD

ArXiv ePrint: 2505.11310

https://doi.org/10.1007/JHEP08(2025)142

Contents

1 Introduction

Measurements of W-boson pair (WW) production cross-sections provide an important test of the Standard Model (SM). The WW production at hadron colliders is sensitive to the properties of electroweak-boson self-interactions and allows predictions of perturbative quantum chromodynamics (QCD) and electroweak (EW) theory to be tested. It also constitutes a large background in measurements of Higgs boson production as well as in some searches for physics beyond the SM. Inclusive and fiducial WW production cross-sections have been measured in proton-proton (pp) collisions at $\sqrt{s} = 5\,\text{TeV}$ [1], 7 TeV [2, 3], 8 TeV [4–6] 13 TeV [7–11], and 13.6 TeV [12], as well as in e^+e^- collisions at LEP [13] and in $p\bar{p}$ collisions at the Tevatron [14–16].

Illustrative Feynman diagrams for WW production are shown in figure 1. In pp collisions, 95% of the WW production rate is due to t-channel and s-channel $q\bar{q}$-induced

JHEP08(2025)142

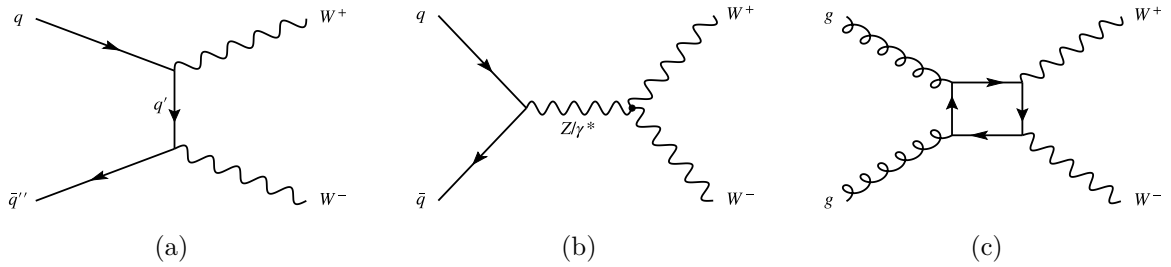

Figure 1. Illustrative examples of Feynman diagrams for the (a) t-channel and (b) s-channel $q\bar{q} \to WW$ production, as well as the (c) $gg \to WW$ production.

WW production ($q\bar{q} \to WW$), shown in figures 1(a) and 1(b) respectively. Loop-induced gluon-gluon fusion, $gg \to WW$ (figure 1(c)), represents 5% of the total WW production cross-section, despite formally being only a next-to-next-to-leading-order (NNLO) QCD correction to WW production. Beyond leading order in perturbation theory, additional partonic initial states can contribute to the processes labelled $q\bar{q} \to WW$ and $gg \to WW$. Resonant $gg \to H \to WW$ production is included in the signal definition and simulation, although it is strongly suppressed by the selection requirement on the electron-muon invariant mass.

This paper reports measurements of integrated and differential $WW \to e^{\pm}\nu\mu^{\mp}\nu$ production cross-sections at $\sqrt{s} = 13\,\text{TeV}$ using pp collision data recorded by the ATLAS experiment in 2015–2018, corresponding to an integrated luminosity of $140\,\text{fb}^{-1}$ [17]. The number of events due to top-quark pair ($t\bar{t}$) production, the largest background for this measurement, is reduced by rejecting events containing jets with b-hadron decays (b-jets). The dilepton invariant mass is required to be greater than 85 GeV, to reduce the background due to Drell-Yan production of leptonically decaying τ-lepton pairs.

Measurements of WW production are challenging because a large top-quark pair production background remains even after rejecting events containing b-jets. In contrast to previous ATLAS measurements [2, 4, 7, 8, 11], no jet veto or other selection requirements are employed here to reduce this background. Instead the background contribution is precisely estimated in situ using two control regions. The control regions provide a way to the reduce the uncertainties due to the theoretical modelling of top-quark pair production and the efficiency of identifying b-jets. This jet-inclusive measurement is advantageous not only from an experimental perspective, but also because it allows a comparison with precise predictions of perturbative QCD that are not subject to the large logarithmic corrections that jet vetoes entail [18].

Backgrounds from W+jets events with a misidentified or non-prompt lepton, another major source of uncertainty in measurements of WW cross-sections, are estimated with a data-driven method. The remaining backgrounds are estimated with simulated event samples.

The integrated cross-section is determined from a fit to the data with a statistical model representing background estimates as well as a state-of-the-art NNLO signal prediction matched to the parton shower with the MiNNLO$_{\text{PS}}$ method [19, 20].

Fiducial differential cross-sections for WW production are measured after background subtraction, using an iterative Bayesian unfolding method [21, 22]. Cross-sections are measured differentially as a function of

JHEP08(2025)142

- the transverse momentum of the leading lepton, $p_{\mathrm{T}}^{\text{lead. lep.}}$,
- the transverse momentum of the sub-leading lepton, $p_{\mathrm{T}}^{\text{sub-lead. lep.}}$,
- the transverse momentum of the dilepton system, $p_{\mathrm{T},e\mu}$,
- the absolute rapidity of the dilepton system, $|y_{e\mu}|$,
- the invariant mass of the lepton pair, $m_{e\mu}$,
- the azimuthal separation of the two leptons, $\Delta\phi_{e\mu}$,
- $|\cos\theta^*| = |\tanh(\Delta\eta_{e\mu}/2)|$, which is sensitive to the spin structure of the W-boson pair [23],[1]
- the magnitude $E_{\mathrm{T}}^{\mathrm{miss}}$ of the missing transverse momentum $\vec{p}_{\mathrm{T}}^{\,\mathrm{miss}}$, defined as the negative vectorial sum of the transverse momenta of all visible particles,
- the scalar sum of $E_{\mathrm{T}}^{\mathrm{miss}}$ and the lepton transverse momenta, $H_{\mathrm{T}}^{\text{lep.+MET}}$,
- the transverse mass of the dilepton system and the missing transverse momentum,[2] $m_{\mathrm{T},e\mu}$,
- the scalar sum of all jet and lepton transverse momenta, S_{T}, and
- the jet multiplicity.

The $|y_{e\mu}|$ and $p_{\mathrm{T},e\mu}$ observables are also measured in three regions of $m_{e\mu}$. These two observables are proxies for the longitudinal and transverse boost of the WW system, and their measurement at different invariant masses can be used to constrain parton distribution functions (PDFs).

Two cross-section asymmetries are measured, each defined as

$$A = \frac{\sigma_{\text{fid}}^{x>0} - \sigma_{\text{fid}}^{x<0}}{\sigma_{\text{fid}}},$$

where σ_{fid} is the fiducial cross-section and $\sigma_{\text{fid}}^{x>0}$ ($\sigma_{\text{fid}}^{x<0}$) is the fiducial cross-section for the phase space for which the relevant observable x is greater than (less than) zero:

- A_{C}, the asymmetry in the distribution of the difference of the absolute pseudorapidities of positively and negatively charged leptons, $|\eta_{\ell^+}| - |\eta_{\ell^-}|$, which is predicted to be non-zero due to the charge asymmetry of the partonic initial state [24] and is useful in the study of PDFs [25].

[1] ATLAS uses a right-handed coordinate system with its origin at the nominal interaction point (IP) in the centre of the detector and the z-axis along the beam pipe. The x-axis points from the IP to the centre of the LHC ring, and the y-axis points upwards. Cylindrical coordinates (r, ϕ) are used in the transverse plane, ϕ being the azimuthal angle around the z-axis. The rapidity is defined as $y = (1/2)\ln[(E + p_z)/(E - p_z)]$ while the pseudorapidity is defined in terms of the polar angle θ as $\eta = -\ln\tan(\theta/2)$. Angular distance is measured in units of $\Delta R \equiv \sqrt{(\Delta\eta)^2 + (\Delta\phi)^2}$.

[2] The transverse mass is defined as $m_{\mathrm{T},e\mu} = \sqrt{(E_{\mathrm{T},e\mu} + E_{\mathrm{T}}^{\mathrm{miss}})^2 - (\vec{p}_{\mathrm{T},e\mu} + \vec{p}_{\mathrm{T}}^{\,\mathrm{miss}})^2}$, where $E_{\mathrm{T},e\mu} = \sqrt{|\vec{p}_{\mathrm{T},e\mu}|^2 + m_{e\mu}^2}$.

JHEP08(2025)142

- A_{CP}, the asymmetry in the CP-odd observable $O_z = \left((\vec{p}_{\ell^-} \times \vec{p}_{\ell^+})_z \operatorname{sign}\left(p_{\ell^-,z} - p_{\ell^+,z}\right)\right)$ [26, 27], constructed as the cross product of the lepton three-momenta projected onto the beam direction, with the sign fixed, by convention, by the difference of the longitudinal lepton momenta. The expectation value of the asymmetry is zero and it is sensitive to additional sources of CP violation not predicted by the SM.

Finally, limits on boson-quark couplings and boson self-couplings are obtained in the framework of the Standard Model Effective Field Theory (SMEFT) [28, 29] by analysing the unfolded $m_{\mathrm{T},e\mu}$ distribution.

This paper is organized as follows. Section 2 gives a brief overview of the ATLAS detector. The recorded dataset and the simulated event samples used are listed in section 3. The criteria used to define the object and event selection in the signal region are given in section 4. Section 5 presents estimates of the top-quark, non-prompt-lepton, Drell-Yan and other backgrounds, as well as an overview of the selected WW candidate events. The statistical analysis used to determine the fiducial and differential cross-sections is presented in section 6, while section 7 considers the systematic uncertainties and their treatment. State-of-the-art predictions of fiducial cross-sections (both integrated and differential) are introduced in section 8. Section 9 reports the measured fiducial and total cross-sections, along with asymmetries, compares them to theoretical predictions, and provides an interpretation in the SMEFT framework. The paper ends with the conclusions in section 10.

2 The ATLAS detector

The ATLAS experiment [30] at the LHC [31] is a multipurpose particle detector with a forward-backward symmetric cylindrical geometry and nearly 4π coverage in solid angle. It consists of an inner tracking detector surrounded by a thin superconducting solenoid providing a 2 T axial magnetic field, electromagnetic and hadron calorimeters, and a muon spectrometer with three large superconducting toroidal magnets with eight coils each.

The inner tracking detector (ID) covers the pseudorapidity range $|\eta| < 2.5$. It contains a high-granularity silicon pixel detector, including the insertable B-layer installed before Run 2 [32, 33], followed by a silicon microstrip tracker. The silicon detectors are complemented by a transition radiation tracking detector, enabling extended track reconstruction within $|\eta| < 2.0$.

Lead/liquid-argon (LAr) sampling calorimeters provide electromagnetic (EM) energy measurements with high granularity. A steel/scintillator-tile hadron calorimeter covers the central pseudorapidity range ($|\eta| < 1.7$). The endcap and forward regions are instrumented with copper/LAr and tungsten/LAr calorimeters for EM and hadronic energy measurements up to $|\eta| = 4.9$.

The muon spectrometer surrounds the calorimeters and is based on three large air-core toroidal superconducting magnets with eight coils each. The field integral of the toroids ranges between 2.0 and 6.0 Tm across most of the spectrometer. The muon spectrometer includes a system of precision chambers for tracking and fast detectors for triggering.

JHEP08(2025)142

Process	Generator	Parton shower	Matrix element $\mathcal{O}(\alpha_s)$	Normalization
$q\bar{q} \to WW$	MiNNLO	Pythia 8.2	NNLO	Generator
$gg \to WW$	Sherpa 2.2.2	Sherpa	LO (0–1 jet)	NLO
$q\bar{q} \to WWjj$	Sherpa 2.2.2	Sherpa	LO (EWK only)	Generator
$t\bar{t}$	Powheg Box v2	Pythia 8.2	NLO	NNLO+NNLL
Wt	Powheg Box v2	Pythia 8.2	NLO	NLO+NNLL
Z+jets	Sherpa 2.2.1	Sherpa	NLO (0–2 jets), LO (3–4 jets)	NNLO
WZ, ZZ	Sherpa 2.2.2	Sherpa	NLO (0–1 jet), LO (2–3 jets)	Generator†
$W\gamma, Z\gamma$	Sherpa 2.2.8	Sherpa	NLO (0–1 jet), LO (2–3 jets)	Generator†

†: the cross-section calculated by Sherpa is found to be in good agreement with the NNLO result [39–43].

Table 1. Summary of the nominal Monte Carlo simulated events samples used in the analysis. The $gg \to WW$ simulation includes Higgs boson contributions. The last two columns give the order in the strong coupling constant, α_s, of the matrix-element calculation and the overall cross-section normalization. All nominal Monte Carlo samples use the NNPDF3.0 PDF set. The samples generated with Sherpa use its default set of tuned parton-shower parameters, while for the Powheg Box and MiNNLO samples the A14 set of tuned parameters and the NNPDF2.3lo PDF set are used for the parton shower.

Events are selected using a two-level trigger system. The first-level trigger is implemented in hardware and uses a subset of the detector information to accept events at a rate of about 100 kHz. It is followed by a software-based trigger that reduces the accepted event rate to about1.25 kHz.

An extensive software suite [34] is used in data simulation, in the reconstruction and analysis of real and simulated data, in detector operations, and in the trigger and data acquisition systems of the experiment.

3 Data and Monte Carlo samples

The analysis uses data collected from proton-proton collisions at a centre-of-mass energy of 13 TeV from 2015 to 2018. After applying data quality criteria [35], the dataset corresponds to an integrated luminosity of 140 fb^{-1}, with an uncertainty of 0.83% [17], determined using the LUCID-2 detector [36] for the primary luminosity measurements.

Monte Carlo (MC) simulated event samples are used to correct the signal yield for detector effects and to estimate background contributions. All samples were passed through a full simulation of the ATLAS detector [37], based on Geant4 [38]. Table 1 lists the configurations for the nominal MC simulations used in the analysis.

Signal $q\bar{q} \to WW$ events were modelled using Powheg MiNNLO [19, 20], which is accurate at NNLO in QCD for inclusive observables. This signal sample and all other WW production processes described in the following were generated using the NNPDF3.0nnlo PDF set [44]. The events were interfaced to Pythia 8.245 [45] for the modelling of the parton shower, hadronization, and underlying event, with parameter values set according to the A14 set of tuned parameters (tune) [46]. The matrix-element calculation of $gg \to WW$ production, which includes off-shell effects and Higgs boson contributions, incorporates

JHEP08(2025)142

up to one additional parton emission at LO. This contribution was simulated with the Sherpa 2.2.2 [47, 48] generator, and the matrix element was matched and merged with the Sherpa parton shower based on the Catani-Seymour dipole factorization [49, 50] using the MEPS@NLO prescription [51–54]. The virtual QCD corrections were provided by the OpenLoops library [55, 56]. The Sherpa 2.2.2 [47] generator was also used to simulate electroweak production of a diboson in association with two jets. The LO-accurate matrix elements were matched to a parton shower based on Catani-Seymour dipole factorization using the MEPS@LO prescription [51–54]. A dedicated set of tuned parton-shower parameters developed by the Sherpa authors was used for all Sherpa samples.

The production of $t\bar{t}$ and single-top Wt events was modelled using the Powheg Box v2 [57–61] generator at NLO with the NNPDF3.0nlo [44] PDFs. The events were interfaced to Pythia 8.230 [45] to model the parton shower, hadronization, and underlying event, using the A14 tune and the NNPDF2.3lo set of PDFs [62]. For $t\bar{t}$ event generation, the h_{damp} parameter[3] was set to 1.5 times the top quark mass [63]. The diagram-removal scheme [64] was employed to handle the interference between the Wt and $t\bar{t}$ production processes [63]. Alternative samples were generated to assess the uncertainties in the top-background modelling. The uncertainty due to initial-state radiation and higher-order QCD effects was estimated by simultaneous variations of the h_{damp} parameter and the renormalization and factorization scales, and by choosing the VAR3c up/down variants of the A14 tune. The VAR3c variations correspond to alternative values of α_{s} in the parton shower, as described in refs. [46, 65]. The impact of final-state radiation was evaluated with weights that account for the effect of raising or lowering the renormalization scale for final-state parton-shower emissions by a factor of two. To assess the measurement's dependence on the $t\bar{t}$-Wt overlap removal scheme, the diagram-subtraction scheme [64] was employed as an alternative to the diagram-removal scheme. The uncertainty due to the parton shower and hadronization model was evaluated by comparing the nominal sample of events with an event sample generated by Powheg Box v2 and interfaced to Herwig 7.04 [66, 67], using the H7UE set of tuned parameters [67] and the MMHT2014lo PDF set [68]. To estimate the uncertainty from the matching of NLO matrix elements to the parton shower, the nominal sample was compared with a sample generated by MadGraph5_aMC@NLO 2.6.2 [69] at NLO in QCD using the five-flavour scheme and the NNPDF2.3nlo PDF set. The events were interfaced to Pythia 8.230, as done for the nominal sample. The $t\bar{t}$ sample was normalized to the cross-section prediction at NNLO in QCD including the resummation of next-to-next-to-leading logarithmic (NNLL) soft-gluon terms calculated using Top++ 2.0 [70–76]. The inclusive cross-section for single-top Wt production was corrected to the theory prediction calculated at NLO in QCD with NNLL soft-gluon corrections [77, 78].

The background due to Z/γ^*+jets production was simulated with the Sherpa 2.2.1 generator using NLO-accurate matrix elements for up to two associated jets, and LO-accurate matrix elements for three or four jets, calculated with the Comix and OpenLoops libraries. They were matched with the Sherpa parton shower using the MEPS@NLO prescription and

[3]The h_{damp} parameter is a resummation damping factor and one of the parameters that control the matching of Powheg matrix elements to the parton shower and thus effectively regulates the high-p_{T} radiation against which the $t\bar{t}$ system recoils.

JHEP08(2025)142

the set of tuned parameters developed by the Sherpa authors. The NNPDF3.0nnlo set of PDFs was used, and the samples were normalized to an NNLO prediction [79].

The production of diboson final states was simulated with the Sherpa 2.2.2 (VZ with $V = W, Z$) and Sherpa 2.2.8 ($V\gamma$) generators using OpenLoops at NLO QCD accuracy for up to one additional parton and LO accuracy for two to three additional parton emissions, matched and merged with the Sherpa parton shower. The VZ simulation includes $V\gamma^*$ contributions for $m(\ell\ell) > 4\,\text{GeV}$. Samples were generated using the NNPDF3.0nnlo PDF set and normalized to the cross-section calculated by the event generator.

Samples generated with Powheg Box or MadGraph5_aMC@NLO used the EvtGen program [80] to model the decay of bottom and charm hadrons. The effect of multiple interactions in the same and neighbouring bunch crossings (pile-up) was modelled by overlaying the hard-scattering event with simulated inelastic pp events generated with Pythia 8.186 [81] using the NNPDF2.3lo set of PDFs and the A3 set of tuned parameters [82].

4 Event reconstruction and selection

Candidate WW events are selected by requiring exactly one electron and one muon with opposite electric charges. These leptons are required to be isolated, i.e. there should be little hadronic activity in the vicinity of the lepton, to suppress backgrounds due to misidentified leptons or leptons from hadron decays. Events with two isolated leptons of the same flavour are not considered in the analysis, due to the higher background from Drell-Yan events.

Events were selected online by either single-electron or single-muon triggers. During the data-taking period, the lowest p_{T} threshold was raised from 24 GeV to 26 GeV for electrons and from 20 GeV to 26 GeV for muons, both requiring 'loose' to 'medium' isolation criteria [83, 84]. Triggers with higher p_{T} thresholds and looser isolation requirements are used to increase the efficiency. The trigger selection efficiency is more than 99% for signal events fulfilling all other selection requirements detailed in this section.

Trajectories of charged particles are reconstructed as tracks in the ID, whose common vertices are used to identify interaction vertex candidates. Candidate events are required to have at least one vertex having at least two associated tracks with $p_{\text{T}} > 500\,\text{MeV}$. The vertex with the highest $\sum p_{\text{T}}^2$ of the associated tracks is taken as the primary vertex.

Electrons are reconstructed from energy deposits in the calorimeter that are matched to tracks [85]. Electron candidates are required to meet the `TightLH` likelihood-based identification criteria as defined in ref. [85]. Furthermore, they are required to have $p_{\text{T}} > 27\,\text{GeV}$ and $|\eta| < 2.47$, excluding the transition region between the barrel and endcap calorimeter regions, $1.37 < |\eta| < 1.52$.

Muon candidates are reconstructed by combining a track in the inner detector with a track in the muon spectrometer [86]. Muons are required to have $p_{\text{T}} > 27\,\text{GeV}$ and $|\eta| < 2.5$ and to satisfy the `Medium` identification selection, as defined in ref. [86].

Leptons are required to be compatible with the primary vertex by imposing constraints on the impact parameters of their tracks. The transverse impact parameter's significance, d_0/σ_{d_0}, is required to satisfy $|d_0/\sigma_{d_0}| < 5\,(3)$ for electrons (muons). The longitudinal impact parameter z_0 must satisfy $|z_0 \cdot \sin\theta| < 0.5\,\text{mm}$, where θ is the polar angle of the track. Additionally, leptons are required to be isolated using information from the ID tracks and

JHEP08(2025)142

calorimeter energy clusters in a cone around the lepton. The `Gradient` working point is used for electrons [85], while for muons the `Tight_FixedRad` working point is used. The latter is similar to the `Tight` selection defined in ref. [87] but with a fixed cone size for muons with $p_{\mathrm{T}} > 50\,\mathrm{GeV}$ in order to increase the background rejection. The electron or muon trigger object is required to match the respective reconstructed lepton.

Jets are reconstructed from particle-flow objects [88] by using the anti-k_t algorithm [89, 90] with a radius parameter of $R = 0.4$. They are required to have $p_{\mathrm{T}} > 30\,\mathrm{GeV}$ and $|\eta| < 4.5$. To suppress jets that originate from pile-up, a jet-vertex tagger [91] is applied to jets with $p_{\mathrm{T}} < 60\,\mathrm{GeV}$ and $|\eta| < 2.4$. The jet energy scale is calibrated using an η- and p_{T}-dependent correction [92]. Jets with $p_{\mathrm{T}} > 20\,\mathrm{GeV}$ and $|\eta| < 2.5$ containing decay products of a b-hadron are identified using the DL1r b-tagging algorithm [93] at the 85% efficiency working point. The lower p_{T} threshold of 20 GeV when selecting b-jets allows a larger fraction of the $t\bar{t}$ background to be rejected.

To resolve the overlap between particles reconstructed as multiple physics objects in the detector, an overlap removal procedure is applied. Non-b-tagged jets are removed if they overlap, within $\Delta R < 0.2$, with an electron, or with a muon if the jet has less than three associated tracks with $p_{\mathrm{T}} > 500\,\mathrm{MeV}$ and satisfies $p_{\mathrm{T}}^{\mu}/p_{\mathrm{T}}^{\mathrm{jet}} > 0.5$, and the ratio of the muon p_{T} to the sum of the track p_{T} associated with the jet is greater than 0.7. Subsequently, electrons or muons overlapping within $\Delta R < 0.4$ with any jet, including b-tagged jets, are removed.

The missing transverse momentum, $E_{\mathrm{T}}^{\mathrm{miss}}$, computed as the negative vectorial sum of the transverse momenta of calibrated objects in the detector [94], measures the momentum imbalance produced by weakly interacting particles, such as neutrinos in the $W^+W^- \to e^{\pm}\nu\mu^{\mp}\nu$ decays. It includes a track-based term to account for the energy from particles that are not associated with a reconstructed lepton or jet.

Events with one or more b-tagged jets are vetoed to reduce the dominant background from top-quark pair production. To reduce the Drell-Yan backgrounds, dominated by Z+jets events with $Z \to \tau^+\tau^-$ decays, the invariant mass of the electron-muon pair is required to be $m_{e\mu} > 85\,\mathrm{GeV}$. This requirement also reduces the contribution from resonant $gg \to H \to WW$ production.

Events with additional leptons that have $p_{\mathrm{T}} > 10\,\mathrm{GeV}$ and satisfy `Loose` isolation and `LooseLH` (`Loose`) identification requirements for electrons (muons) are vetoed to reduce backgrounds due to WZ and ZZ production.

Table 2 gives a summary of the lepton, jet, and event selection criteria used to define the signal region. The expected $W^+W^- \to e^{\pm}\nu\mu^{\mp}\nu$ acceptance and efficiency are approximately 25% and 50%, respectively, with a predicted signal yield of 56900 ± 1100 events.

5 Background estimate

About 60% of the events passing the event selection are background events. The top-quark background, from either $t\bar{t}$ or single-top Wt production, is the largest background and comprises about 80% of the total background. Additional backgrounds considered come from Z+jets production, events with non-prompt or misidentified leptons, and diboson production (WZ, $W\gamma$, ZZ, and $Z\gamma$).

JHEP08(2025)142

	Requirement	Criteria
Electron	p_{T}	$> 27\,\mathrm{GeV}$
	$\lvert\eta\rvert$	$\in [0\,,\,1.37) \cup (1.52\,,\,2.47)$
	Identification	`TightLH` working point
	Isolation	`Gradient`
	Impact parameters	$\lvert d_0/\sigma_{d_0}\rvert < 5$; $\lvert z_0 \cdot \sin\theta\rvert < 0.5\,\mathrm{mm}$
Muon	p_{T}	$> 27\,\mathrm{GeV}$
	$\lvert\eta\rvert$	< 2.5
	Identification	`Medium` working point
	Isolation	`Tight_FixedRad`
	Impact parameters	$\lvert d_0/\sigma_{d_0}\rvert < 3$; $\lvert z_0 \cdot \sin\theta\rvert < 0.5\,\mathrm{mm}$
b-jets	p_{T}	$> 20\,\mathrm{GeV}$
	$\lvert\eta\rvert$	< 2.5
	Pile-up suppression	jet-vertex tagger [91] for $p_{\mathrm{T}} < 60\,\mathrm{GeV}$ and $\lvert\eta\rvert < 2.4$
	b-tagging	DL1r, 85% efficiency working point
Jets	p_{T}	$> 30\,\mathrm{GeV}$
	$\lvert\eta\rvert$	< 4.5
	Pile-up suppression	jet-vertex tagger [91] for $p_{\mathrm{T}} < 60\,\mathrm{GeV}$ and $\lvert\eta\rvert < 2.4$
Event	Leptons	1 electron and 1 muon of opposite electric charge; no additional lepton with $p_{\mathrm{T}} > 10\,\mathrm{GeV}$, `Loose` isolation, and `LooseLH` (electron) / `Loose` (muon) identification
	Number of b-jets	0
	$m_{e\mu}$	$> 85\,\mathrm{GeV}$

Table 2. Summary of the object and event selection criteria.

5.1 Top-quark background

An estimate of the $t\bar{t}$ background is obtained using a data-driven technique referred to as the b-tag counting method, which is applied separately in each bin of the differential measurements. Following the procedure established in a measurement of the $t\bar{t}$ production cross-section [95] and in the measurement of WW+jets production [10], two control regions are defined, requiring exactly one or exactly two b-tagged jets respectively. All other selection criteria are the same as in the signal region. The contribution of non-$t\bar{t}$ events in the 1-b-jet and 2-b-jet control regions is 13% and 4% of the expected events, respectively, of which more than 80% can be attributed to single-top Wt production.

After subtracting the estimated non-$t\bar{t}$ backgrounds, the $t\bar{t}$ event yields in the two control regions and the signal region are parameterized by three quantities. The first, $N^{t\bar{t}}$, is the total number of $t\bar{t}$ events without requirements on the b-jet multiplicity. The second, ε_b, is the

JHEP08(2025)142

efficiency of identifying and selecting a b-jet in a $t\bar{t}$ event, reflecting both the efficiency of the b-tagging algorithm and the acceptance for b-jets. The third parameter is the b-jet correlation factor C_b, which accounts for the fact that the probability of identifying both b-jets in a $t\bar{t}$ event is not exactly ε_b^2 but rather $C_b\varepsilon_b^2$, due to correlation effects that depend on the interplay of event selection and $t\bar{t}$ kinematics, as well as the presence of additional light-flavour jets and b-jets. The number of $t\bar{t}$ events with exactly i b-tagged jets, $N_{ib}^{t\bar{t}}$, is given by

$$\begin{aligned} N_{2b}^{t\bar{t}} &= N^{t\bar{t}} \cdot C_b\varepsilon_b^2 \,, \\ N_{1b}^{t\bar{t}} &= N^{t\bar{t}} \cdot 2\varepsilon_b \left(1 - C_b\varepsilon_b\right) \,, \\ N_{0b}^{t\bar{t}} &= N^{t\bar{t}} \cdot \left(1 - 2\varepsilon_b + C_b\varepsilon_b^2\right) \,. \end{aligned}$$

Using these equations, the number of $t\bar{t}$ events in the signal region can be expressed as

$$N_{0b}^{t\bar{t}} = \frac{C_b}{4} \frac{\left(N_{1b}^{t\bar{t}} + 2N_{2b}^{t\bar{t}}\right)^2}{N_{2b}^{t\bar{t}}} - N_{1b}^{t\bar{t}} - N_{2b}^{t\bar{t}} \,,$$

where ε_b and $N^{t\bar{t}}$ are expressed in terms of the observed yields in the two control regions, $N_{1b}^{t\bar{t}}$ and $N_{2b}^{t\bar{t}}$, which are obtained after the subtraction of minor backgrounds. Consequently, the only input from $t\bar{t}$ simulation is the correction factor C_b, which is typically very close to unity — between 0.99 and 1.01 across jet-inclusive distributions such as $m_{e\mu}$ (figure 2(a)). Since uncertainties in the modelling of top-quark processes and b-tagging primarily affect ε_b and $N^{t\bar{t}}$ but not C_b, the uncertainty in C_b is less than 1% in most analysis bins.

In certain configurations, for example in events with exactly one jet with $p_{\mathrm{T}} > 30\,\mathrm{GeV}$, C_b can be as low as 0.8 (figure 2(b)). Although identifying two b-jets is possible in events with only one jet with $p_{\mathrm{T}} > 30\,\mathrm{GeV}$, given that the b-jet p_{T} threshold is 20 GeV, the probability of tagging both b-jets is substantially lower than ε_b^2, as reflected by $C_b < 1$. This is due to the fact that, in such a configuration, the second jet is often outside the tracker acceptance or has a transverse momentum between 20 GeV and 30 GeV, resulting in a smaller b-tagging efficiency. The disparity in kinematics also leads to a lower correlation between the uncertainties associated with finding the first and second jet, which in turn increases the uncertainty on C_b.

The b-jet counting method significantly reduces experimental and theoretical uncertainties in the $t\bar{t}$ background estimate, thereby lowering its total uncertainty to about 3%, approximately a factor of five less than an estimate based purely on MC simulation.

The single-top Wt background is estimated using simulation. The subtraction of Wt backgrounds in the $t\bar{t}$ control regions introduces an anti-correlation between the estimated Wt and $t\bar{t}$ yields in the signal region so that modelling uncertainties in Wt have a reduced impact on the measurement.

In a few analysis bins, the 2-b-jet control region contains only a limited number of events, leading to a large statistical uncertainty in the $t\bar{t}$ background estimate. To mitigate this, the top-quark background is instead estimated using a transfer-factor method in these bins. The $t\bar{t}$ yield from the corresponding bins of a control region, constructed by requiring at least one b-jet, with the other selection criteria being the same as in the signal region, is extrapolated into the signal region using a transfer factor calculated from $t\bar{t}$ simulation. Although this transfer factor has a systematic uncertainty of about 10% (larger than that of the b-tag

JHEP08(2025)142

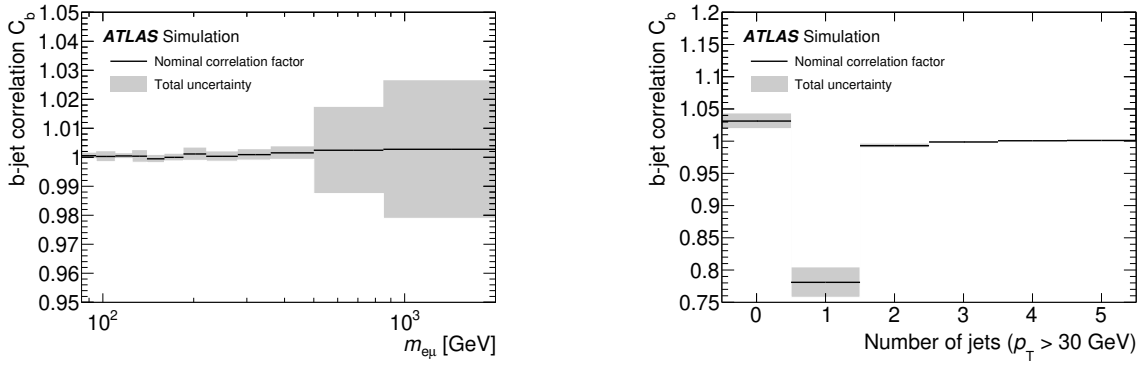

(a) (b)

Figure 2. The b-jet correlation correction factor C_b as evaluated from simulation as a function of (a) $m_{e\mu}$ and (b) the number of jets. The error bands show the total uncertainty, including systematic effects.

counting method), it still reduces the impact of experimental and theoretical uncertainties relative to an estimate based purely on simulation.

The top-quark background estimate is validated in a top-enriched region that overlaps with the signal region, by requiring at least one jet and $m_{\ell j} < 140\,\text{GeV}$, as well as $\Delta\phi_{e\mu} < \pi/2$ in addition to the normal event selection. Here $m_{\ell j}$ is the invariant mass of the leading jet and the closest lepton. This region is approximately 70% pure in top-quark events and shows good agreement between the data and the combined signal and background prediction. Figures 3(a) and 3(b) show the distributions of $p_{\text{T}}^{\text{lead. lep.}}$ and the jet multiplicity, confirming that lepton and jet-related properties are accurately modelled in events without b-jets.

5.2 Backgrounds with non-prompt or misidentified leptons

Reducible backgrounds arising from events with non-prompt or misidentified leptons — referred to as fake-lepton backgrounds or "fakes" — originate from heavy-flavour hadron decays and jets misidentified as electrons. These fake-lepton events, which stem mostly from W+jets production, constitute about 4% of the selected events.

The fake-lepton background is estimated using a data-driven technique. A control region is defined by selecting events in which one of the two lepton candidates fails the nominal selection but meets a looser set of requirements. This strategy enhances the contribution of fake-lepton events while ensuring that the fake lepton's characteristics remain similar to those in the signal region. Specifically, the lepton that fails the nominal selection is required to fulfil a loose (instead of a tight) isolation requirement and either the medium (instead of tight) identification criteria if it is an electron or, if it is a muon, an impact parameter significance requirement of $|d_0/\sigma_{d_0}| < 10$ (instead of $|d_0/\sigma_{d_0}| < 3$). Although this control region is enriched in fake leptons, approximately 75% of its events still contain two prompt leptons (including electrons or muons from prompt τ-lepton decays). These prompt-lepton contributions are modelled using simulated event samples, with a dedicated correction factor applied to adjust the probability with which leptons pass the loose, but not the tight, isolation and identification cuts. Signal contamination in the control region is estimated using the WW simulation, corrected in each bin by the ratio of background-subtracted data events

JHEP08(2025)142

to the WW simulation yield in the signal region. An uncertainty of 5% is assigned to this correction to account for uncertainties in the signal subtraction. Although the method can, in principle, be applied iteratively to refine the background subtraction involved, it is found to converge after just one iteration.

The fake-lepton background in the signal region is then obtained by scaling the number of data events in the control region — after subtracting processes with two prompt leptons — by an extrapolation factor. This factor, determined from a data sample dominated by fake leptons, depends on the p_{T}, $|\eta|$, and flavour of the lepton. The sample is selected by requiring a dijet-like configuration where one lepton candidate recoils against a jet, with $\Delta\phi_{\ell j} > 2.8$. To further suppress contamination from W+jets events, the sum of the $E_{\mathrm{T}}^{\mathrm{miss}}$ and the transverse mass of the lepton-and-$E_{\mathrm{T}}^{\mathrm{miss}}$ system is required to be smaller than 50 GeV. The extrapolation factor is defined as the ratio of the number of events in which a lepton satisfies the nominal selection to the number in which it meets only the looser criteria. Systematic uncertainties associated with the contributions from different sources of fake leptons are estimated by varying the selection of the data sample in which the extrapolation factors are determined. The variations include selecting events with a b-jet recoiling against the lepton candidate, selecting only events without a b-jet, and changing the $E_{\mathrm{T}}^{\mathrm{miss}}$ requirements to increase the fake-lepton contributions. The total uncertainty in the fake-lepton background is about 25%.

To validate the fake-lepton background estimate, the opposite-charge requirement in the signal region selection is inverted, and events containing same-charge electron-muon pairs are selected instead. This selection increases the contribution of W+jets events to about 25% by suppressing prompt-lepton processes, which are mostly charge asymmetric. The modelling of the fake-lepton background can be validated despite the relatively low purity since the dominant WZ background in this region is known with a precision of about 10%. Good agreement between the prediction and the data is observed, as is shown for the $p_{\mathrm{T}}^{\text{sub-lead. lep.}}$ distribution in figure 3(c).

5.3 Drell-Yan background

The Drell-Yan Z+jets background is estimated using MC simulation. The $m_{e\mu} > 85$ GeV requirement strongly suppresses this background. The contribution of this background to the selected events in the signal region is about 5%, almost entirely due to $Z/\gamma^*(\to \tau^+\tau^-)$+jets events.

The Z+jets estimate is checked in a validation region requiring a dilepton invariant mass between 45 GeV and 80 GeV, and either $p_{\mathrm{T},e\mu} < 30$ GeV or $E_{\mathrm{T}}^{\mathrm{miss}} < 20$ GeV, in addition to the b-jet veto. The Z+jets purity of this region is about 85% and the data is observed to be well modelled. Figure 3(d) shows the distribution of the dilepton invariant mass $m_{e\mu}$ in the validation region, which features the resonant $Z \to \tau\tau$ distribution over a rising background of top-quark events.

In addition to the theoretical uncertainty of 5% in the Z+jets cross-section [96], uncertainties in the Z+jets background are estimated by varying the renormalization and factorization scales used in the matrix-element calculation by factors of two and one-half, avoiding variations in opposite directions.

JHEP08(2025)142

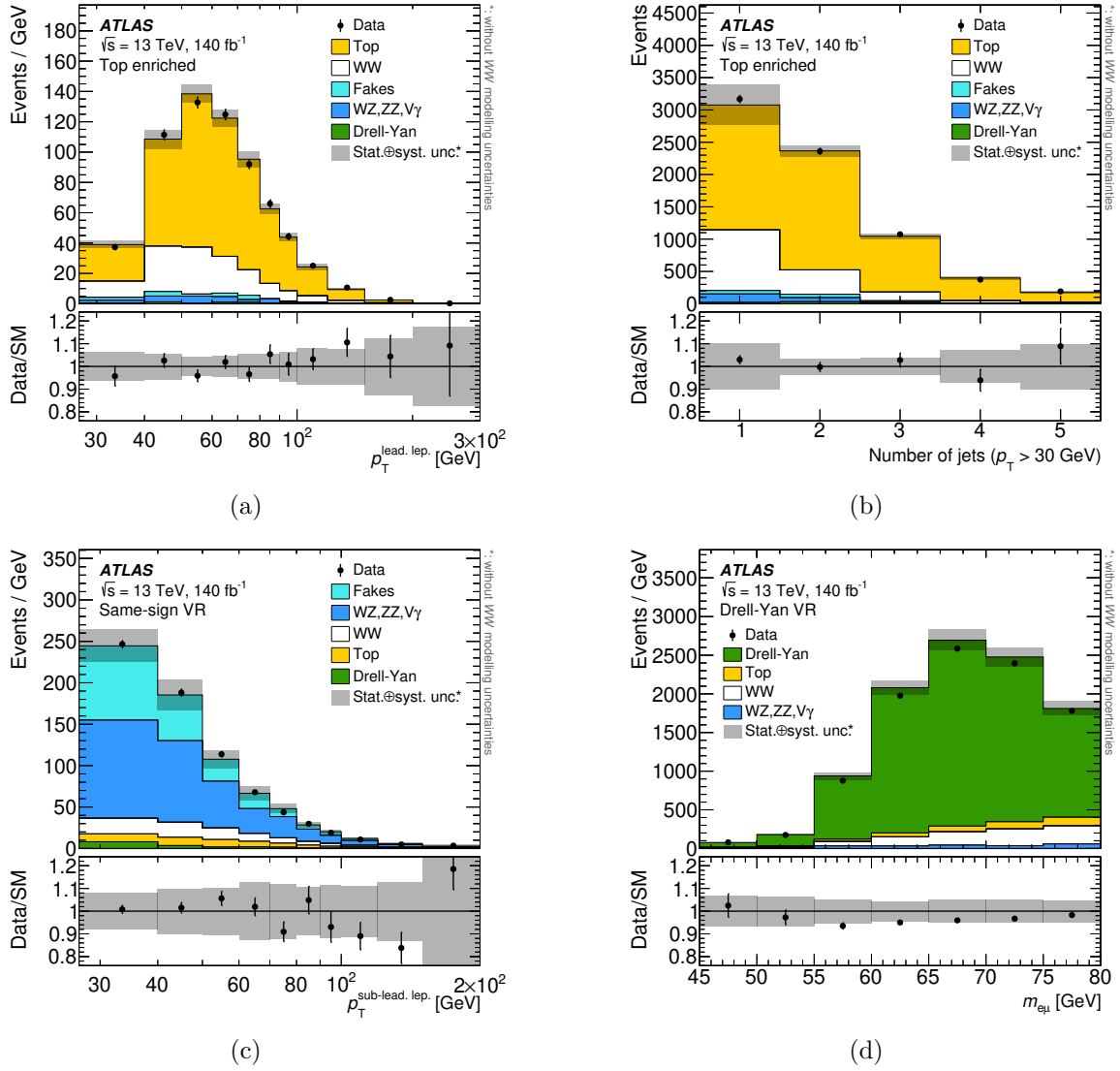

Figure 3. Detector-level distributions of (a) $p_{\mathrm{T}}^{\text{lead. lep.}}$ and (b) the jet multiplicity in the top-enriched region, (c) $p_{\mathrm{T}}^{\text{sub-lead. lep.}}$ in the same-sign validation region (VR), and (d) $m_{e\mu}$ in the Drell-Yan VR. The rightmost bin contains overflow events. Data are shown as black markers, together with histograms of the predictions for signal and background processes. The top-quark background in the top-enriched region is estimated using the data-driven method explained in section 5.1; in the other two regions its contribution is small and the nominal MC prediction is used instead. The lower panels show the ratio of the data to the total prediction. The uncertainty bands shown include statistical and systematic uncertainties. Theory uncertainties in the signal are negligible and not shown.

JHEP08(2025)142

5.4 Other backgrounds

Backgrounds from WZ, ZZ, $W\gamma$ and $Z\gamma$ production are estimated from simulation, and are found to contribute about 4% of the selected events. The dominant contribution comes from WZ events, which are observed to be well described by the nominal Sherpa simulation in ref. [97]. Uncertainties due to missing higher-order QCD corrections are derived by varying the factorization and renormalization scales used in the matrix-element calculations by factors of two, avoiding variations in opposite directions. Additionally, an uncertainty of 10% is assigned to the diboson production cross-section [98, 99].

The VZ (WZ and ZZ) prediction is validated in events containing a third lepton that has $p_{\mathrm{T}} \geq 10\,\mathrm{GeV}$ and satisfies loosened identification criteria. The invariant mass of the resulting same-flavour opposite-charge pair of leptons is required to be between 80 GeV and 100 GeV, close to the Z-boson mass, while the remaining selection criteria are identical to those in the signal region. These selections give a very pure sample of diboson events, and the prediction is in good agreement with the data, as seen in figure 4(a), where the $E_{\mathrm{T}}^{\mathrm{miss}}$ distribution in the VZ validation region shows separation between ZZ and WZ events.

Some $V\gamma$ ($W\gamma$ and $Z\gamma$) events enter the signal region as backgrounds when the photon is reconstructed and selected as an electron candidate. To validate estimates of these backgrounds, the electron identification requirements are loosened and electron track requirements changed such that contributions from photon conversions increase. As the electron candidates reconstructed from photon conversion are charge symmetric, both electron-candidate charge states are selected, regardless of the selected muon's charge. Figure 4(b) shows the p_{T} distribution of the electron candidates in the $V\gamma$ validation region with opposite-charge $e-\mu$ pairs. It is dominated by electrons from photon conversion. Excellent agreement with the data is found in both validation regions.

5.5 Selected WW candidate events

Table 3 lists the number of selected WW candidate events, as well as the breakdown of the background predictions. Details of the systematic uncertainties are given in section 7. Figure 5 shows distributions at detector level and compares the observed data with the signal prediction and the background estimate. A small excess of data events is observed, in particular at low jet-activity values. In these bins, WW production is expected to make the dominant contribution to the event yield.

6 Fiducial and differential cross-section determination

The WW cross-section is evaluated in the fiducial volume defined in table 4 at particle level, i.e. without detector effects and reconstruction inefficiencies. Exactly one prompt electron and one prompt muon of opposite electric charge are required. Prompt leptons are defined as leptons that do not originate from τ-lepton or hadron decays. The momenta of photons not originating from hadron decays but emitted in a cone of size $\Delta R = 0.1$ around the lepton direction are added to the lepton momentum to form infrared-safe "dressed" leptons. Kinematic requirements on leptons reflect the analysis requirements of table 2, and the invariant mass of the two leptons, $m_{e\mu}$, is required to be greater than 85 GeV. Events with

JHEP08(2025)142

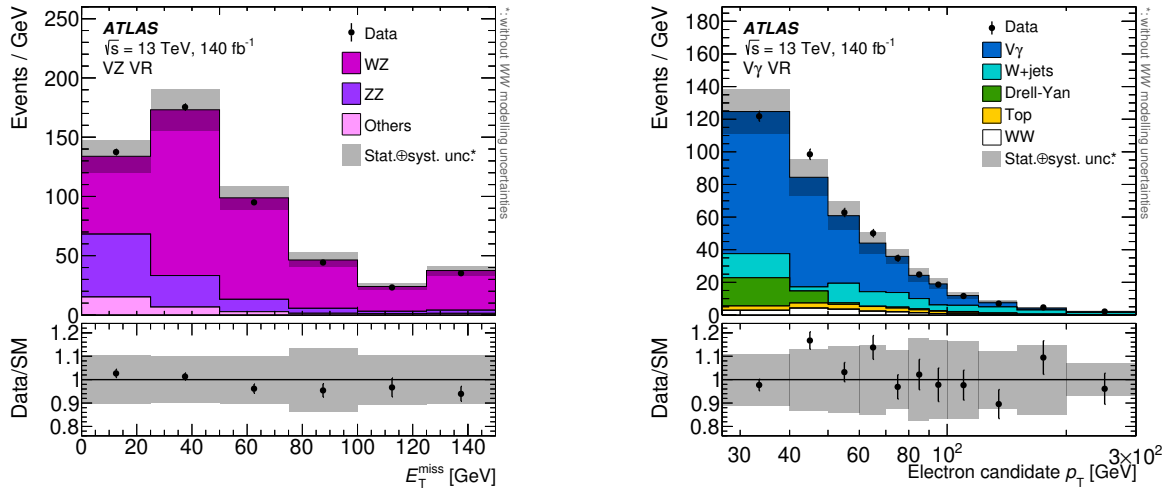

(a) (b)

Figure 4. Detector-level distributions of (a) $E_{\mathrm{T}}^{\mathrm{miss}}$ in the VZ validation region (VR) and (b) the electron candidate p_{T} in the $V\gamma$ VR with opposite-charge leptons. The rightmost bin contains overflow events. Data are shown as black markers, together with histograms of the predictions for signal and background processes. The nominal MC prediction is used for the top-quark background in both regions. The lower panels show the ratio of the data to the total prediction. The uncertainty bands shown include statistical and systematic uncertainties. Theory uncertainties in the signal are negligible and not shown.

Category	Event yield	Fraction
Data	144221	
Total SM	139500 ± 2400	
WW	56900 ± 1100	41%
Total background	82600 ± 2100	59%
Top	66500 ± 1900	48%
Drell-Yan	6500 ± 400	5%
Fakes	5000 ± 1300	4%
WZ, ZZ, $V\gamma$	4500 ± 600	3%

Table 3. Selected WW candidate events in data, together with the signal prediction and the background estimates. The uncertainties include statistical and systematic contributions, excluding theory uncertainties in the signal. The fractions in percent give the relative contribution to the total SM prediction. The individual uncertainties are correlated, and do not add up in quadrature to the total uncertainty.

JHEP08(2025)142

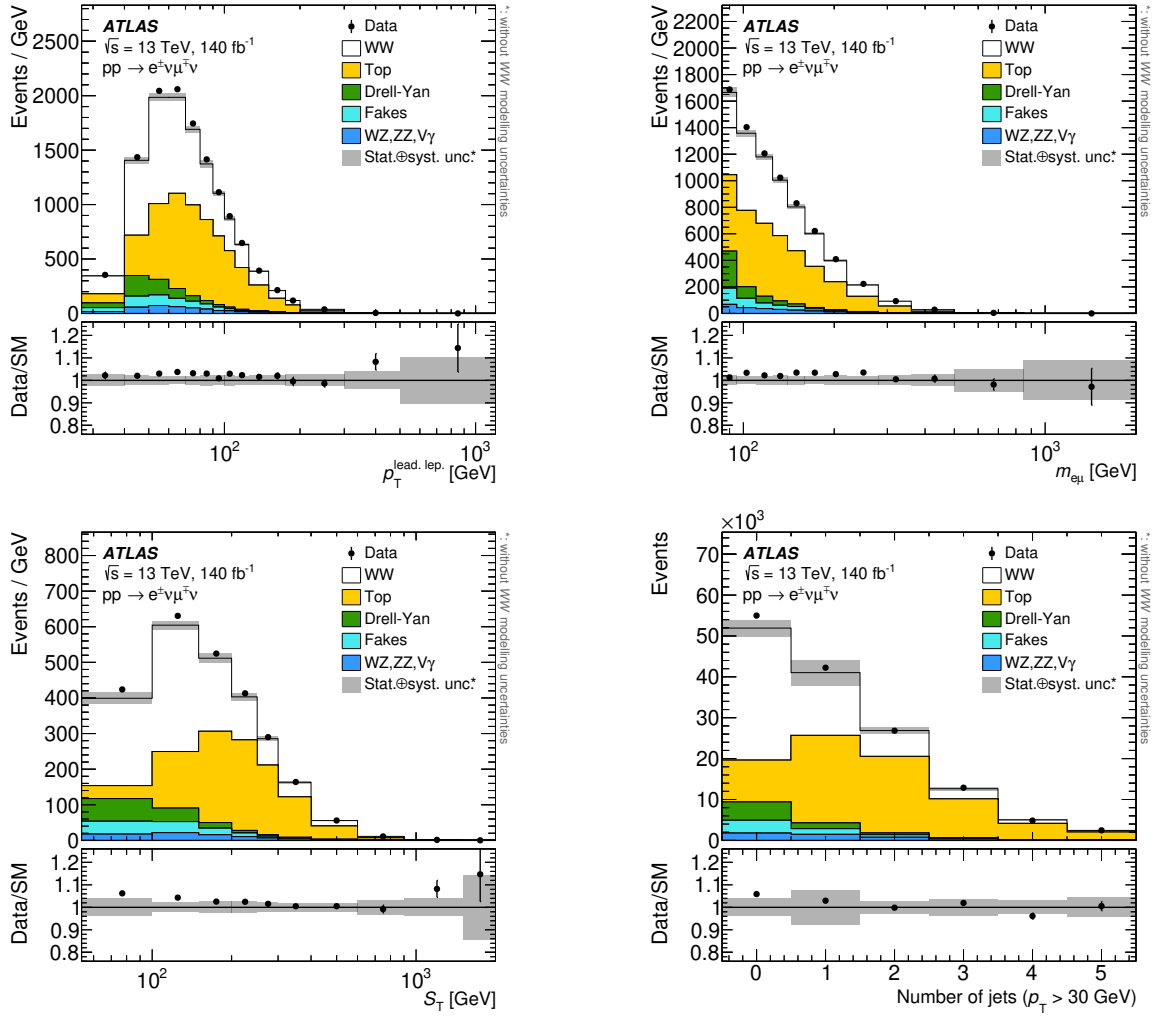

(c) (d)

Figure 5. Detector-level distributions of (a) $p_{\mathrm{T}}^{\text{lead. lep.}}$, (b) $m_{e\mu}$, (c) S_{T}, and (d) the jet multiplicity. Data are shown as black markers together with histograms of the predictions for signal and background processes. The rightmost bin contains overflow events. The lower panels show the ratio of the data to the total prediction. Top-quark and fake-lepton backgrounds are determined using data-driven methods. The uncertainty bands shown include statistical and systematic uncertainties, excluding theory uncertainties in the signal, which largely cancel out in the measurement of WW cross-sections.

additional prompt leptons fulfilling a looser p_{T} requirement are vetoed. Stable final-state particles,[4] excluding prompt neutrinos as well as prompt charged leptons and the associated photons, are clustered into particle-level jets using the anti-k_t algorithm with radius parameter $R = 0.4$. The nominal definition of the fiducial phase space includes a veto on particle-level b-jets with $p_{\mathrm{T}} > 20\,\mathrm{GeV}$ that are defined by ghost-association [100] of b-hadrons. The missing transverse momentum is defined at particle level as the negative vectorial sum of the transverse momenta of visible particles.

[4]Particles are considered stable if their decay length $c\tau$ is greater than 1 cm.

JHEP08(2025)142

Object	Requirement	Criteria
Prompt lepton	p_{T}	$> 27\,\mathrm{GeV}$
	$\lvert\eta\rvert$	< 2.5
Loose lepton	p_{T}	$> 10\,\mathrm{GeV}$
	$\lvert\eta\rvert$	< 2.5
b-jets	p_{T}	$> 20\,\mathrm{GeV}$
	$\lvert\eta\rvert$	< 2.5
Jets	p_{T}	$> 30\,\mathrm{GeV}$
	$\lvert\eta\rvert$	< 4.5
Event	Leptons	1 prompt electron and 1 prompt muon of opposite electric charge. No additional loose leptons
	Number of b-jets	0
	$m_{e\mu}$	$> 85\,\mathrm{GeV}$

Table 4. Definition of the particle-level objects and fiducial phase space. Jets containing b-hadrons are labelled *b-jet* while other jets are labelled *jet*.

The integrated fiducial cross-section is determined using a profile likelihood fit of the S_{T} distribution. The fit of the S_{T} distribution reduces uncertainties associated with the top-quark background, which dominates at high S_{T}, and, to a lesser extent, uncertainties in Drell-Yan and fake-lepton backgrounds, which are most important at low S_{T}. A model based on the sum of background estimates, which for top-pair production and fake-lepton events are determined using the data-driven methods presented in sections 5.1 and 5.2, is fitted to the data, along with the signal prediction, which includes $q\bar{q} \to WW$ and $gg \to WW$ production as well as electroweak $WWjj$ production. The number of events in each bin is modelled as the predicted number of signal events scaled by a signal-strength modifier μ, plus the number of background events. Systematic uncertainties in the signal and background predictions are parameterized by nuisance parameters. The likelihood is modelled using RooFit [101] as a product of Poissonian distributions multiplied by Gaussian constraints on the nuisance parameters. The fiducial cross-section is obtained by multiplying the unconditional maximum-likelihood estimate of μ by the particle-level fiducial cross-section prediction of the signal model. Since the fit relies on a correct prediction of the signal shape from MC simulation, it is subject to signal modelling uncertainties and only valid for a WW signal like that in the SM.

The differential cross-sections are determined using an iterative Bayesian unfolding method [21, 22]. In contrast to the integrated cross-section measurement, these results depend only weakly on the signal model, which is only used to estimate detector resolution and efficiency, and remain approximately valid in the presence of physics beyond the SM. Background events are subtracted in accord with the estimates discussed in section 5. A fiducial correction is applied to take into account events that are reconstructed in the

JHEP08(2025)142

signal region, but originate from outside the fiducial region at particle level (about 13% of selected events, mostly events with leptons from τ decays). The unfolding procedure corrects for migrations between bins in the distributions during the reconstruction of the events. Finally, efficiency corrections take into account events inside the fiducial region that are not reconstructed in the signal region due to detector inefficiencies (about 44% of events). To reduce the bias from using the chosen theory prediction to give the "true" distribution, the method can be applied with multiple iterations, at the cost of increased statistical uncertainty. Due to the good modelling of the data by simulation and the relatively small migration effects, the method converges quickly and only two iterations are required for most observables, the only exception being the jet multiplicity distribution, which is subject to larger modelling uncertainties and is unfolded using three iterations. The bias from using the simulation distributions as priors in the unfolding is estimated by reweighting the simulation with a smooth function such that it closely resembles the background-subtracted data. This reweighted detector-level prediction is unfolded using the nominal unfolding setup. The unfolding procedure is able to very accurately recover the generator-level distribution, indicating that any potential bias introduced by the unfolding method can be neglected.

7 Uncertainties

Systematic uncertainties in the WW cross-section measurements arise from experimental sources, the background determination, the procedures used to correct for detector effects, and theoretical uncertainties in the signal modelling. Systematic uncertainties in the differential cross-sections are evaluated by repeating the unfolding procedure with simulations making varied assumptions in the signal, background, and detector model. The resulting uncertainties are symmetrized and treated as being uncorrelated. In the likelihood that is used to determine the integrated fiducial cross-section, the same uncertainty sources are instead modelled by nuisance parameters that are profiled in the fit.

The dominant experimental systematic uncertainties arise in the determination of the b-tagging efficiency and mis-tag rates [102], the calibration of the jet energy scale and resolution [92], and the luminosity measurement [17]. Experimental uncertainties also encompass uncertainties in the correction of lepton trigger [83, 84], reconstruction, identification and isolation efficiencies [85, 86], the calibration of the lepton momentum or energy scale and resolution [85, 103], and the modelling of pile-up. All experimental uncertainties are evaluated by varying the respective calibrations, and propagating their effects through the analysis, affecting both the background estimates and the unfolding of detector effects. Both the effect on the total rate and the effect on the shape of distributions are taken into account for all sources of systematic uncertainty.

The estimate of the top-quark background is affected by the statistical uncertainty of the number of events in the control region, and by uncertainties in the modelling of $t\bar{t}$ and single-top Wt events, such as the uncertainty in the matrix-element calculation, the parton-shower modelling, the QCD scales, the amount of initial- and final-state radiation, and the modelling of interference between $t\bar{t}$ and single-top Wt events [104]. These are evaluated by using the alternative simulations described in section 3 and propagating the results through the top-quark background estimation.

JHEP08(2025)142

Systematic uncertainties in the estimate of fake leptons are derived by changing the selection used to estimate the extrapolation weights, in order to change the contributions from different sources of fake leptons. Additionally, the subtraction of the prompt-lepton sources in the control region is varied, and the statistical uncertainties of the weights are propagated. More details of the uncertainties affecting the fake-lepton estimate can be found in section 5.

The uncertainty in additional backgrounds is estimated by varying each of their cross-sections within its uncertainty and by using scale variations to account for missing higher-order QCD corrections and parton-shower modelling uncertainties. The impact of these uncertainties on the cross-section measurements is small compared to the uncertainties associated with the fake-lepton and top-quark background.

The uncertainty due to missing higher-order QCD corrections in the signal simulation is evaluated by varying the renormalization and factorization scales by factors of two and one-half, avoiding variations in opposite directions. The renormalization scales are varied independently in the matrix element and the parton shower. Additional uncertainties from the parton shower are evaluated by varying the parameters of the A14 tune within their uncertainties, with the largest uncertainty resulting from the variation VAR3c [46], affecting the modelling of initial-state radiation. An uncertainty due to the modelling of heavy-flavour jets is estimated by varying the fraction of events containing at least one jet originating from a b-quark or a c-quark by 30%, which covers the difference between predictions from Pythia 8.230 and Sherpa 2.2.2.

Statistical uncertainties in the unfolded distributions are evaluated by creating pseudo-data samples by varying the data within their Poisson uncertainties in each bin and then propagating these varied samples through the unfolding. The statistical uncertainties in the background estimates, which include statistical uncertainties in MC predictions and others due to the control regions used in estimating the top-quark and fake-lepton backgrounds, are evaluated using the same method.

Table 5 gives a breakdown of the uncertainties in the fiducial cross-section measured in the profile likelihood fit. Figures 6(a) and 6(b) display the uncertainties as a function of the unfolded $m_{e\mu}$ and S_{T} distributions, respectively.

8 Theoretical predictions

Fiducial differential cross-section measurements are compared with fixed-order predictions as well as three predictions where the matrix element is matched to a parton shower. Fixed-order predictions are calculated using Matrix 2.1 [43, 55, 56, 105–114], which includes the NNLO QCD correction to $q\bar{q} \to WW$ production, and the NLO QCD correction to $gg \to WW$ production. The latter correction constitutes part of the N^{3}LO correction to WW production and the combined prediction is thus labelled nNNLO. The prediction also accounts for photon-induced contributions and NLO electroweak corrections by using OpenLoops. The electroweak correction is combined, by default, multiplicatively with the QCD correction to $q\bar{q} \to WW$. An additive application of the NLO EW correction is preferred for the $p_{\mathrm{T},e\mu}$, $E_{\mathrm{T}}^{\mathrm{miss}}$, and jet multiplicity distributions because their tails are populated by events with hard radiation that arise only beyond leading order. Since the LO prediction is zero or close to zero while the NLO prediction is finite, multiplicative NLO corrections are ill-

JHEP08(2025)142

Uncertainty source	Effect
Total uncertainty	3.1%
Statistical uncertainty	1.1%
Top modelling	1.6%
Fake-lepton background	1.5%
Flavour tagging	0.7%
Other background	0.9%
Signal modelling	1.0%
Jet calibration	0.6%
Luminosity	0.8%
Other systematic uncertainties	0.9%

Table 5. Effects of uncertainties on the integrated fiducial cross-section measurement with the profile likelihood fit. They are evaluated by fixing each nuisance parameter individually to the boundaries of its post-fit 68% confidence interval, repeating the fit, and adding in quadrature the effects for each uncertainty group. "Top modelling" and "Signal modelling" are uncertainties in the theoretical modelling of the respective processes, "Fake-lepton background" is the uncertainty in the fake-lepton estimate while "Other background" is the uncertainty due to minor prompt-lepton backgrounds, "Flavour tagging" is all uncertainties in the flavour-tagging efficiency and mis-tag rate, "Jet calibration" uncertainties encompass jet energy scale and resolution uncertainties, and "Luminosity" is the uncertainty in the luminosity measurement. All systematic uncertainties belonging to none of the above categories are included in "Other systematic uncertainties". Statistical uncertainties arise in both the signal region and the control region used for the data-driven top-quark and fake-lepton estimates, and from backgrounds estimated using MC simulations.

defined. The NNPDF3.1NNLO [115] set of PDFs was used, with a prediction of the photon PDF with the LUXQED method [116]. The cross-section uncertainty associated with the NNPDF3.1NNLO LUXQED set is estimated as the standard deviation of replicas, yielding a value of 1.2%. The factorization and renormalization scales were set to half the sum of the W-boson transverse masses [105]. Theoretical uncertainties due to missing higher-order QCD corrections are evaluated by varying the factorization and renormalization scales by factors of two and one-half, avoiding variations in opposite directions. This results in an uncertainty estimate of 2.1%.

The nominal parton-shower-matched prediction is derived from the MiNNLO+Pythia 8 $q\bar{q} \to WW$ sample in combination with the Sherpa 2.2.2 $gg \to WW$ sample. These samples are also used to estimate efficiencies and resolution, in order to model the WW signal in the maximum-likelihood fit, and were introduced in section 3. The NNPDF3.0NNLO set of PDFs was used in the generation of these samples while the more recent NNPDF3.1NNLO was used for the Matrix prediction introduced above. The cross-section uncertainty associated with the NNPDF3.0NNLO set is 1.4%. Compared to the results from Matrix, this prediction lacks photon-induced contributions as well as NLO electroweak corrections beyond the effects of photon radiation included in the Pythia parton shower. On the other hand, the inclusion of

JHEP08(2025)142

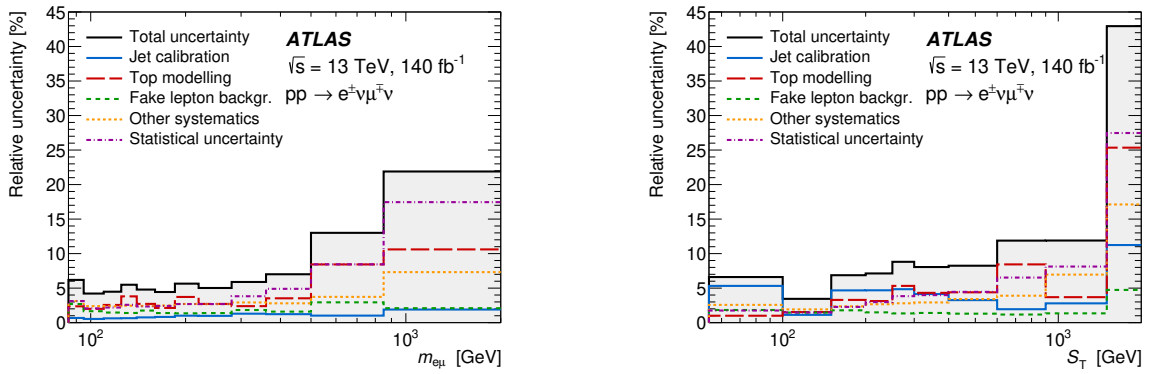

(a) (b)

Figure 6. Uncertainties in the unfolded (a) $m_{e\mu}$ and (b) S_{T} distributions. "Jet calibration" uncertainties encompass jet energy scale and resolution uncertainties, "Top modelling" is the uncertainty in the theoretical modelling of the top-quark background, and "Fake lepton backgr." is the uncertainty in the estimate of the fake-lepton background. All systematic uncertainties related to minor prompt-lepton backgrounds, flavour-tagging efficiencies and mis-tag rates, the luminosity, lepton calibration, pile-up reweighting, and signal modelling, are included in "Other systematics". "Statistical uncertainty" combines statistical uncertainties arising in the signal region and the control regions used for the data-driven top-quark and fake-lepton estimates, and those in backgrounds estimated using MC simulations.

the parton-shower effects improves the modelling of jets as well as observables correlated with the transverse momentum of the WW system. The Sherpa 2.2.2 simulation of $gg \to WW$ includes an additional jet at matrix-element level but lacks the full NLO correction included in the Matrix prediction.

An alternative NNLO+PS prediction is computed using the Geneva method to produce an MC sample of $q\bar{q} \to WW$ events [117]. The matching is achieved using a resummed calculation for the hardest jet transverse momentum, instead of the colour-singlet transverse momentum resummation employed for the MiNNLO prediction. The event simulation uses the NNPDF3.1nnlo parton distribution functions and is interfaced with the Pythia 8.307 parton shower using the Monash tune [118]. As in the MiNNLO prediction, the expected yields are augmented with the Sherpa 2.2.2 $gg \to WW$ sample.

A third parton-shower-matched prediction is generated using Sherpa 2.2.12 [47]. The prediction has NLO accuracy in QCD for up to one additional parton, and leading-order accuracy for two to three additional parton emissions for $q\bar{q}$ initial states. The matrix-element calculations are matched and merged with the Sherpa parton shower based on Catani-Seymour dipole factorization using the MEPS@NLO prescription. The virtual QCD corrections are provided by the OpenLoops library [55, 56, 111]. The NNPDF3.0nnlo set of PDFs is used, along with the dedicated set of tuned parton-shower parameters developed by the Sherpa authors. This generator combination lacks the full NNLO QCD corrections but does include an extra parton emission at LO, which improves the modelling of high-multiplicity events.

JHEP08(2025)142

Process	Code	PDF	Perturbative order	Fid. cross-section	
$q\bar{q} \to WW$	Matrix 2.1	NNPDF3.1	NNLO QCD	672 fb	±1.8 %
$q\bar{q} \to WW$	Geneva+Pythia 8.3	NNPDF3.1	NNLO QCD + PS	659 fb	±0.6 %
$q\bar{q} \to WW$	MiNNLO+Pythia 8.2	NNPDF3.0	NNLO QCD + PS	642 fb	±1.1 %
$q\bar{q} \to WW$	Sherpa 2.2.12	NNPDF3.0	NLO QCD + PS †	630 fb	±7.2 %
$gg \to WW$	Matrix 2.1	NNPDF3.1	NLO QCD	32 fb	±13 %
$gg \to WW$	Sherpa 2.2.2	NNPDF3.0	LO QCD + PS †	15 fb	±30 %
$\gamma\gamma \to WW$	Matrix 2.1	NNPDF3.1	LO	5 fb	±16 %
$\gamma\gamma \to WW$	Matrix 2.1	NNPDF3.1	NLO EW	11 fb	±2.3 %
$q\bar{q} \to WWjj$ (EW)	Sherpa 2.2.12	NNPDF3.0	LO + PS	4 fb	±7.0 %
For calculation of NLO EW correction:					
$q\bar{q} \to WW$	Matrix 2.1	NNPDF3.1	LO	436 fb	±5.1 %
$q\bar{q} \to WW$	Matrix 2.1	NNPDF3.1	NLO EW	418 fb	±5.1 %

†: includes matrix elements with additional parton emissions, matched and merged with the parton shower, which increases the accuracy of the simulation of high jet-multiplicity events but also increases the nominal scale uncertainty.

Table 6. Comparison of theoretical predictions of fiducial cross-sections for various subprocesses contributing to WW production, with the corresponding scale uncertainties. The specified process, for example in $q\bar{q} \to WW$, corresponds to the initial state at leading order. Other partons contribute to each sub-process at higher orders in perturbation theory. The names of the NNPDF3.0nnlo and NNPDF3.1nnlo luxQED PDF sets are shortened in the table.

In comparisons with differential distributions, the parton-shower-matched predictions are augmented by a simulation of electroweak production of a diboson pair in association with two jets ($VVjj$), which was generated with Sherpa 2.2.12. The contribution from this subprocess is negligible, inclusively, but $WWjj$ production with vector-boson scattering kinematics constitutes a correction of several percent in bins dominated by events with at least two jets.

An overview of fiducial cross-section predictions is given in table 6. The Powheg MiNNLO prediction for $q\bar{q} \to WW$, using NNPDF3.0nnlo, is 5% smaller than the fixed-order NNLO prediction using NNPDF3.1nnlo. The different PDF choice results in a 3% change in cross-section, while parton-shower effects, particularly final-state photon radiation, reduce the lepton momenta and thus the signal acceptance by 2%. The latter effect is also modelled by the Geneva prediction, but this uses NNPDF3.1nnlo, resulting in a larger cross-section. Sherpa 2.2.12 predicts a fiducial cross-section that is compatible with those from the NNLO generators, albeit with a larger scale uncertainty. The Sherpa 2.2.2 $gg \to WW$ prediction at LO is significantly smaller than the Matrix NLO QCD prediction. A K-factor of 1.7, calculated as the ratio of the NLO to Sherpa cross-section in the total phase space, is applied to the $gg \to WW$ sample and only partially compensates for the difference, due to the different acceptances predicted by the two models. The NLO electroweak correction to $q\bar{q} \to WW$, given by the ratio of the NLO EW prediction to the LO prediction, decreases the $q\bar{q} \to WW$ cross-section by 4% while doubling the photon-induced contribution.

JHEP08(2025)142

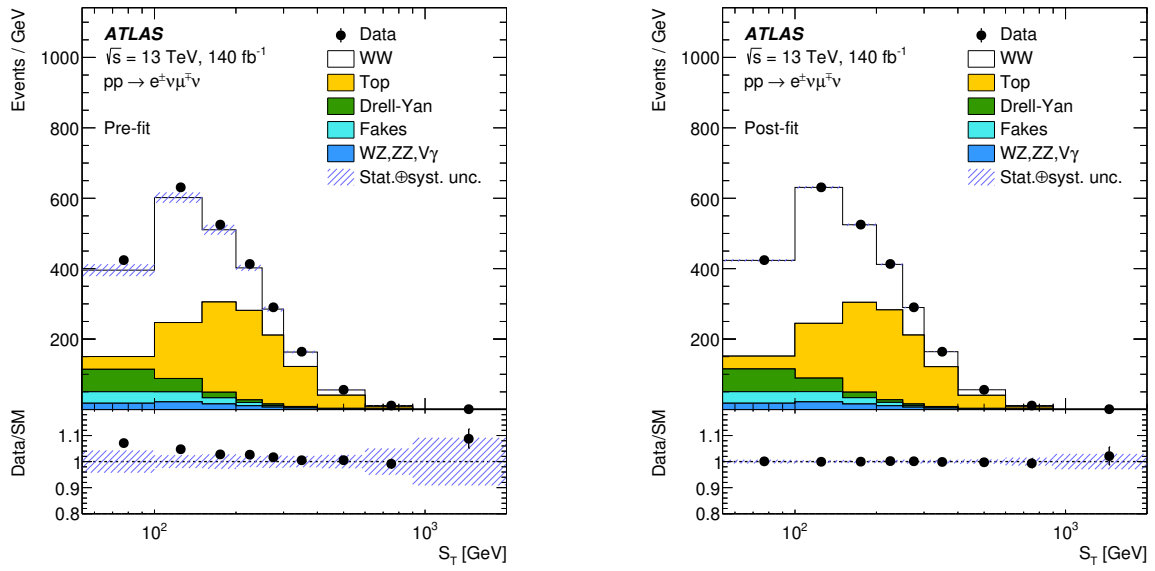

(a) (b)

Figure 7. (a) Pre-fit and (b) post-fit S_{T} distributions in the profile likelihood fit. Data are shown as black markers together with the predictions for the signal and background production processes. The rightmost bin contains overflow events. The lower panels show the ratio of the data to the total prediction. Top-quark and fake-lepton backgrounds are determined using data-driven methods. The uncertainty bands shown include statistical and systematic uncertainties. Theory uncertainties affecting the shape and selection efficiency of the signal are included.

9 Results

9.1 Cross-sections

The measured fiducial cross-section for WW production, with $WW \to e^{\pm}\nu\mu^{\mp}\nu$, in pp collisions at $\sqrt{s} = 13\,\mathrm{TeV}$, for the fiducial volume defined in table 4 is determined from the profile likelihood fit to be

$$\sigma_{\mathrm{fid}} = 707 \pm 7\ (\mathrm{stat.}) \pm 20\ (\mathrm{syst.}) \pm 6\ (\mathrm{lumin.})\,\mathrm{fb},$$

with a total uncertainty of 3.1%. Figures 7(a) and 7(b) present the pre-fit and post-fit distributions of S_{T}, respectively. In the fit, nuisance parameters remain very close to their initial values and the background normalizations are changed by less than 2% from their estimates based on control regions and theoretical calculations.

In figure 8 the result is compared with several theoretical predictions: the nominal MiNNLO model used in the analysis, a second NNLO+PS prediction from Geneva, the Sherpa NLO prediction, and two pairs of nNNLO prediction from Matrix 2.1. One of the Matrix prediction pairs includes NLO electroweak corrections while predictions within each pair differ based on the NNPDF version. The measured cross-section is about two standard deviations larger than the cross-section predicted by MiNNLO, but is in good agreement with Matrix predictions. The main reasons for the larger cross-section predicted by Matrix are the updated NNPDF PDF version, which increases the cross-section by 28 fb, and an 11 fb

JHEP08(2025)142

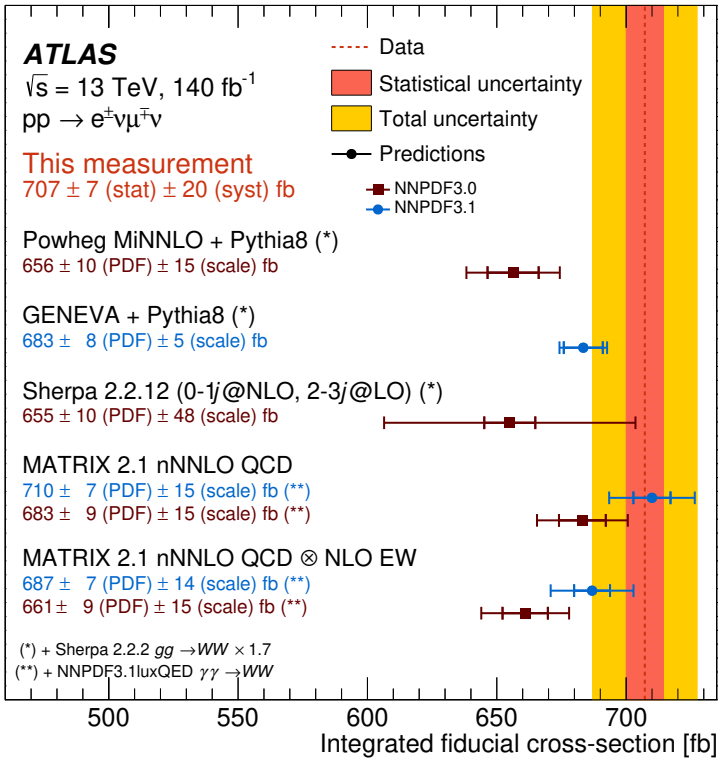

Figure 8. Measured fiducial cross-section compared with theoretical predictions from Powheg MiNNLO+Pythia 8, Geneva+Pythia 8, Sherpa 2.2.12, and Matrix 2.1. The predictions are based on the NNPDF3.0 (red squares) and NNPDF3.1 luxQED (blue dots) PDF sets. The nNNLO predictions include photon-induced contributions (always using NNPDF3.1 luxQED) and NLO QCD corrections to the gluon-gluon initial state. The $q\bar{q} \to WW$ predictions from Powheg MiNNLO, Geneva and Sherpa 2.2.12 are combined with a Sherpa 2.2.2 prediction of gluon-induced WW production, scaled by an inclusive NLO K-factor of 1.7. Inner (outer) error bars on the theory predictions correspond to PDF (the combination of scale and PDF) uncertainties. The Matrix nNNLO QCD $\otimes$ NLO EW prediction using NNPDF3.1 luxQED, the best available prediction of the integrated fiducial cross-section, is in good agreement with the measurement.

increase in the cross-section due to photon-induced contributions, as detailed in section 8. The parton-shower-matched $q\bar{q} \to WW$ predictions from MiNNLO, Geneva, and Sherpa are combined with the Sherpa 2.2.2 prediction of gluon-induced WW production. The Matrix prediction without EW corrections is the only prediction not modelling photon FSR; including photon FSR would reduce the predicted cross-section by 2%. For all measured distributions, correction factors that provide "Born-level" cross-sections, which exclude photon FSR effects, are available at the HEPdata entry associated with this paper.

The measurement is extrapolated to the full phase space of WW production, accounting for a W-boson leptonic decay branching ratio of 10.86% [119], and an acceptance of 23.7% for $W^+W^- \to e^\pm\nu\mu^\mp\nu$ events that was calculated at nNNLO with Matrix and includes NLO electroweak corrections. The uncertainty in the acceptance is 1.1%, estimated by comparing the multiplicative and additive schemes for electroweak corrections, evaluating the PDF

JHEP08(2025)142

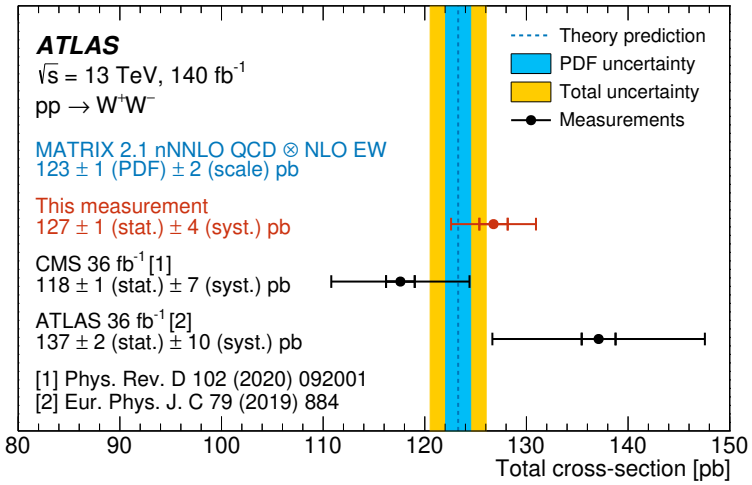

Figure 9. Measured total WW cross-section, compared with a theoretical prediction from MATRIX and previous measurements by ATLAS [8] and CMS [9]. The theoretical prediction uses the NNPDF3.1NNLO LUXQED set of parton distribution functions, has NNLO accuracy in QCD for $q\bar{q} \to WW$ production and includes NLO QCD corrections to $gg \to WW$ production, which constitute part of the N^{3}LO correction. It includes photon-induced contributions and is combined multiplicatively with NLO EW corrections to $q\bar{q} \to WW$. Inner (outer) error bars on experimental measurements correspond to statistical (total) uncertainties. The inner (outer) error band includes PDF uncertainties (PDF and scale uncertainties added in quadrature).

uncertainty, and varying the renormalization and factorization scales by factors of two and one-half, avoiding variations in opposite directions. The choice of combination scheme for electroweak corrections is the dominant source of uncertainty in the signal acceptance. After the extrapolation, the measured total production cross-section for W-boson pairs is found to be

$$\sigma_{\text{total}} = 127 \pm 1\ (\text{stat.}) \pm 4\ (\text{syst.}) \pm 1\ (\text{lumin.})\ \text{pb}.$$

In figure 9 the total cross-section is compared with measurements by ATLAS [8] and CMS [9] that are based on datasets of 36 fb^{-1}. The present measurement is more precise than its predecessor [8] because of more precise data-driven top-quark and fake-lepton estimates, an improved luminosity determination [17], and the use of a jet-inclusive phase space, which reduces jet-related uncertainties as well as theoretical uncertainties in the extrapolation to the full phase space.

Differential fiducial cross-sections are presented in figures 10–12. Excellent agreement with the fixed-order MATRIX prediction is observed for jet-inclusive distributions. The most notable discrepancy is a local three-standard-deviation difference in the lowest bin of the H_{T} distribution. A broader tension with the data is also observed for lower values of $\Delta\phi_{e\mu}$, a region characterized by relatively large systematic uncertainties in the modeling of the $t\bar{t}$ background, as well as in the signal cross-section prediction, particularly due to the $gg \to WW$ contribution.

Electroweak corrections, applied with the multiplicative combination scheme, improve the modelling of high-mass events for some distributions (e.g. $m_{e\mu}$) but over-correct for

JHEP08(2025)142

other distributions (e.g. $p_{\mathrm{T}}^{\text{lead. lep.}}$). Over-corrections are expected because the multiplicative combination scheme does not always yield an appropriate estimate of mixed QCD-EW effects, particularly in regions of phase space that are dominated by events with hard QCD radiation, as is the case for high $p_{\mathrm{T}}^{\text{lead. lep.}}$ [105].

The parton-shower-matched predictions also model the data well, except for underestimates of the cross-section by the Sherpa and MiNNLO predictions, which can be explained by the different PDF choice used in the generation of these samples. The parton shower allows the simulated events to have more than two jets, and improves the modelling of the S_{T} distribution in particular.

Figure 13 displays the measured $p_{\mathrm{T},e\mu}$ and $|y_{e\mu}|$ distributions in low ($85\,\text{GeV} < m_{e\mu} < 150\,\text{GeV}$), intermediate ($150\,\text{GeV} < m_{e\mu} < 250\,\text{GeV}$), and high ($m_{e\mu} > 250\,\text{GeV}$) $m_{e\mu}$ regions. The two observables are proxies for the transverse and longitudinal boost of the WW system and their measurement in different invariant mass regions offers sensitivity to parton distribution functions. The measurement is in good agreement with modern four-flavour NNLO PDF sets, of which CT18 [120], MSHT20 [121], NNPDF3.0 [44], NNPDF3.1 [115], and NNPDF4.0 [122] are shown.

9.2 Asymmetries

In this subsection the measurement of two asymmetries, A_{C} and A_{CP}, is presented. To determine these asymmetries free from detector effects, the distributions of the underlying observables, introduced in section 1, are background-subtracted and unfolded, analogously to the differential cross-section measurements described in the previous subsection.

In WW production a rapidity-dependent charge asymmetry is expected [24]. In the dominant $u\bar{u}$ production mode the W^+ boson tends to follow the more highly boosted up-quark direction, so the W^+ bosons tend to be more forward than W^- bosons. However, contributions from other production modes and the angular dependence of the boson decays lead to a much smaller observable charge asymmetry in the lepton rapidities, with the negatively charged lepton being more forward slightly more often. Based on the MiNNLO+Pythia 8 sample and including the NNPDF3.0nnlo PDF uncertainty, the predicted lepton asymmetry A_{C} (as introduced in section 1) is -0.023 ± 0.003. Its measured value is

$$A_{\mathrm{C}} = -0.004 \pm 0.008\ (\text{stat.}) \pm 0.006\ (\text{syst.})\,,$$

which differs from the theoretical prediction by about two standard deviations.

The charge asymmetry is also measured as a function of the absolute difference of the absolute values of the lepton rapidities, $||\eta_{\ell^+}| - |\eta_{\ell^-}||$, and the invariant mass of the dilepton system, $m_{e\mu}$. An increase in the asymmetry is predicted for larger values of these quantities, as shown in figure 14. Differences between predictions discussed in the previous section are small compared to the uncertainty of the measurement. The significance of the measured differential asymmetry is evaluated using a hypothesis test based on the profile-likelihood-ratio test statistic. The measurement as a function of $||\eta_{\ell^+}| - |\eta_{\ell^-}||$ is compatible, within two standard deviations, with both the SM prediction and the hypothesis of no asymmetry. However, for the asymmetry distribution as a function of $m_{e\mu}$, the absolute value of A_{C} significantly increases

JHEP08(2025)142

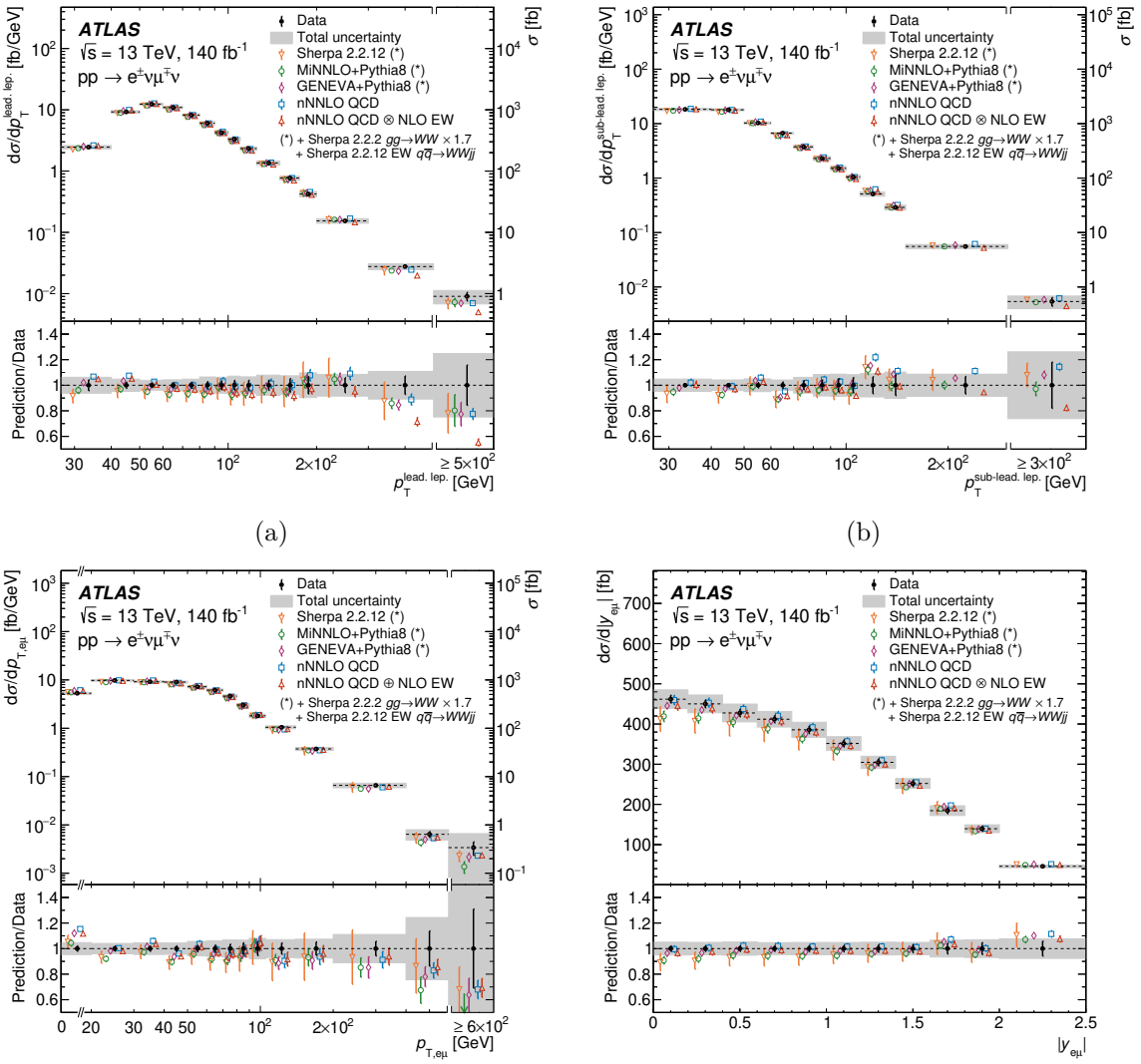

Figure 10. Fiducial differential cross-sections as a function of (a) $p_{\mathrm{T}}^{\text{lead. lep.}}$, (b) $p_{\mathrm{T}}^{\text{sub-lead. lep.}}$, (c) $p_{\mathrm{T},e\mu}$, and (d) $|y_{e\mu}|$. The measured cross-section values are shown as points with error bars giving the statistical uncertainty and solid bands indicating the size of the total uncertainty. For distributions in which the rightmost bin is inclusive, the right-hand-side axis indicates the integrated cross-section of the rightmost bin. The results are compared with fixed-order nNNLO QCD (+ NLO EW) predictions from MATRIX 2.1, the NNLO+PS predictions from POWHEG MINNLO+PYTHIA 8 and GENEVA+PYTHIA 8, and the SHERPA 2.2.12 NLO+PS predictions. The last three predictions are combined with the ones from SHERPA 2.2.2 for the gg initial state and SHERPA 2.2.12 for electroweak $WWjj$ production. These contributions are modelled at LO but an NLO QCD K-factor of 1.7 is applied for gluon-induced production. Theoretical predictions are indicated as markers with vertical lines denoting PDF, scale and parton-shower uncertainties. Markers are staggered for better visibility.

JHEP08(2025)142

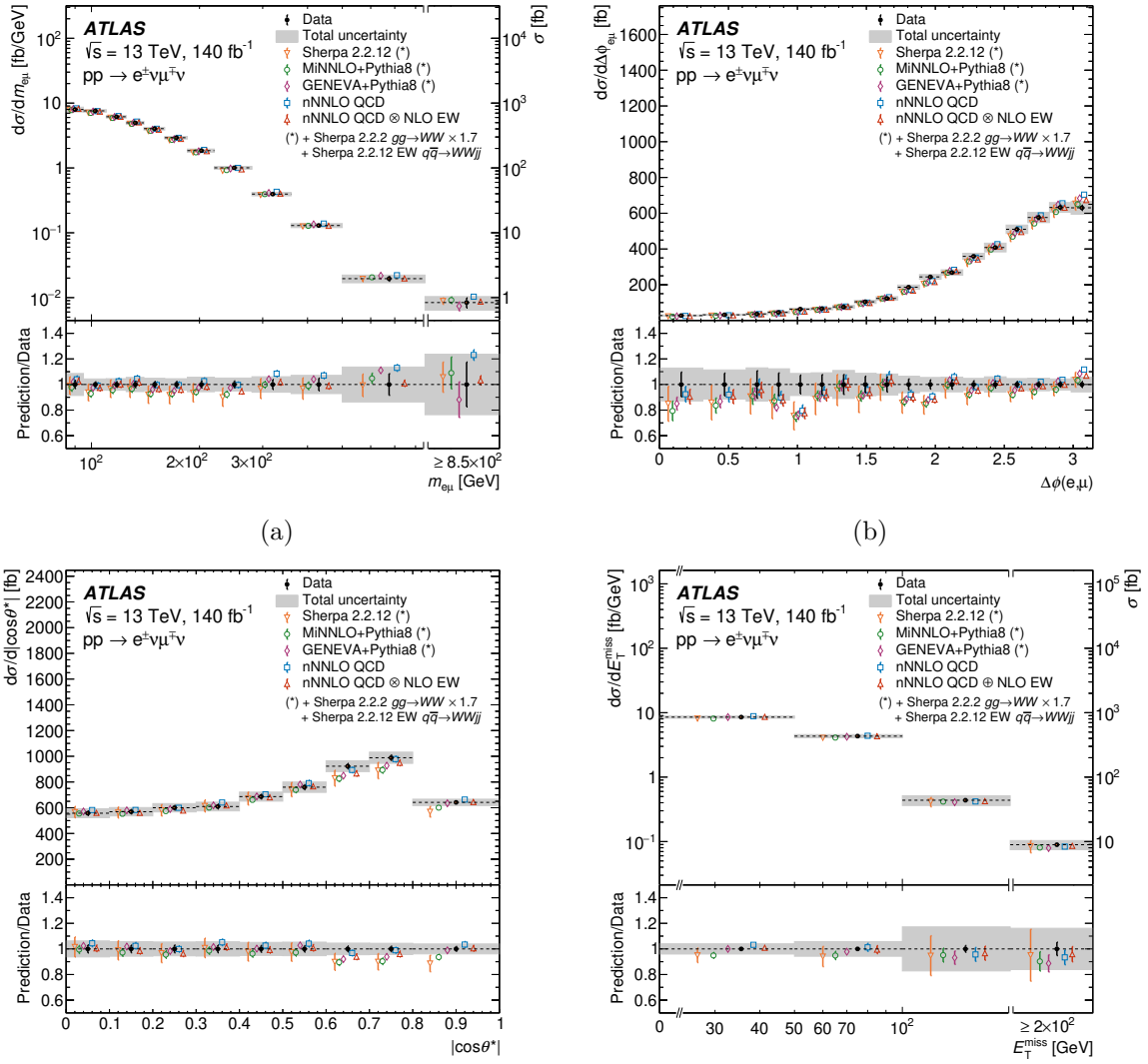

Figure 11. Fiducial differential cross-sections as a function of (a) $m_{e\mu}$, (b) $\Delta\phi_{e\mu}$, (c) $|\cos\theta^*|$, and (d) $E_{\mathrm{T}}^{\mathrm{miss}}$. The measured cross-section values are shown as points with error bars giving the statistical uncertainty and solid bands indicating the size of the total uncertainty. For distributions in which the rightmost bin is inclusive, the right-hand-side axis indicates the integrated cross-section of the rightmost bin. The results are compared with fixed-order nNNLO QCD (+ NLO EW) predictions from MATRIX 2.1, the NNLO+PS predictions from POWHEG MINNLO+PYTHIA 8 and GENEVA+PYTHIA 8, and the SHERPA 2.2.12 NLO+PS predictions. The last three predictions are combined with the ones from SHERPA 2.2.2 for the gg initial state and SHERPA 2.2.12 for electroweak $WWjj$ production. These contributions are modelled at LO but an NLO QCD K-factor of 1.7 is applied for gluon-induced production. Theoretical predictions are indicated as markers with vertical lines denoting PDF, scale and parton-shower uncertainties. Markers are staggered for better visibility.

JHEP08(2025)142

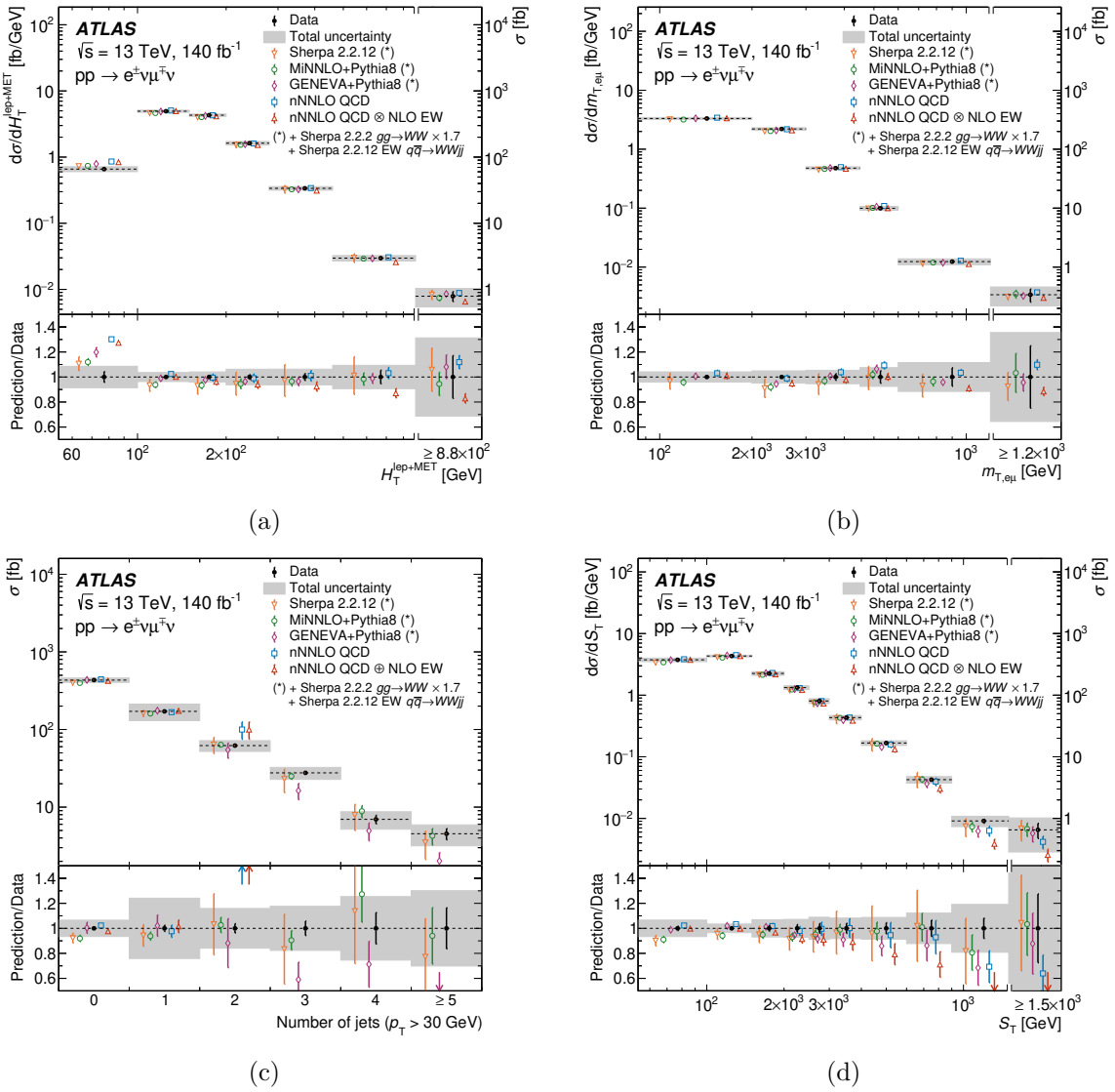

Figure 12. Fiducial differential cross-sections as a function of (a) $H_{\mathrm{T}}^{\mathrm{lep.+MET}}$, (b) $m_{\mathrm{T},e\mu}$, (c) the jet multiplicity of the event, and (d) S_{T}. The measured cross-section values are shown as points with error bars giving the statistical uncertainty and solid bands indicating the size of the total uncertainty. For distributions in which the rightmost bin is inclusive, the right-hand-side axis indicates the integrated cross-section of the rightmost bin. The results are compared with fixed-order nNNLO QCD (+ NLO EW) predictions from Matrix 2.1, the NNLO+PS predictions from Powheg MiNNLO+Pythia 8 and Geneva+Pythia 8, and the Sherpa 2.2.12 NLO+PS predictions. The last three predictions are combined with the ones from Sherpa 2.2.2 for the gg initial state and Sherpa 2.2.12 for electroweak $WWjj$ production. These contributions are modelled at LO but an NLO QCD K-factor of 1.7 is applied for gluon-induced production. Theoretical predictions are indicated as markers with vertical lines denoting PDF, scale and parton-shower uncertainties. Markers are staggered for better visibility.

JHEP08(2025)142

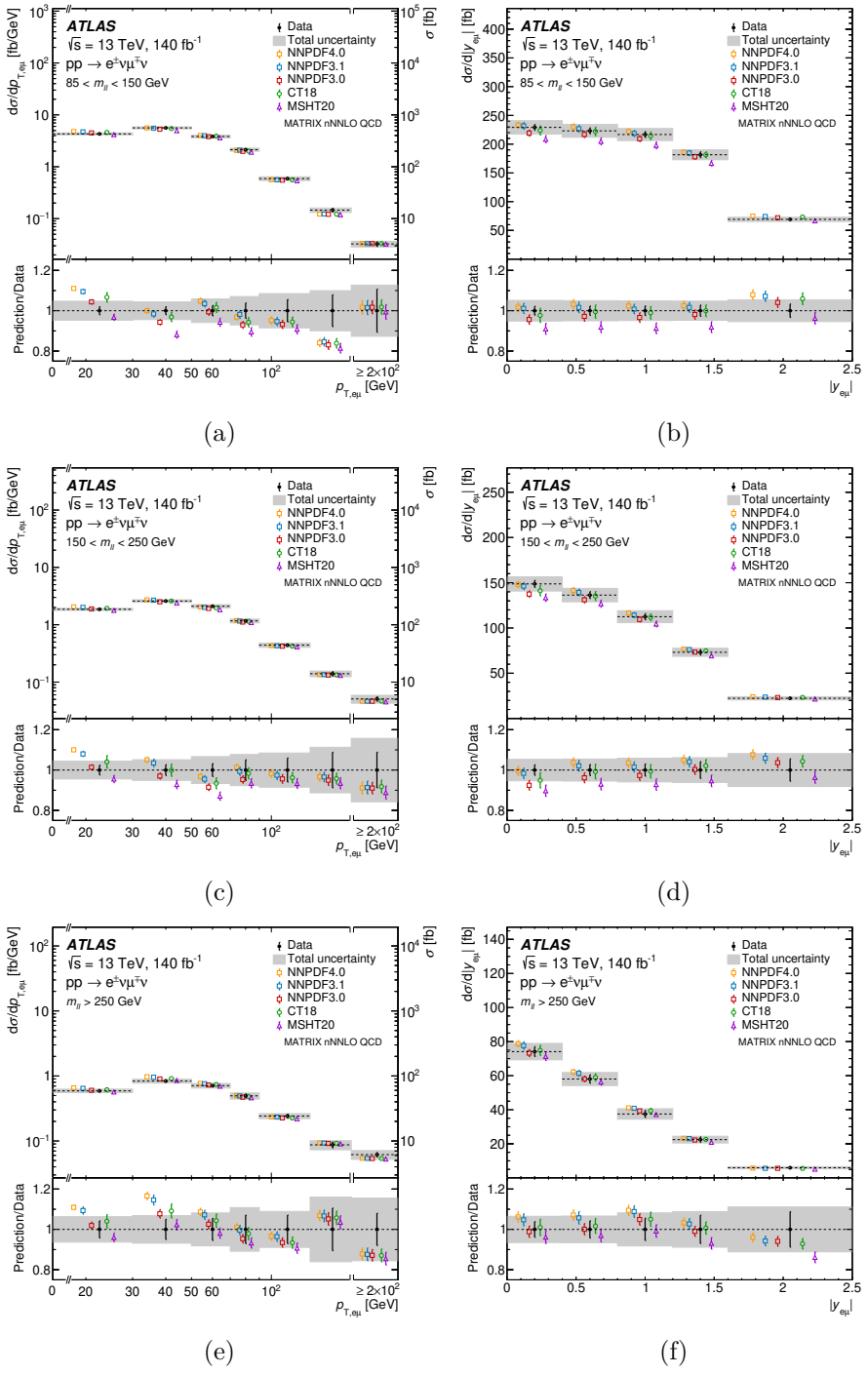

Figure 13. Fiducial differential cross-sections for $p_{\mathrm{T},e\mu}$ and $|y_{e\mu}|$ for the nNNLO MATRIX prediction and various four-flavour PDF sets in three $m_{e\mu}$ regions: ((a) and (b)) $85\,\mathrm{GeV} < m_{e\mu} < 150\,\mathrm{GeV}$, ((c) and (d)) $150\,\mathrm{GeV} < m_{e\mu} < 250\,\mathrm{GeV}$, and ((e) and (f)) $150\,\mathrm{GeV} < m_{e\mu} < 250\,\mathrm{GeV}$. The measured cross-section values are shown as points with error bars giving the statistical uncertainty and solid bands indicating the size of the total uncertainty. For $p_{\mathrm{T},e\mu}$, the right-hand-side axis indicates the integrated cross-section of the rightmost bin. The measurement is compared with fixed-order nNNLO QCD + NLO EW predictions from MATRIX 2.1 using five different four-flavour NNLO PDF sets: NNPDF4.0, NNPDF3.1, NNPDF3.0, CT18, and MSHT20.

JHEP08(2025)142

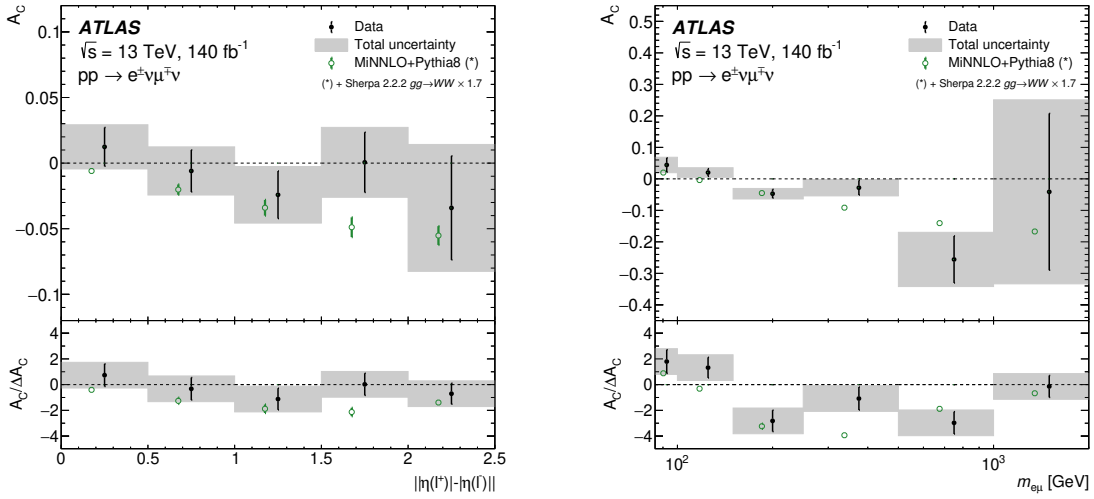

(a) (b)

Figure 14. Charge asymmetry A_C measured as a function of (a) the absolute difference of the leptons' absolute rapidities $||\eta_{\ell^+}| - |\eta_{\ell^-}||$, and (b) the invariant mass of the dilepton system, $m_{e\mu}$. The measured values are shown as points, whose error bars represent the statistical uncertainty, while the solid bands indicate the size of the total uncertainty. In the bottom panel, the central value of the charge asymmetry divided by the total uncertainty of the A_C measurement is shown. The measurement is compared with the NNLO+PS predictions from POWHEG MiNNLO+PYTHIA 8 with vertical lines denoting PDF uncertainties. For A_C as a function of $m_{e\mu}$, PDF uncertainties are smaller than the marker size and not visible.

for larger values of $m_{e\mu}$, in agreement with the SM. In this case, the no-asymmetry hypothesis is rejected in favour of the SM with a significance of approximately three standard deviations.

A non-zero asymmetry in a CP-odd observable would signal CP violation. Since the SM does not predict any CP-violating effects in WW production, such a finding would point to CP-violating new physics. In this paper, the asymmetry A_{CP} of the O_z observable, introduced in section 1, is measured for the first time. It is found to be

$$A_{\mathrm{CP}} = 0.014 \pm 0.008\ (\mathrm{stat.}) \pm 0.008\ (\mathrm{syst.}),$$

which is compatible with the SM expectation of zero within about one standard deviation.

9.3 Effective field theory interpretation

The Standard Model effective field theory [28, 29] provides a framework for describing the effects of theories beyond the Standard Model (BSM theories) that introduce new physics at a scale Λ much larger than the electroweak scale v. The SMEFT allows observables to be expanded in v/Λ and E/Λ, where E is the typical energy exchanged in the process. This is achieved by adding to the SM Lagrangian a series of operators $\mathcal{O}_i^{(d)}$, which consist of gauge invariant combinations of SM fields with an energy dimension d greater than four:

$$\mathcal{L}_{\mathrm{SMEFT}} = \mathcal{L}_{\mathrm{SM}} + \sum_i \frac{c_i^{(5)}}{\Lambda}\mathcal{O}_i^{(5)} + \sum_i \frac{c_i^{(6)}}{\Lambda^2}\mathcal{O}_i^{(6)} + \ldots.$$

JHEP08(2025)142

Measurements of observables sensitive to the effect of SMEFT operators constrain $c_i^{(d)}/\Lambda^{d-4}$, where $c_i^{(d)}$ are the Wilson coefficients associated with the dimension-d operator $\mathcal{O}_i^{(d)}$. Operators of odd dimensionality introduce lepton and baryon number violation and are thus irrelevant for this analysis. The leading effects of BSM physics are expected to manifest themselves as dimension-six operators, as higher-dimensional operators are suppressed by greater powers of Λ.

The Warsaw basis [29] provides a complete set of dimension-six operators consistent with the SM gauge symmetries. For this analysis a $\mathrm{U}(2)_q \times \mathrm{U}(2)_u \times \mathrm{U}(2)_d$ flavour symmetry is assumed, which requires identical couplings for quarks of the first two generations. A quadratic parameterization of dimension-six SMEFT effects is obtained by reweighting [123] a sample of simulated events generated with MadGraph 2.9.9 [69] and the SMEFTsim 3.0 [124, 125] model. Both the $e^{\pm}\nu\mu^{\mp}\nu$ and $e^{\pm}\nu\mu^{\mp}\nu$+1-jet final states are simulated at leading order at matrix-element level, then showered with Pythia 8.307, and merged via the CKKW-L merging scheme [126, 127] to avoid the double counting of jet emissions from the parton-shower and the matrix-element generators. The merged sample shows good agreement with NLO QCD predictions generated with SMEFT@NLO [128] for the SM, and for effects linear and quadratic in the Wilson coefficients. SMEFT effects are also simulated for the $\gamma\gamma$ initial states; these contribute about 10% of the predicted high-mass WW modification due to anomalous triple-gauge-boson couplings.

Seven dimension-six Wilson coefficients that impact WW production are analyzed. Three of these coefficients — c_W, c_{HWB}, and c_{HD} — modify triple-gauge-boson couplings (and in the case of c_{HWB} and c_{HD} also Z-boson couplings to fermions), which strongly affects the high-mass WW cross-section. The remaining four coefficients — $c_{Hq}^{(1)}$, $c_{Hq}^{(3)}$, c_{Hu}, and c_{Hd} — alter the couplings between quarks and weak bosons, resulting in significant effects at high invariant mass by disrupting the cancellations present in the SM amplitudes. Other coefficients are not studied, either because their contributions do not increase with the WW invariant mass (thus offering limited sensitivity) or because they correspond to four-fermion interactions that are more tightly constrained by high-mass Drell-Yan measurements.

The unfolded $m_{\mathrm{T},e\mu}$ distribution in figure 12 is found to offer the best sensitivity to the targeted SMEFT effects. It is verified, using simulated data, that the unfolding procedure accurately recovers the effects of the studied dimension-six operators. Figure 15 shows the measured $m_{\mathrm{T},e\mu}$ distribution again, now compared to the SM and SMEFT predictions described below

The precise Matrix nNNLO QCD $\otimes$ NLO EW prediction introduced in section 8 serves as the basis for the SM prediction. Theoretical uncertainties in this prediction arise from parton distribution functions, the QCD scales, and the unknown effect of mixed EW-QCD higher-order corrections. The last is the dominant uncertainty, estimated as the difference of multiplicative and additive application of QCD and EW corrections, which affects the predicted yield in the last bin of the distribution by 10%.

While the jet-merged SMEFT prediction agrees well with NLO QCD results from SMEFT@NLO, residual differences remain relative to the best SM prediction because NLO EW and NNLO QCD corrections to WW production have not been computed within the SMEFT framework. As an approximation, it is assumed that the SM NLO EW and NNLO

JHEP08(2025)142

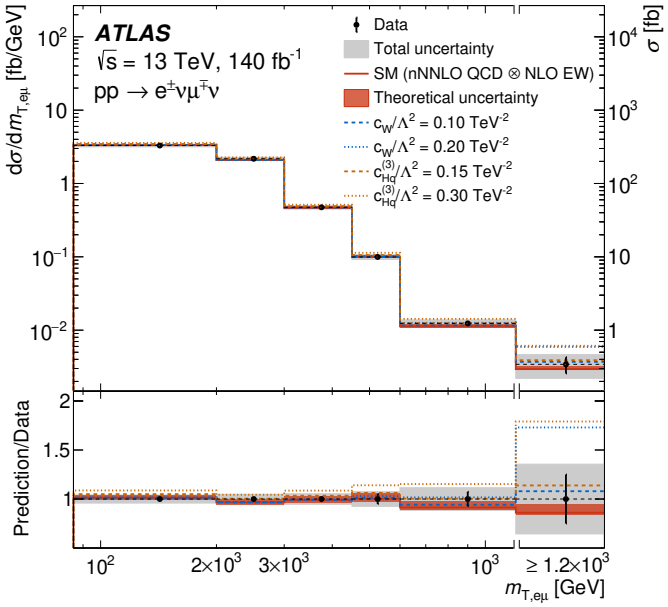

Figure 15. Measured $m_{\mathrm{T},e\mu}$ distribution used in the SMEFT analysis, compared to the MATRIX nNNLO QCD $\otimes$ NLO EW prediction obtained using NNPDF3.1 LUXQED, as well as SMEFT predictions for illustrative values of the Wilson coefficients c_W and $c_{Hq}^{(3)}$. Measured cross-section values are shown as points, with error bars representing statistical uncertainties and solid bands indicating the total experimental uncertainty. The right-hand vertical axis displays the integrated cross-section in the inclusive overflow bin. The SM prediction is shown as a red line, with a shaded band denoting the total theoretical uncertainty used in the SMEFT fit, combined in quadrature. The uncertainty is asymmetric due to the dominant contribution from the two-point uncertainty defined by the difference between multiplicative and additive combinations of QCD and EW corrections.

QCD corrections are applicable to the SMEFT prediction in each bin of the $m_{\mathrm{T},e\mu}$ distribution. The QCD correction increases the SMEFT contribution in all bins by approximately 10%, while the EW correction reduces it by up to 30% in the last bin. This approach is conservative in the sense that not applying higher-order corrections would result in Wilson coefficient limits that are roughly 10% more stringent.

To constrain the Wilson coefficients, a multivariate normal likelihood function is used. Statistical and systematic uncertainties are captured by the covariance of the multivariate distribution, while signal theory uncertainties are incorporated through Gaussian-constrained nuisance parameters. Confidence intervals are derived using a profile-likelihood-ratio test statistic [129], which is assumed to be χ^2-distributed according to Wilks' theorem [130]. The validity of the χ^2-approximation is confirmed using pseudo-experiments.

Table 7 summarizes the expected and observed 95% confidence level (CL) limits on Wilson coefficients, considering either only linear contributions, of $O(c_i/\Lambda^2)$ — arising from the interference between SM and BSM amplitudes — or also quadratic terms of order $O(c_i^2/\Lambda^4)$ — arising purely from the BSM amplitudes. Limits that account only for the linear contribution of the Wilson coefficients are much weaker, despite formally missing only a higher-order correction in Λ^{-1}. This is largely due to helicity suppression of the $O(\Lambda^{-2})$ interference

JHEP08(2025)142

	$O(\Lambda^{-2})$, individual		$O(\Lambda^{-4})$, individual		$O(\Lambda^{-4})$, profiled	
	Expected	Observed	Expected	Observed	Expected	Observed
c_W	$[-3.5, 3.2]$	$[-3.5, 3.4]$	$[-0.16, 0.16]$	$[-0.18, 0.18]$	$[-0.17, 0.16]$	$[-0.18, 0.18]$
c_{HD}	$[-8.9, 9.8]$	$[-11, 8]$	$[-7, 21]$	$[-8, 21]$	$[-7, 21]$	$[-8, 21]$
c_{HWB}	$[-8.4, 9.2]$	$[-10, 8]$	$[-1.5, 1.7]$	$[-1.7, 1.9]$	$[-1.7, 1.7]$	$[-1.8, 1.9]$
$c_{Hq}^{(1)}$	$[-2.5, 2.4]$	$[-2.2, 2.8]$	$[-0.27, 0.24]$	$[-0.29, 0.27]$	$[-0.29, 0.29]$	$[-0.31, 0.31]$
$c_{Hq}^{(3)}$	$[-0.69, 0.66]$	$[-0.7, 0.68]$	$[-0.28, 0.22]$	$[-0.31, 0.24]$	$[-0.3, 0.27]$	$[-0.34, 0.29]$
c_{Hu}	$[-3.2, 3.0]$	$[-3.0, 3.4]$	$[-0.31, 0.29]$	$[-0.35, 0.32]$	$[-0.32, 0.31]$	$[-0.35, 0.33]$
c_{Hd}	$[-11, 11]$	$[-11, 11]$	$[-0.45, 0.46]$	$[-0.5, 0.51]$	$[-0.49, 0.49]$	$[-0.52, 0.53]$

Table 7. Expected and observed 95% CL limits for various assumptions. For $O(\Lambda^{-2})$, only the interference effect of dimension-six operators is considered, while for $O(\Lambda^{-4})$, both the interference and quadratic effects are included. "Profiled"' means that all seven Wilson coefficients are fit simultaneously. Profiled limits cannot be obtained in the $O(\Lambda^{-2})$ fit, which is degenerate. Confidence intervals are given for $\Lambda = 1\,\text{TeV}$ and increase quadratically with the value of Λ.

effects [131] and does not necessarily indicate a breakdown of the SMEFT expansion [132]. In the case of the combined linear and quadratic parameterization, profiled limits can be derived by fitting all other parameters to their conditional best-fit values. The linear fit suffers from degeneracies, as there are more degrees of freedom than data points, allowing constraints only on combinations of Wilson coefficients rather than individual parameters.

Limits driven by quadratic dimension-six contributions exhibit increased model dependence, as they are only valid for BSM models where linear contributions from dimension-eight operators are small relative to the quadratic dimension-six contributions — despite both contributions being of the order Λ^{-4}. To facilitate an *a posteriori* assessment of the validity of limits for specific BSM models, a "clipping" scan is implemented following a recommendation of the LHC EFT Working Group [133]. In this approach, the effect of dimension-six operators is disregarded for a WW invariant mass exceeding a cut-off, M_{cut}, allowing the extraction of limits sensitive only to data below a defined energy scale, enabling an estimation of unknown higher-order SMEFT contributions. Profiled 95% CL limits as a function of the cut-off value are shown in figure 16.

The limits on the triple-gauge-boson coupling coefficient c_W, considering also quadratic contributions, represent an improvement on the previous ATLAS WW measurement [8], which provided constraints on c_{WWW} in the HISZ basis [134, 135] that translate into a 95% confidence interval of $[-0.24, 0.24]$ for the Warsaw basis coefficient c_W. However, they are weaker than those obtained in WZ [136] and $W\gamma$ [137, 138] final states, which are the most stringent constraints from diboson data. In the linear approximation, limits are much stronger than in the previous WW measurement, owing to the inclusion of final states with jets, which partially mitigate the helicity surpression of the interference [139]. Nonetheless, in the linear case the sensitivity is still an order of magnitude weaker than in the ATLAS analysis of electroweak Zjj production [140] and the CMS analysis of $W\gamma$ production [137], for which angular observables specifically sensitive to the interference can be constructed.

JHEP08(2025)142

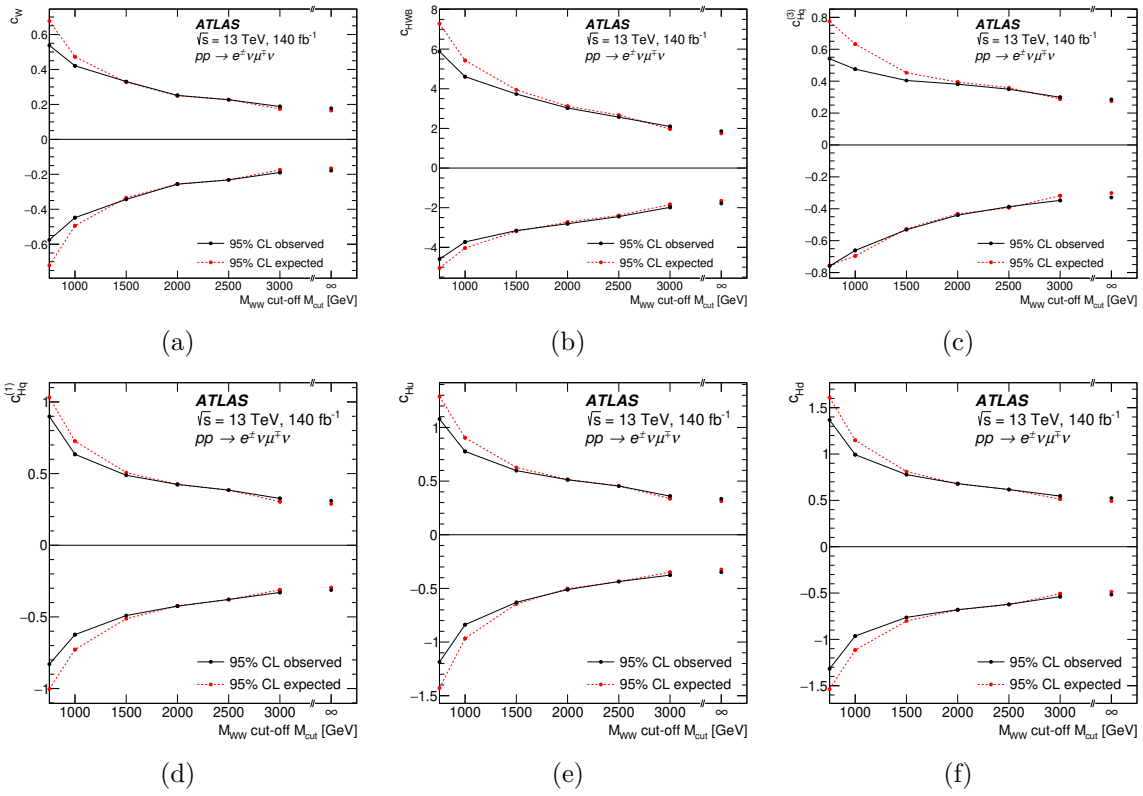

Figure 16. Borders of the 95% confidence intervals as a function of an upper mass cut-off M_{cut}, applied to the SMEFT effects only, for (a) c_W, (b) c_{HWB}, (c) $c_{Hq}^{(3)}$, (d) $c_{Hq}^{(1)}$, (e) c_{Hu}, and (f) c_{Hd}. The six remaining Wilson coefficients are profiled in the fit. Not shown is c_{HD}, which has no relevant M_{WW} dependence.

The individual constraints on the quark-coupling-modifying Wilson coefficients $c_{Hq}^{(1)}$, $c_{Hq}^{(3)}$, c_{Hu}, and c_{Hd} are weaker than those obtained from global fits [141] that include electroweak precision data [142]. However, these global constraints are highly correlated, and profiled limits on these coefficients are considerably weaker and cannot effectively distinguish between anomalous couplings to left-handed light quarks (as introduced by $c_{Hq}^{(1)}$ and $c_{Hq}^{(3)}$) and right-handed light quarks (as introduced by c_{Hu} and c_{Hd}). When profiling over other coefficients, this WW measurement particularly improves constraints on the Wilson coefficients that modify right-handed quark couplings, as no sensitivity to these operators exists in WZ or $W\gamma$ final states. However, the improvements are mainly driven by quadratic contributions in the Wilson coefficients and thus carry larger model dependence than those from precision data. While constraints on $c_{Hq}^{(1)}$, $c_{Hq}^{(3)}$, c_{Hu}, and c_{Hd} from Higgs boson production in association with a vector boson (VH) are typically stronger by a factor of two [143, 144], the WW measurement offers complementary sensitivity, as VH is also affected by additional Wilson coefficients.

10 Conclusion

Differential and integrated fiducial cross-sections for the production of W-boson pairs decaying into final states with one electron and one muon of opposite electric charge are measured using a 140 fb^{-1} dataset of $\sqrt{s} = 13$ TeV pp collisions recorded by the ATLAS detector at the LHC.

JHEP08(2025)142

A jet-inclusive event selection allows comparisons of the measured cross-sections with precise theoretical calculations. Improved data-driven estimates of the top-quark and fake-lepton backgrounds reduce the uncertainty in the fiducial cross-section to 3.1%. The measurement is extrapolated to the full phase space, resulting in a total WW cross-section of $127 \pm 4\,\text{pb}$. Differential cross-sections are measured as a function of twelve observables.

The measurements are compared with several state-of-the-art theoretical predictions. A fixed-order prediction at nNNLO in QCD using the NNPDF3.1NNLO LUXQED set of PDFs is in excellent agreement with the measured total cross-section and gives a good description of differential cross-sections. Its multiplicative combination with EW corrections improves the description of some observables, although it does not provide an adequate description in other cases because the combination cannot take into account non-factorizing EW-QCD effects. Furthermore, parton-shower-matched predictions from POWHEG MINNLO+PYTHIA 8, GENEVA+PYTHIA 8, and SHERPA 2.2.12 are able to correctly describe observables sensitive to jet emission. Given the experimental and theoretical uncertainties, excellent agreement between the measurements and predictions is observed.

The rapidity-dependent charge asymmetry in WW production, A_{C}, is measured differentially in the dilepton invariant mass $m_{e\mu}$ and in the absolute difference of the leptons' absolute rapidities. A significant asymmetry is observed as a function of $m_{e\mu}$, in accordance with the SM expectation. Furthermore, an asymmetry A_{CP} in a CP-odd observable is found to be compatible with no CP violation.

Limits on Wilson coefficients that modify triple-gauge-boson couplings and the coupling of quarks to bosons are set in the SMEFT framework. When considering the effects of dimension-six operators at order Λ^{-4}, the limits on c_W, c_{Hu}, and c_{Hd} are competitive with those derived from electroweak precision data, as well as those from weak-boson pair and ZH measurements at the LHC, although they do not provide the strongest constraints on any of these coefficients.

Acknowledgments

We thank CERN for the very successful operation of the LHC and its injectors, as well as the support staff at CERN and at our institutions worldwide without whom ATLAS could not be operated efficiently.

The crucial computing support from all WLCG partners is acknowledged gratefully, in particular from CERN, the ATLAS Tier-1 facilities at TRIUMF/SFU (Canada), NDGF (Denmark, Norway, Sweden), CC-IN2P3 (France), KIT/GridKA (Germany), INFN-CNAF (Italy), NL-T1 (Netherlands), PIC (Spain), RAL (U.K.) and BNL (U.S.A.), the Tier-2 facilities worldwide and large non-WLCG resource providers. Major contributors of computing resources are listed in ref. [145].

We gratefully acknowledge the support of ANPCyT, Argentina; YerPhI, Armenia; ARC, Australia; BMWFW and FWF, Austria; ANAS, Azerbaijan; CNPq and FAPESP, Brazil; NSERC, NRC and CFI, Canada; CERN; ANID, Chile; CAS, MOST and NSFC, China; Minciencias, Colombia; MEYS CR, Czech Republic; DNRF and DNSRC, Denmark; IN2P3-CNRS and CEA-DRF/IRFU, France; SRNSFG, Georgia; BMFTR, HGF and MPG, Germany; GSRI, Greece; RGC and Hong Kong SAR, China; ISF and Benoziyo Center, Israel; INFN,

JHEP08(2025)142

Italy; MEXT and JSPS, Japan; CNRST, Morocco; NWO, Netherlands; RCN, Norway; MEiN, Poland; FCT, Portugal; MNE/IFA, Romania; MESTD, Serbia; MSSR, Slovakia; ARIS and MVZI, Slovenia; DSI/NRF, South Africa; MICINN, Spain; SRC and Wallenberg Foundation, Sweden; SERI, SNSF and Cantons of Bern and Geneva, Switzerland; NSTC, Taipei; TENMAK, Türkiye; STFC/UKRI, United Kingdom; DOE and NSF, United States of America.

Individual groups and members have received support from BCKDF, CANARIE, CRC and DRAC, Canada; CERN-CZ, PRIMUS 21/SCI/017 and UNCE SCI/013, Czech Republic; COST, ERC, ERDF, Horizon 2020, ICSC-NextGenerationEU and Marie Skłodowska-Curie Actions, European Union; Investissements d'Avenir Labex, Investissements d'Avenir Idex and ANR, France; DFG and AvH Foundation, Germany; Herakleitos, Thales and Aristeia programmes co-financed by EU-ESF and the Greek NSRF, Greece; BSF-NSF and MINERVA, Israel; Norwegian Financial Mechanism 2014-2021, Norway; NCN and NAWA, Poland; La Caixa Banking Foundation, CERCA Programme Generalitat de Catalunya and PROMETEO and GenT Programmes Generalitat Valenciana, Spain; Göran Gustafssons Stiftelse, Sweden; The Royal Society and Leverhulme Trust, United Kingdom.

In addition, individual members wish to acknowledge support from Chile: Agencia Nacional de Investigación y Desarrollo (FONDECYT 1190886, FONDECYT 1210400); China: National Natural Science Foundation of China (NSFC — 12175119, NSFC 12275265, NSFC-12075060); Czech Republic: PRIMUS Research Programme (PRIMUS/21/SCI/017); EU: H2020 European Research Council (ERC — 101002463, H2020-MSCA-IF-2020: HPOFHIC — 10103); European Union: European Research Council (ERC — 948254), Horizon 2020 Framework Programme (MUCCA — CHIST-ERA-19-XAI-00), European Union, Future Artificial Intelligence Research (FAIR-NextGenerationEU PE00000013), Italian Center for High Performance Computing, Big Data and Quantum Computing (ICSC, NextGenerationEU), Marie Sklodowska-Curie Actions (EU H2020 MSC IF GRANT NO 101033496); France: Agence Nationale de la Recherche (ANR-20-CE31-0013, ANR-21-CE31-0013, ANR-21-CE31-0022), Investissements d'Avenir Idex (ANR-11-LABX-0012), Investissements d'Avenir Labex (ANR-11-LABX-0012); Germany: Baden-Württemberg Stiftung (BW Stiftung-Postdoc Eliteprogramme), Deutsche Forschungsgemeinschaft (DFG — CR 312/5-1); Italy: Istituto Nazionale di Fisica Nucleare (FELLINI G.A. n. 754496, ICSC, NextGenerationEU); Japan: Japan Society for the Promotion of Science (JSPS KAKENHI JP21H05085, JSPS KAKENHI JP22H01227, JSPS KAKENHI JP22H04944); Netherlands: Netherlands Organisation for Scientific Research (NWO Veni 2020 — VI.Veni.202.179); Norway: Research Council of Norway (RCN-314472); Poland: Polish National Agency for Academic Exchange (PPN/PPO/2020/1/00002/U/00001), Polish National Science Centre (NCN 2021/42/E/ST2/00350, NCN UMO-2019/34/E/ST2/00393, NCN & H2020 MSCA 945339, UMO-2020/37/B/ST2/01043, UMO-2021/40/C/ST2/00187); Portugal: Foundation for Science and Technology (FCT); Slovenia: Slovenian Research Agency (ARIS grant J1-3010); Spain: BBVA Foundation (LEO22-1-603), Generalitat Valenciana (Artemisa, FEDER, IDIFEDER/2018/048), La Caixa Banking Foundation (LCF/BQ/PI20/11760025), Ministry of Science and Innovation (MCIN & NextGenEU PCI2022-135018-2, MICIN & FEDER PID2021-125273NB, RYC2019-028510-I, RYC2020-030254-I, RYC2021-031273-I, RYC2022-038164-I), PROMETEO and GenT Programmes Generalitat Valenciana (CIDEGENT/2019/023,

CIDEGENT/2019/027); Sweden: Swedish Research Council (VR 2018-00482, VR 2021-03651, VR 2022-03845, VR 2022-04683), Knut and Alice Wallenberg Foundation (KAW 2017.0100, KAW 2018.0157, KAW 2018.0458, KAW 2019.0447); Switzerland: Swiss National Science Foundation (SNSF — PCEFP2_194658); United Kingdom: Leverhulme Trust (Leverhulme Trust RPG-2020-004); United States of America: U.S. Department of Energy (ECA DE-AC02-76SF00515), Neubauer Family Foundation.

Data Availability Statement. This article has no associated data or the data will not be deposited.

Code Availability Statement. This article has no associated code or the code will not be deposited.

References

[1] CMS collaboration, *Measurements of the electroweak diboson production cross sections in proton-proton collisions at $\sqrt{s} = 5.02$ TeV using leptonic decays*, *Phys. Rev. Lett.* **127** (2021) 191801 [arXiv:2107.01137] [INSPIRE].

[2] ATLAS collaboration, *Measurement of W^+W^- production in pp collisions at $\sqrt{s} = 7$ TeV with the ATLAS detector and limits on anomalous WWZ and $WW\gamma$ couplings*, *Phys. Rev. D* **87** (2013) 112001 [*Erratum ibid.* **88** (2013) 079906] [arXiv:1210.2979] [INSPIRE].

[3] CMS collaboration, *Measurement of the W^+W^- cross section in pp collisions at $\sqrt{s} = 7$ TeV and limits on anomalous $WW\gamma$ and WWZ couplings*, *Eur. Phys. J. C* **73** (2013) 2610 [arXiv:1306.1126] [INSPIRE].

[4] ATLAS collaboration, *Measurement of total and differential W^+W^- production cross sections in proton-proton collisions at $\sqrt{s} = 8$ TeV with the ATLAS detector and limits on anomalous triple-gauge-boson couplings*, *JHEP* **09** (2016) 029 [arXiv:1603.01702] [INSPIRE].

[5] CMS collaboration, *Measurement of the W^+W^- cross section in pp collisions at $\sqrt{s} = 8$ TeV and limits on anomalous gauge couplings*, *Eur. Phys. J. C* **76** (2016) 401 [arXiv:1507.03268] [INSPIRE].

[6] ATLAS collaboration, *Measurement of W^+W^- production in association with one jet in proton-proton collisions at $\sqrt{s} = 8$ TeV with the ATLAS detector*, *Phys. Lett. B* **763** (2016) 114 [arXiv:1608.03086] [INSPIRE].

[7] ATLAS collaboration, *Measurement of the W^+W^- production cross section in pp collisions at a centre-of-mass energy of $\sqrt{s} = 13$ TeV with the ATLAS experiment*, *Phys. Lett. B* **773** (2017) 354 [arXiv:1702.04519] [INSPIRE].

[8] ATLAS collaboration, *Measurement of fiducial and differential W^+W^- production cross-sections at $\sqrt{s} = 13$ TeV with the ATLAS detector*, *Eur. Phys. J. C* **79** (2019) 884 [arXiv:1905.04242] [INSPIRE].

[9] CMS collaboration, *W^+W^- boson pair production in proton-proton collisions at $\sqrt{s} = 13$ TeV*, *Phys. Rev. D* **102** (2020) 092001 [arXiv:2009.00119] [INSPIRE].

JHEP08(2025)142

[10] ATLAS collaboration, *Measurements of $W^+W^-+\geq 1$ jet production cross-sections in pp collisions at $\sqrt{s} = 13$ TeV with the ATLAS detector*, *JHEP* **06** (2021) 003 [arXiv:2103.10319] [INSPIRE].

[11] ATLAS collaboration, *Measurements of W^+W^- production in decay topologies inspired by searches for electroweak supersymmetry*, *Eur. Phys. J. C* **83** (2023) 718 [arXiv:2206.15231] [INSPIRE].

[12] CMS collaboration, *Measurement of inclusive and differential cross sections for W^+W^- production in proton-proton collisions at $\sqrt{s} = 13.6$ TeV*, *Phys. Lett. B* **861** (2025) 139231 [arXiv:2406.05101] [INSPIRE].

[13] ALEPH et al. collaborations, *Electroweak measurements in electron-positron collisions at W-boson-pair energies at LEP*, *Phys. Rept.* **532** (2013) 119 [arXiv:1302.3415] [INSPIRE].

[14] CDF collaboration, *Observation of W^+W^- production in $\bar{p}p$ collisions at $\sqrt{s} = 1.8$ TeV*, *Phys. Rev. Lett.* **78** (1997) 4536 [INSPIRE].

[15] CDF collaboration, *Measurement of the W^+W^- production cross section and search for anomalous $WW\gamma$ and WWZ couplings in $p\bar{p}$ collisions at $\sqrt{s} = 1.96$ TeV*, *Phys. Rev. Lett.* **104** (2010) 201801 [arXiv:0912.4500] [INSPIRE].

[16] D0 collaboration, *Measurement of the WW production cross section with dilepton final states in $p\bar{p}$ collisions at $\sqrt{s} = 1.96$ TeV and limits on anomalous trilinear gauge couplings*, *Phys. Rev. Lett.* **103** (2009) 191801 [arXiv:0904.0673] [INSPIRE].

[17] ATLAS collaboration, *Luminosity determination in pp collisions at $\sqrt{s} = 13$ TeV using the ATLAS detector at the LHC*, *Eur. Phys. J. C* **83** (2023) 982 [arXiv:2212.09379] [INSPIRE].

[18] P. Meade, H. Ramani and M. Zeng, *Transverse momentum resummation effects in W^+W^- measurements*, *Phys. Rev. D* **90** (2014) 114006 [arXiv:1407.4481] [INSPIRE].

[19] D. Lombardi, M. Wiesemann and G. Zanderighi, *W^+W^- production at NNLO+PS with MINNLO$_{PS}$*, *JHEP* **11** (2021) 230 [arXiv:2103.12077] [INSPIRE].

[20] P.F. Monni et al., *MiNNLO$_{PS}$: a new method to match NNLO QCD to parton showers*, *JHEP* **05** (2020) 143 [*Erratum ibid.* **02** (2022) 031] [arXiv:1908.06987] [INSPIRE].

[21] G. D'Agostini, *A multidimensional unfolding method based on Bayes' theorem*, *Nucl. Instrum. Meth. A* **362** (1995) 487 [INSPIRE].

[22] G. D'Agostini, *Improved iterative Bayesian unfolding*, in the proceedings of the *Alliance workshop on unfolding and data correction*, (2010) [arXiv:1010.0632] [INSPIRE].

[23] A.J. Barr, *Measuring slepton spin at the LHC*, *JHEP* **02** (2006) 042 [hep-ph/0511115] [INSPIRE].

[24] E. Re, M. Wiesemann and G. Zanderighi, *NNLOPS accurate predictions for W^+W^- production*, *JHEP* **12** (2018) 121 [arXiv:1805.09857] [INSPIRE].

[25] S. Yang et al., *Boost asymmetry of the diboson productions in pp collisions*, *Phys. Rev. D* **106** (2022) L051301 [arXiv:2207.02072] [INSPIRE].

[26] T. Han and Y. Li, *Genuine CP-odd observables at the LHC*, *Phys. Lett. B* **683** (2010) 278 [arXiv:0911.2933] [INSPIRE].

[27] C. Degrande and J. Touchèque, *A reduced basis for CP violation in SMEFT at colliders and its application to diboson production*, *JHEP* **04** (2022) 032 [arXiv:2110.02993] [INSPIRE].

[28] W. Buchmüller and D. Wyler, *Effective Lagrangian analysis of new interactions and flavor conservation*, *Nucl. Phys. B* **268** (1986) 621 [INSPIRE].

JHEP08(2025)142

[29] B. Grzadkowski, M. Iskrzyński, M. Misiak and J. Rosiek, *Dimension-six terms in the Standard Model Lagrangian*, *JHEP* **10** (2010) 085 [arXiv:1008.4884] [INSPIRE].

[30] ATLAS collaboration, *The ATLAS experiment at the CERN Large Hadron Collider*, 2008 *JINST* **3** S08003 [INSPIRE].

[31] L. Evans and P. Bryant, *LHC machine*, 2008 *JINST* **3** S08001 [INSPIRE].

[32] ATLAS collaboration, *ATLAS Insertable B-Layer technical design report*, CERN-LHCC-2010-013, CERN, Geneva, Switzerland (2010).

[33] ATLAS IBL collaboration, *Production and integration of the ATLAS Insertable B-Layer*, 2018 *JINST* **13** T05008 [arXiv:1803.00844] [INSPIRE].

[34] ATLAS collaboration, *Software and computing for run 3 of the ATLAS experiment at the LHC*, *Eur. Phys. J. C* **85** (2025) 234 [arXiv:2404.06335] [INSPIRE].

[35] ATLAS collaboration, *ATLAS data quality operations and performance for 2015–2018 data-taking*, 2020 *JINST* **15** P04003 [arXiv:1911.04632] [INSPIRE].

[36] G. Avoni et al., *The new LUCID-2 detector for luminosity measurement and monitoring in ATLAS*, 2018 *JINST* **13** P07017 [INSPIRE].

[37] ATLAS collaboration, *The ATLAS simulation infrastructure*, *Eur. Phys. J. C* **70** (2010) 823 [arXiv:1005.4568] [INSPIRE].

[38] GEANT4 collaboration, *GEANT4 — a simulation toolkit*, *Nucl. Instrum. Meth. A* **506** (2003) 250 [INSPIRE].

[39] M. Grazzini, S. Kallweit, D. Rathlev and M. Wiesemann, $W^{\pm}Z$ *production at hadron colliders in NNLO QCD*, *Phys. Lett. B* **761** (2016) 179 [arXiv:1604.08576] [INSPIRE].

[40] M. Grazzini, S. Kallweit, D. Rathlev and M. Wiesemann, $W^{\pm}Z$ *production at the LHC: fiducial cross sections and distributions in NNLO QCD*, *JHEP* **05** (2017) 139 [arXiv:1703.09065] [INSPIRE].

[41] M. Grazzini, S. Kallweit and D. Rathlev, ZZ *production at the LHC: fiducial cross sections and distributions in NNLO QCD*, *Phys. Lett. B* **750** (2015) 407 [arXiv:1507.06257] [INSPIRE].

[42] F. Cascioli et al., *ZZ production at hadron colliders in NNLO QCD*, *Phys. Lett. B* **735** (2014) 311 [arXiv:1405.2219] [INSPIRE].

[43] M. Grazzini et al., W^+W^- *production at the LHC: fiducial cross sections and distributions in NNLO QCD*, *JHEP* **08** (2016) 140 [arXiv:1605.02716] [INSPIRE].

[44] NNPDF collaboration, *Parton distributions for the LHC run II*, *JHEP* **04** (2015) 040 [arXiv:1410.8849] [INSPIRE].

[45] T. Sjöstrand et al., *An introduction to PYTHIA 8.2*, *Comput. Phys. Commun.* **191** (2015) 159 [arXiv:1410.3012] [INSPIRE].

[46] ATLAS collaboration, *ATLAS Pythia 8 tunes to 7 TeV data*, ATL-PHYS-PUB-2014-021, CERN, Geneva, Switzerland (2014).

[47] SHERPA collaboration, *Event generation with Sherpa 2.2*, *SciPost Phys.* **7** (2019) 034 [arXiv:1905.09127] [INSPIRE].

[48] F. Cascioli et al., *Precise Higgs-background predictions: merging NLO QCD and squared quark-loop corrections to four-lepton + 0,1 jet production*, *JHEP* **01** (2014) 046 [arXiv:1309.0500] [INSPIRE].

JHEP08(2025)142

[49] T. Gleisberg and S. Höche, *Comix, a new matrix element generator*, *JHEP* **12** (2008) 039 [arXiv:0808.3674] [INSPIRE].

[50] S. Schumann and F. Krauss, *A parton shower algorithm based on Catani-Seymour dipole factorisation*, *JHEP* **03** (2008) 038 [arXiv:0709.1027] [INSPIRE].

[51] S. Höche, F. Krauss, M. Schönherr and F. Siegert, *A critical appraisal of NLO+PS matching methods*, *JHEP* **09** (2012) 049 [arXiv:1111.1220] [INSPIRE].

[52] S. Höche, F. Krauss, M. Schönherr and F. Siegert, *QCD matrix elements + parton showers: the NLO case*, *JHEP* **04** (2013) 027 [arXiv:1207.5030] [INSPIRE].

[53] S. Catani, F. Krauss, R. Kuhn and B.R. Webber, *QCD matrix elements + parton showers*, *JHEP* **11** (2001) 063 [hep-ph/0109231] [INSPIRE].

[54] S. Höche, F. Krauss, S. Schumann and F. Siegert, *QCD matrix elements and truncated showers*, *JHEP* **05** (2009) 053 [arXiv:0903.1219] [INSPIRE].

[55] F. Cascioli, P. Maierhöfer and S. Pozzorini, *Scattering amplitudes with OpenLoops*, *Phys. Rev. Lett.* **108** (2012) 111601 [arXiv:1111.5206] [INSPIRE].

[56] A. Denner, S. Dittmaier and L. Hofer, *Collier: a fortran-based Complex One-Loop LIbrary in Extended Regularizations*, *Comput. Phys. Commun.* **212** (2017) 220 [arXiv:1604.06792] [INSPIRE].

[57] S. Frixione, P. Nason and G. Ridolfi, *A positive-weight next-to-leading-order Monte Carlo for heavy flavour hadroproduction*, *JHEP* **09** (2007) 126 [arXiv:0707.3088] [INSPIRE].

[58] P. Nason, *A new method for combining NLO QCD with shower Monte Carlo algorithms*, *JHEP* **11** (2004) 040 [hep-ph/0409146] [INSPIRE].

[59] S. Frixione, P. Nason and C. Oleari, *Matching NLO QCD computations with parton shower simulations: the POWHEG method*, *JHEP* **11** (2007) 070 [arXiv:0709.2092] [INSPIRE].

[60] S. Alioli, P. Nason, C. Oleari and E. Re, *A general framework for implementing NLO calculations in shower Monte Carlo programs: the POWHEG BOX*, *JHEP* **06** (2010) 043 [arXiv:1002.2581] [INSPIRE].

[61] E. Re, *Single-top Wt-channel production matched with parton showers using the POWHEG method*, *Eur. Phys. J. C* **71** (2011) 1547 [arXiv:1009.2450] [INSPIRE].

[62] R.D. Ball et al., *Parton distributions with LHC data*, *Nucl. Phys. B* **867** (2013) 244 [arXiv:1207.1303] [INSPIRE].

[63] ATLAS collaboration, *Studies on top-quark Monte Carlo modelling for Top2016*, ATL-PHYS-PUB-2016-020, CERN, Geneva, Switzerland (2016).

[64] S. Frixione et al., *Single-top hadroproduction in association with a W boson*, *JHEP* **07** (2008) 029 [arXiv:0805.3067] [INSPIRE].

[65] ATLAS collaboration, *Studies on top-quark Monte Carlo modelling with Sherpa and MG5_aMC@NLO*, ATL-PHYS-PUB-2017-007, CERN, Geneva, Switzerland (2017).

[66] M. Bähr et al., *Herwig++ physics and manual*, *Eur. Phys. J. C* **58** (2008) 639 [arXiv:0803.0883] [INSPIRE].

[67] J. Bellm et al., *Herwig 7.0/Herwig++ 3.0 release note*, *Eur. Phys. J. C* **76** (2016) 196 [arXiv:1512.01178] [INSPIRE].

[68] L.A. Harland-Lang, A.D. Martin, P. Motylinski and R.S. Thorne, *Parton distributions in the LHC era: MMHT 2014 PDFs*, *Eur. Phys. J. C* **75** (2015) 204 [arXiv:1412.3989] [INSPIRE].

JHEP08(2025)142

[69] J. Alwall et al., *The automated computation of tree-level and next-to-leading order differential cross sections, and their matching to parton shower simulations*, *JHEP* **07** (2014) 079 [arXiv:1405.0301] [INSPIRE].

[70] M. Beneke, P. Falgari, S. Klein and C. Schwinn, *Hadronic top-quark pair production with NNLL threshold resummation*, *Nucl. Phys. B* **855** (2012) 695 [arXiv:1109.1536] [INSPIRE].

[71] M. Cacciari et al., *Top-pair production at hadron colliders with next-to-next-to-leading logarithmic soft-gluon resummation*, *Phys. Lett. B* **710** (2012) 612 [arXiv:1111.5869] [INSPIRE].

[72] P. Bärnreuther, M. Czakon and A. Mitov, *Percent level precision physics at the Tevatron: first genuine NNLO QCD corrections to $q\bar{q} \to t\bar{t} + X$*, *Phys. Rev. Lett.* **109** (2012) 132001 [arXiv:1204.5201] [INSPIRE].

[73] M. Czakon and A. Mitov, *NNLO corrections to top-pair production at hadron colliders: the all-fermionic scattering channels*, *JHEP* **12** (2012) 054 [arXiv:1207.0236] [INSPIRE].

[74] M. Czakon and A. Mitov, *NNLO corrections to top pair production at hadron colliders: the quark-gluon reaction*, *JHEP* **01** (2013) 080 [arXiv:1210.6832] [INSPIRE].

[75] M. Czakon, P. Fiedler and A. Mitov, *Total top-quark pair-production cross section at hadron colliders through $O(\alpha_S^4)$*, *Phys. Rev. Lett.* **110** (2013) 252004 [arXiv:1303.6254] [INSPIRE].

[76] M. Czakon and A. Mitov, *Top++: a program for the calculation of the top-pair cross-section at hadron colliders*, *Comput. Phys. Commun.* **185** (2014) 2930 [arXiv:1112.5675] [INSPIRE].

[77] N. Kidonakis, *Two-loop soft anomalous dimensions for single top quark associated production with a W^- or H^-*, *Phys. Rev. D* **82** (2010) 054018 [arXiv:1005.4451] [INSPIRE].

[78] N. Kidonakis, *Top quark production*, in the proceedings of the *Helmholtz international summer school on physics of heavy quarks and hadrons*, (2014) [DOI:10.3204/DESY-PROC-2013-03/Kidonakis] [arXiv:1311.0283] [INSPIRE].

[79] C. Anastasiou, L.J. Dixon, K. Melnikov and F. Petriello, *High precision QCD at hadron colliders: electroweak gauge boson rapidity distributions at NNLO*, *Phys. Rev. D* **69** (2004) 094008 [hep-ph/0312266] [INSPIRE].

[80] D.J. Lange, *The EvtGen particle decay simulation package*, *Nucl. Instrum. Meth. A* **462** (2001) 152 [INSPIRE].

[81] T. Sjöstrand, S. Mrenna and P.Z. Skands, *A brief introduction to PYTHIA 8.1*, *Comput. Phys. Commun.* **178** (2008) 852 [arXiv:0710.3820] [INSPIRE].

[82] ATLAS collaboration, *The Pythia 8 A3 tune description of ATLAS minimum bias and inelastic measurements incorporating the Donnachie-Landshoff diffractive model*, ATL-PHYS-PUB-2016-017, CERN, Geneva, Switzerland (2016).

[83] ATLAS collaboration, *Performance of electron and photon triggers in ATLAS during LHC run 2*, *Eur. Phys. J. C* **80** (2020) 47 [arXiv:1909.00761] [INSPIRE].

[84] ATLAS collaboration, *Performance of the ATLAS muon triggers in run 2*, 2020 *JINST* **15** P09015 [arXiv:2004.13447] [INSPIRE].

[85] ATLAS collaboration, *Electron and photon performance measurements with the ATLAS detector using the 2015–2017 LHC proton-proton collision data*, 2019 *JINST* **14** P12006 [arXiv:1908.00005] [INSPIRE].

JHEP08(2025)142

[86] ATLAS collaboration, *Muon reconstruction and identification efficiency in ATLAS using the full run 2 pp collision data set at* $\sqrt{s} = 13$ *TeV*, *Eur. Phys. J. C* **81** (2021) 578 [arXiv:2012.00578] [INSPIRE].

[87] ATLAS collaboration, *Muon reconstruction performance of the ATLAS detector in proton–proton collision data at* $\sqrt{s} = 13$ *TeV*, *Eur. Phys. J. C* **76** (2016) 292 [arXiv:1603.05598] [INSPIRE].

[88] ATLAS collaboration, *Jet reconstruction and performance using particle flow with the ATLAS detector*, *Eur. Phys. J. C* **77** (2017) 466 [arXiv:1703.10485] [INSPIRE].

[89] M. Cacciari, G.P. Salam and G. Soyez, *The anti-*k_t *jet clustering algorithm*, *JHEP* **04** (2008) 063 [arXiv:0802.1189] [INSPIRE].

[90] M. Cacciari, G.P. Salam and G. Soyez, *FastJet user manual*, *Eur. Phys. J. C* **72** (2012) 1896 [arXiv:1111.6097] [INSPIRE].

[91] ATLAS collaboration, *Performance of pile-up mitigation techniques for jets in pp collisions at* $\sqrt{s} = 8$ *TeV using the ATLAS detector*, *Eur. Phys. J. C* **76** (2016) 581 [arXiv:1510.03823] [INSPIRE].

[92] ATLAS collaboration, *Jet energy scale and resolution measured in proton–proton collisions at* $\sqrt{s} = 13$ *TeV with the ATLAS detector*, *Eur. Phys. J. C* **81** (2021) 689 [arXiv:2007.02645] [INSPIRE].

[93] ATLAS collaboration, *ATLAS flavour-tagging algorithms for the LHC run 2 pp collision dataset*, *Eur. Phys. J. C* **83** (2023) 681 [arXiv:2211.16345] [INSPIRE].

[94] ATLAS collaboration, *The performance of missing transverse momentum reconstruction and its significance with the ATLAS detector using* $140\,fb^{-1}$ *of* $\sqrt{s} = 13$ *TeV pp collisions*, *Eur. Phys. J. C* **85** (2025) 606 [arXiv:2402.05858] [INSPIRE].

[95] ATLAS collaboration, *Measurement of the* $t\bar{t}$ *production cross-section and lepton differential distributions in* $e\mu$ *dilepton events from pp collisions at* $\sqrt{s} = 13$ *TeV with the ATLAS detector*, *Eur. Phys. J. C* **80** (2020) 528 [arXiv:1910.08819] [INSPIRE].

[96] ATLAS collaboration, *Measurement of* $W^{\pm}$ *and Z-boson production cross sections in pp collisions at* $\sqrt{s} = 13$ *TeV with the ATLAS detector*, *Phys. Lett. B* **759** (2016) 601 [arXiv:1603.09222] [INSPIRE].

[97] ATLAS collaboration, *Measurement of* $W^{\pm}Z$ *production cross sections and gauge boson polarisation in pp collisions at* $\sqrt{s} = 13$ *TeV with the ATLAS detector*, *Eur. Phys. J. C* **79** (2019) 535 [arXiv:1902.05759] [INSPIRE].

[98] ATLAS collaboration, *Multi-boson simulation for 13 TeV ATLAS analyses*, ATL-PHYS-PUB-2016-002, CERN, Geneva, Switzerland (2016).

[99] M. Grazzini, S. Kallweit and D. Rathlev, $W\gamma$ *and* $Z\gamma$ *production at the LHC in NNLO QCD*, *JHEP* **07** (2015) 085 [arXiv:1504.01330] [INSPIRE].

[100] M. Cacciari and G.P. Salam, *Pileup subtraction using jet areas*, *Phys. Lett. B* **659** (2008) 119 [arXiv:0707.1378] [INSPIRE].

[101] W. Verkerke and D.P. Kirkby, *The RooFit toolkit for data modeling*, *eConf C* **0303241** (2003) MOLT007 [physics/0306116] [INSPIRE].

[102] ATLAS collaboration, *ATLAS b-jet identification performance and efficiency measurement with* $t\bar{t}$ *events in pp collisions at* $\sqrt{s} = 13$ *TeV*, *Eur. Phys. J. C* **79** (2019) 970 [arXiv:1907.05120] [INSPIRE].

JHEP08(2025)142

[103] ATLAS collaboration, *Studies of the muon momentum calibration and performance of the ATLAS detector with pp collisions at* $\sqrt{s} = 13$ *TeV*, *Eur. Phys. J. C* **83** (2023) 686 [arXiv:2212.07338] [INSPIRE].

[104] ATLAS collaboration, *Study of top-quark pair modelling and uncertainties using ATLAS measurements at* $\sqrt{s} = 13$ *TeV*, ATL-PHYS-PUB-2020-023, CERN, Geneva, Switzerland (2020).

[105] M. Grazzini et al., *NNLO QCD + NLO EW with Matrix+OpenLoops: precise predictions for vector-boson pair production*, *JHEP* **02** (2020) 087 [arXiv:1912.00068] [INSPIRE].

[106] M. Grazzini, S. Kallweit, M. Wiesemann and J.Y. Yook, W^+W^- *production at the LHC: NLO QCD corrections to the loop-induced gluon fusion channel*, *Phys. Lett. B* **804** (2020) 135399 [arXiv:2002.01877] [INSPIRE].

[107] T. Gehrmann et al., W^+W^- *production at hadron colliders in next to next to leading order QCD*, *Phys. Rev. Lett.* **113** (2014) 212001 [arXiv:1408.5243] [INSPIRE].

[108] M. Grazzini, S. Kallweit and M. Wiesemann, *Fully differential NNLO computations with MATRIX*, *Eur. Phys. J. C* **78** (2018) 537 [arXiv:1711.06631] [INSPIRE].

[109] A. von Manteuffel and L. Tancredi, *The two-loop helicity amplitudes for* $gg \to V_1V_2 \to 4$ leptons, *JHEP* **06** (2015) 197 [arXiv:1503.08835] [INSPIRE].

[110] T. Gehrmann, A. von Manteuffel and L. Tancredi, *The two-loop helicity amplitudes for* $q\overline{q}' \to V_1V_2 \to 4$ *leptons*, *JHEP* **09** (2015) 128 [arXiv:1503.04812] [INSPIRE].

[111] F. Buccioni et al., *OpenLoops 2*, *Eur. Phys. J. C* **79** (2019) 866 [arXiv:1907.13071] [INSPIRE].

[112] F. Buccioni, S. Pozzorini and M. Zoller, *On-the-fly reduction of open loops*, *Eur. Phys. J. C* **78** (2018) 70 [arXiv:1710.11452] [INSPIRE].

[113] S. Catani et al., *Vector boson production at hadron colliders: hard-collinear coefficients at the NNLO*, *Eur. Phys. J. C* **72** (2012) 2195 [arXiv:1209.0158] [INSPIRE].

[114] S. Catani and M. Grazzini, *An NNLO subtraction formalism in hadron collisions and its application to Higgs boson production at the LHC*, *Phys. Rev. Lett.* **98** (2007) 222002 [hep-ph/0703012] [INSPIRE].

[115] NNPDF collaboration, *Parton distributions from high-precision collider data*, *Eur. Phys. J. C* **77** (2017) 663 [arXiv:1706.00428] [INSPIRE].

[116] NNPDF collaboration, *Illuminating the photon content of the proton within a global PDF analysis*, *SciPost Phys.* **5** (2018) 008 [arXiv:1712.07053] [INSPIRE].

[117] A. Gavardi, M.A. Lim, S. Alioli and F.J. Tackmann, *NNLO+PS* W^+W^- *production using jet veto resummation at NNLL'*, *JHEP* **12** (2023) 069 [arXiv:2308.11577] [INSPIRE].

[118] P. Skands, S. Carrazza and J. Rojo, *Tuning PYTHIA 8.1: the Monash 2013 tune*, *Eur. Phys. J. C* **74** (2014) 3024 [arXiv:1404.5630] [INSPIRE].

[119] PARTICLE DATA GROUP collaboration, *Review of particle physics*, *Phys. Rev. D* **110** (2024) 030001 [INSPIRE].

[120] T.-J. Hou et al., *New CTEQ global analysis of quantum chromodynamics with high-precision data from the LHC*, *Phys. Rev. D* **103** (2021) 014013 [arXiv:1912.10053] [INSPIRE].

[121] S. Bailey et al., *Parton distributions from LHC, HERA, Tevatron and fixed target data: MSHT20 PDFs*, *Eur. Phys. J. C* **81** (2021) 341 [arXiv:2012.04684] [INSPIRE].

[122] NNPDF collaboration, *The path to proton structure at 1% accuracy*, *Eur. Phys. J. C* **82** (2022) 428 [arXiv:2109.02653] [INSPIRE].

JHEP08(2025)142

[123] O. Mattelaer, *On the maximal use of Monte Carlo samples: re-weighting events at NLO accuracy*, *Eur. Phys. J. C* **76** (2016) 674 [arXiv:1607.00763] [INSPIRE].

[124] I. Brivio, Y. Jiang and M. Trott, *The SMEFTsim package, theory and tools*, *JHEP* **12** (2017) 070 [arXiv:1709.06492] [INSPIRE].

[125] I. Brivio, *SMEFTsim 3.0 — a practical guide*, *JHEP* **04** (2021) 073 [arXiv:2012.11343] [INSPIRE].

[126] L. Lönnblad, *Correcting the color dipole cascade model with fixed order matrix elements*, *JHEP* **05** (2002) 046 [hep-ph/0112284] [INSPIRE].

[127] L. Lönnblad and S. Prestel, *Matching tree-level matrix elements with interleaved showers*, *JHEP* **03** (2012) 019 [arXiv:1109.4829] [INSPIRE].

[128] C. Degrande et al., *Automated one-loop computations in the standard model effective field theory*, *Phys. Rev. D* **103** (2021) 096024 [arXiv:2008.11743] [INSPIRE].

[129] G.J. Feldman and R.D. Cousins, *A unified approach to the classical statistical analysis of small signals*, *Phys. Rev. D* **57** (1998) 3873 [physics/9711021] [INSPIRE].

[130] S.S. Wilks, *The large-sample distribution of the likelihood ratio for testing composite hypotheses*, *Annals Math. Statist.* **9** (1938) 60 [INSPIRE].

[131] A. Azatov, R. Contino, C.S. Machado and F. Riva, *Helicity selection rules and noninterference for BSM amplitudes*, *Phys. Rev. D* **95** (2017) 065014 [arXiv:1607.05236] [INSPIRE].

[132] A. Falkowski et al., *Anomalous triple gauge couplings in the effective field theory approach at the LHC*, *JHEP* **02** (2017) 115 [arXiv:1609.06312] [INSPIRE].

[133] I. Brivio et al., *Truncation, validity, uncertainties*, arXiv:2201.04974 [INSPIRE].

[134] K. Hagiwara, S. Ishihara, R. Szalapski and D. Zeppenfeld, *Low-energy effects of new interactions in the electroweak boson sector*, *Phys. Rev. D* **48** (1993) 2182 [INSPIRE].

[135] C. Degrande et al., *Effective field theory: a modern approach to anomalous couplings*, *Annals Phys.* **335** (2013) 21 [arXiv:1205.4231] [INSPIRE].

[136] CMS collaboration, *Measurement of the inclusive and differential WZ production cross sections, polarization angles, and triple gauge couplings in pp collisions at* $\sqrt{s} = 13$ *TeV*, *JHEP* **07** (2022) 032 [arXiv:2110.11231] [INSPIRE].

[137] CMS collaboration, *Measurement of* $W^{\pm}\gamma$ *differential cross sections in proton-proton collisions at* $\sqrt{s} = 13$ *TeV and effective field theory constraints*, *Phys. Rev. D* **105** (2022) 052003 [arXiv:2111.13948] [INSPIRE].

[138] CMS collaboration, *Measurement of the* $W\gamma$ *production cross section in proton-proton collisions at* $\sqrt{s} = 13$ *TeV and constraints on effective field theory coefficients*, *Phys. Rev. Lett.* **126** (2021) 252002 [arXiv:2102.02283] [INSPIRE].

[139] A. Azatov, J. Elias-Miró, Y. Reyimuaji and E. Venturini, *Novel measurements of anomalous triple gauge couplings for the LHC*, *JHEP* **10** (2017) 027 [arXiv:1707.08060] [INSPIRE].

[140] ATLAS collaboration, *Differential cross-section measurements for the electroweak production of dijets in association with a Z boson in proton–proton collisions at ATLAS*, *Eur. Phys. J. C* **81** (2021) 163 [arXiv:2006.15458] [INSPIRE].

[141] J. Ellis et al., *Top, Higgs, diboson and electroweak fit to the standard model effective field theory*, *JHEP* **04** (2021) 279 [arXiv:2012.02779] [INSPIRE].

JHEP08(2025)142

[142] ALEPH et al. collaborations, *Precision electroweak measurements on the Z resonance*, *Phys. Rept.* **427** (2006) 257 [hep-ex/0509008] [INSPIRE].

[143] ATLAS collaboration, *Measurements of WH and ZH production in the $H \to b\bar{b}$ decay channel in pp collisions at 13 TeV with the ATLAS detector*, *Eur. Phys. J. C* **81** (2021) 178 [arXiv:2007.02873] [INSPIRE].

[144] ATLAS collaboration, *Measurement of the associated production of a Higgs boson decaying into b-quarks with a vector boson at high transverse momentum in pp collisions at $\sqrt{s} = 13$ TeV with the ATLAS detector*, *Phys. Lett. B* **816** (2021) 136204 [arXiv:2008.02508] [INSPIRE].

[145] ATLAS collaboration, *ATLAS computing acknowledgements*, ATL-SOFT-PUB-2025-001, CERN, Geneva, Switzerland (2025).

JHEP08(2025)142

The ATLAS collaboration

G. Aad[102], B. Abbott[120], K. Abeling[55], N.J. Abicht[49], S.H. Abidi[29], A. Aboulhorma[35e], H. Abramowicz[152], H. Abreu[151], Y. Abulaiti[117], A.C. Abusleme Hoffman[137a], B.S. Acharya[69a,69b,n], C. Adam Bourdarios[4], L. Adamczyk[86a], L. Adamek[155], S.V. Addepalli[26], M.J. Addison[101], J. Adelman[115], A. Adiguzel[21c], T. Adye[134], A.A. Affolder[136], Y. Afik[36], M.N. Agaras[13], J. Agarwala[73a,73b], A. Aggarwal[100], C. Agheorghiesei[27c], F. Ahmadov[38,aa], W.S. Ahmed[104], S. Ahuja[95], X. Ai[62a], G. Aielli[76a,76b], M. Ait Tamlihat[35e], B. Aitbenchikh[35a], I. Aizenberg[169], M. Akbiyik[100], T.P.A. Åkesson[98], A.V. Akimov[37], D. Akiyama[168], N.N. Akolkar[24], K. Al Khoury[41], G.L. Alberghi[23b], J. Albert[165], P. Albicocco[53], G.L. Albouy[60], S. Alderweireldt[52], M. Aleksa[36], I.N. Aleksandrov[38], C. Alexa[27b], T. Alexopoulos[10], A. Alfonsi[114], F. Alfonsi[23b], M. Algren[56], M. Alhroob[120], B. Ali[132], H.M.J. Ali[91], S. Ali[149], S.W. Alibocus[92], M. Aliev[37], G. Alimonti[71a], W. Alkakhi[55], C. Allaire[66], B.M.M. Allbrooke[147], J.F. Allen[52], C.A. Allendes Flores[137f], P.P. Allport[20], A. Aloisio[72a,72b], F. Alonso[90], C. Alpigiani[139], M. Alvarez Estevez[99], A. Alvarez Fernandez[100], M.G. Alviggi[72a,72b], M. Aly[101], Y. Amaral Coutinho[83b], A. Ambler[104], C. Amelung[36], M. Amerl[101], C.G. Ames[109], D. Amidei[106], S.P. Amor Dos Santos[130a], K.R. Amos[163], V. Ananiev[125], C. Anastopoulos[140], T. Andeen[11], J.K. Anders[36], S.Y. Andrean[47a,47b], A. Andreazza[71a,71b], S. Angelidakis[9], A. Angerami[41,ad], A.V. Anisenkov[37], A. Annovi[74a], C. Antel[56], M.T. Anthony[140], E. Antipov[146], M. Antonelli[53], D.J.A. Antrim[17a], F. Anulli[75a], M. Aoki[84], T. Aoki[154], J.A. Aparisi Pozo[163], M.A. Aparo[147], L. Aperio Bella[48], C. Appelt[18], A. Apyan[26], N. Aranzabal[36], C. Arcangeletti[53], A.T.H. Arce[51], E. Arena[92], J-F. Arguin[108], S. Argyropoulos[54], J.-H. Arling[48], A.J. Armbruster[36], O. Arnaez[4], H. Arnold[114], Z.P. Arrubarrena Tame[109], G. Artoni[75a,75b], H. Asada[111], K. Asai[118], S. Asai[154], N.A. Asbah[61], J. Assahsah[35d], K. Assamagan[29], R. Astalos[28a], S. Atashi[160], R.J. Atkin[33a], M. Atkinson[162], N.B. Atlay[18], H. Atmani[62b], P.A. Atmasiddha[106], K. Augsten[132], S. Auricchio[72a,72b], A.D. Auriol[20], V.A. Austrup[101], G. Avolio[36], K. Axiotis[56], G. Azuelos[108,ai], D. Babal[28b], H. Bachacou[135], K. Bachas[153,q], A. Bachiu[34], F. Backman[47a,47b], A. Badea[61], P. Bagnaia[75a,75b], M. Bahmani[18], A.J. Bailey[163], V.R. Bailey[162], J.T. Baines[134], L. Baines[94], C. Bakalis[10], O.K. Baker[172], E. Bakos[15], D. Bakshi Gupta[8], R. Balasubramanian[114], E.M. Baldin[37], P. Balek[86a], E. Ballabene[23b,23a], F. Balli[135], L.M. Baltes[63a], W.K. Balunas[32], J. Balz[100], E. Banas[87], M. Bandieramonte[129], A. Bandyopadhyay[24], S. Bansal[24], L. Barak[152], M. Barakat[48], E.L. Barberio[105], D. Barberis[57b,57a], M. Barbero[102], G. Barbour[96], K.N. Barends[33a], T. Barillari[110], M-S. Barisits[36], T. Barklow[144], P. Baron[122], D.A. Baron Moreno[101], A. Baroncelli[62a], G. Barone[29], A.J. Barr[126], J.D. Barr[96], L. Barranco Navarro[47a,47b], F. Barreiro[99], J. Barreiro Guimarães da Costa[14a], U. Barron[152], M.G. Barros Teixeira[130a], S. Barsov[37], F. Bartels[63a], R. Bartoldus[144], A.E. Barton[91], P. Bartos[28a], A. Basan[100], M. Baselga[49], A. Bassalat[66,b], M.J. Basso[156a], C.R. Basson[101], R.L. Bates[59], S. Batlamous[35e], J.R. Batley[32], B. Batool[142], M. Battaglia[136], D. Battulga[18], M. Bauce[75a,75b], M. Bauer[36], P. Bauer[24], L.T. Bazzano Hurrell[30], J.B. Beacham[51], T. Beau[127], P.H. Beauchemin[158], F. Becherer[54], P. Bechtle[24], H.P. Beck[19,p],

JHEP08(2025)142

K. Becker[167], A.J. Beddall[82], V.A. Bednyakov[38], C.P. Bee[146], L.J. Beemster[15], T.A. Beermann[36], M. Begalli[83d], M. Begel[29], A. Behera[146], J.K. Behr[48], J.F. Beirer[55], F. Beisiegel[24], M. Belfkir[159], G. Bella[152], L. Bellagamba[23b], A. Bellerive[34], P. Bellos[20], K. Beloborodov[37], N.L. Belyaev[37], D. Benchekroun[35a], F. Bendebba[35a], Y. Benhammou[152], M. Benoit[29], J.R. Bensinger[26], S. Bentvelsen[114], L. Beresford[48], M. Beretta[53], E. Bergeaas Kuutmann[161], N. Berger[4], B. Bergmann[132], J. Beringer[17a], G. Bernardi[5], C. Bernius[144], F.U. Bernlochner[24], F. Bernon[36,102], T. Berry[95], P. Berta[133], A. Berthold[50], I.A. Bertram[91], S. Bethke[110], A. Betti[75a,75b], A.J. Bevan[94], M. Bhamjee[33c], S. Bhatta[146], D.S. Bhattacharya[166], P. Bhattarai[26], V.S. Bhopatkar[121], R. Bi[29,ak], R.M. Bianchi[129], G. Bianco[23b,23a], O. Biebel[109], R. Bielski[123], M. Biglietti[77a], T.R.V. Billoud[132], M. Bindi[55], A. Bingul[21b], C. Bini[75a,75b], A. Biondini[92], C.J. Birch-sykes[101], G.A. Bird[20,134], M. Birman[169], M. Biros[133], T. Bisanz[49], E. Bisceglie[43b,43a], J.P. Biswal[2], D. Biswas[142], A. Bitadze[101], K. Bjørke[125], I. Bloch[48], C. Blocker[26], A. Blue[59], U. Blumenschein[94], J. Blumenthal[100], G.J. Bobbink[114], V.S. Bobrovnikov[37], M. Boehler[54], B. Boehm[166], D. Bogavac[36], A.G. Bogdanchikov[37], C. Bohm[47a], V. Boisvert[95], P. Bokan[48], T. Bold[86a], M. Bomben[5], M. Bona[94], M. Boonekamp[135], C.D. Booth[95], A.G. Borbély[59], I.S. Bordulev[37], H.M. Borecka-Bielska[108], L.S. Borgna[96], G. Borissov[91], D. Bortoletto[126], D. Boscherini[23b], M. Bosman[13], J.D. Bossio Sola[36], K. Bouaouda[35a], N. Bouchhar[163], J. Boudreau[129], E.V. Bouhova-Thacker[91], D. Boumediene[40], R. Bouquet[5], A. Boveia[119], J. Boyd[36], D. Boye[29], I.R. Boyko[38], J. Bracinik[20], N. Brahimi[62d], G. Brandt[171], O. Brandt[32], F. Braren[48], B. Brau[103], J.E. Brau[123], R. Brener[169], L. Brenner[114], R. Brenner[161], S. Bressler[169], D. Britton[59], D. Britzger[110], I. Brock[24], R. Brock[107], G. Brooijmans[41], W.K. Brooks[137f], E. Brost[29], L.M. Brown[165,156a], L.E. Bruce[61], T.L. Bruckler[126], P.A. Bruckman de Renstrom[87], B. Brüers[48], D. Bruncko[28b,*], A. Bruni[23b], G. Bruni[23b], M. Bruschi[23b], N. Bruscino[75a,75b], T. Buanes[16], Q. Buat[139], D. Buchin[110], A.G. Buckley[59], M.K. Bugge[125], O. Bulekov[37], B.A. Bullard[144], S. Burdin[92], C.D. Burgard[49], A.M. Burger[40], B. Burghgrave[8], O. Burlayenko[54], J.T.P. Burr[32], C.D. Burton[11], J.C. Burzynski[143], E.L. Busch[41], V. Büscher[100], P.J. Bussey[59], J.M. Butler[25], C.M. Buttar[59], J.M. Butterworth[96], W. Buttinger[134], C.J. Buxo Vazquez[107], A.R. Buzykaev[37], G. Cabras[23b], S. Cabrera Urbán[163], L. Cadamuro[66], D. Caforio[58], H. Cai[129], Y. Cai[14a,14e], V.M.M. Cairo[36], O. Cakir[3a], N. Calace[36], P. Calafiura[17a], G. Calderini[127], P. Calfayan[68], G. Callea[59], L.P. Caloba[83b], D. Calvet[40], S. Calvet[40], T.P. Calvet[102], M. Calvetti[74a,74b], R. Camacho Toro[127], S. Camarda[36], D. Camarero Munoz[26], P. Camarri[76a,76b], M.T. Camerlingo[72a,72b], D. Cameron[125], C. Camincher[165], M. Campanelli[96], A. Camplani[42], V. Canale[72a,72b], A. Canesse[104], M. Cano Bret[80], J. Cantero[163], Y. Cao[162], F. Capocasa[26], M. Capua[43b,43a], A. Carbone[71a,71b], R. Cardarelli[76a], J.C.J. Cardenas[8], F. Cardillo[163], T. Carli[36], G. Carlino[72a], J.I. Carlotto[13], B.T. Carlson[129,r], E.M. Carlson[165,156a], L. Carminati[71a,71b], A. Carnelli[135], M. Carnesale[75a,75b], S. Caron[113], E. Carquin[137f], S. Carrá[71a], G. Carratta[23b,23a], F. Carrio Argos[33g], J.W.S. Carter[155], T.M. Carter[52], M.P. Casado[13,i], M. Caspar[48], E.G. Castiglia[172], F.L. Castillo[4], L. Castillo Garcia[13], V. Castillo Gimenez[163], N.F. Castro[130a,130e], A. Catinaccio[36], J.R. Catmore[125],

JHEP08(2025)142

V. Cavaliere[29], N. Cavalli[23b,23a], V. Cavasinni[74a,74b], Y.C. Cekmecelioglu[48], E. Celebi[21a], F. Celli[126], M.S. Centonze[70a,70b], K. Cerny[122], A.S. Cerqueira[83a], A. Cerri[147], L. Cerrito[76a,76b], F. Cerutti[17a], B. Cervato[142], A. Cervelli[23b], G. Cesarini[53], S.A. Cetin[82], Z. Chadi[35a], D. Chakraborty[115], M. Chala[130f], J. Chan[170], W.Y. Chan[154], J.D. Chapman[32], E. Chapon[135], B. Chargeishvili[150b], D.G. Charlton[20], T.P. Charman[94], M. Chatterjee[19], C. Chauhan[133], S. Chekanov[6], S.V. Chekulaev[156a], G.A. Chelkov[38,a], A. Chen[106], B. Chen[152], B. Chen[165], H. Chen[14c], H. Chen[29], J. Chen[62c], J. Chen[143], M. Chen[126], S. Chen[154], S.J. Chen[14c], X. Chen[62c], X. Chen[14b,ah], Y. Chen[62a], C.L. Cheng[170], H.C. Cheng[64a], S. Cheong[144], A. Cheplakov[38], E. Cheremushkina[48], E. Cherepanova[114], R. Cherkaoui El Moursli[35e], E. Cheu[7], K. Cheung[65], L. Chevalier[135], V. Chiarella[53], G. Chiarelli[74a], N. Chiedde[102], G. Chiodini[70a], A.S. Chisholm[20], A. Chitan[27b], M. Chitishvili[163], M.V. Chizhov[38,s], K. Choi[11], A.R. Chomont[75a,75b], Y. Chou[103], E.Y.S. Chow[114], T. Chowdhury[33g], K.L. Chu[169], M.C. Chu[64a], X. Chu[14a,14e], J. Chudoba[131], J.J. Chwastowski[87], D. Cieri[110], K.M. Ciesla[86a], V. Cindro[93], A. Ciocio[17a], F. Cirotto[72a,72b], Z.H. Citron[169,l], M. Citterio[71a], D.A. Ciubotaru[27b], B.M. Ciungu[155], A. Clark[56], P.J. Clark[52], J.M. Clavijo Columbie[48], S.E. Clawson[48], C. Clement[47a,47b], J. Clercx[48], L. Clissa[23b,23a], Y. Coadou[102], M. Cobal[69a,69c], A. Coccaro[57b], R.F. Coelho Barrue[130a], R. Coelho Lopes De Sa[103], S. Coelli[71a], H. Cohen[152], A.E.C. Coimbra[71a,71b], B. Cole[41], J. Collot[60], P. Conde Muiño[130a,130g], M.P. Connell[33c], S.H. Connell[33c], I.A. Connelly[59], E.I. Conroy[126], F. Conventi[72a,aj], H.G. Cooke[20], A.M. Cooper-Sarkar[126], A. Cordeiro Oudot Choi[127], F. Cormier[164], L.D. Corpe[40], M. Corradi[75a,75b], F. Corriveau[104,y], A. Cortes-Gonzalez[18], M.J. Costa[163], F. Costanza[4], D. Costanzo[140], B.M. Cote[119], G. Cowan[95], K. Cranmer[170], D. Cremonini[23b,23a], S. Crépé-Renaudin[60], F. Crescioli[127], M. Cristinziani[142], M. Cristoforetti[78a,78b], V. Croft[114], J.E. Crosby[121], G. Crosetti[43b,43a], A. Cueto[99], T. Cuhadar Donszelmann[160], H. Cui[14a,14e], Z. Cui[7], W.R. Cunningham[59], F. Curcio[43b,43a], P. Czodrowski[36], M.M. Czurylo[63b], M.J. Da Cunha Sargedas De Sousa[62a], J.V. Da Fonseca Pinto[83b], C. Da Via[101], W. Dabrowski[86a], T. Dado[49], S. Dahbi[33g], T. Dai[106], C. Dallapiccola[103], M. Dam[42], G. D'amen[29], V. D'Amico[109], J. Damp[100], J.R. Dandoy[128], M.F. Daneri[30], M. Danninger[143], V. Dao[36], G. Darbo[57b], S. Darmora[6], S.J. Das[29,ak], S. D'Auria[71a,71b], C. David[156b], T. Davidek[133], B. Davis-Purcell[34], I. Dawson[94], H.A. Day-hall[132], K. De[8], R. De Asmundis[72a], N. De Biase[48], S. De Castro[23b,23a], N. De Groot[113], P. de Jong[114], H. De la Torre[107], A. De Maria[14c], A. De Salvo[75a], U. De Sanctis[76a,76b], A. De Santo[147], J.B. De Vivie De Regie[60], D.V. Dedovich[38], J. Degens[114], A.M. Deiana[44], F. Del Corso[23b,23a], J. Del Peso[99], F. Del Rio[63a], F. Deliot[135], C.M. Delitzsch[49], M. Della Pietra[72a,72b], D. Della Volpe[56], A. Dell'Acqua[36], L. Dell'Asta[71a,71b], M. Delmastro[4], P.A. Delsart[60], S. Demers[172], M. Demichev[38], S.P. Denisov[37], L. D'Eramo[40], D. Derendarz[87], F. Derue[127], P. Dervan[92], K. Desch[24], C. Deutsch[24], F.A. Di Bello[57b,57a], A. Di Ciaccio[76a,76b], L. Di Ciaccio[4], A. Di Domenico[75a,75b], C. Di Donato[72a,72b], A. Di Girolamo[36], G. Di Gregorio[5], A. Di Luca[78a,78b], B. Di Micco[77a,77b], R. Di Nardo[77a,77b], C. Diaconu[102], F.A. Dias[114], T. Dias Do Vale[143], M.A. Diaz[137a,137b], F.G. Diaz Capriles[24], M. Didenko[163], E.B. Diehl[106], L. Diehl[54],

JHEP08(2025)142

S. Díez Cornell[48], C. Diez Pardos[142], C. Dimitriadi[24,161], A. Dimitrievska[17a], J. Dingfelder[24], I-M. Dinu[27b], S.J. Dittmeier[63b], F. Dittus[36], F. Djama[102], T. Djobava[150b], J.I. Djuvsland[16], C. Doglioni[101,98], J. Dolejsi[133], Z. Dolezal[133], M. Donadelli[83c], B. Dong[107], J. Donini[40], A. D'Onofrio[77a,77b], M. D'Onofrio[92], J. Dopke[134], A. Doria[72a], N. Dos Santos Fernandes[130a], M.T. Dova[90], A.T. Doyle[59], M.A. Draguet[126], E. Dreyer[169], I. Drivas-koulouris[10], A.S. Drobac[158], M. Drozdova[56], D. Du[62a], T.A. du Pree[114], F. Dubinin[37], M. Dubovsky[28a], E. Duchovni[169], G. Duckeck[109], O.A. Ducu[27b], D. Duda[52], A. Dudarev[36], E.R. Duden[26], M. D'uffizi[101], L. Duflot[66], M. Dührssen[36], C. Dülsen[171], A.E. Dumitriu[27b], M. Dunford[63a], S. Dungs[49], K. Dunne[47a,47b], A. Duperrin[102], H. Duran Yildiz[3a], M. Düren[58], A. Durglishvili[150b], B.L. Dwyer[115], G.I. Dyckes[17a], M. Dyndal[86a], S. Dysch[101], B.S. Dziedzic[87], Z.O. Earnshaw[147], G.H. Eberwein[126], B. Eckerova[28a], S. Eggebrecht[55], M.G. Eggleston[51], E. Egidio Purcino De Souza[127], L.F. Ehrke[56], G. Eigen[16], K. Einsweiler[17a], T. Ekelof[161], P.A. Ekman[98], S. El Farkh[35b], Y. El Ghazali[35b], H. El Jarrari[35e,149], A. El Moussaouy[35a], V. Ellajosyula[161], M. Ellert[161], F. Ellinghaus[171], A.A. Elliot[94], N. Ellis[36], J. Elmsheuser[29], M. Elsing[36], D. Emeliyanov[134], Y. Enari[154], I. Ene[17a], S. Epari[13], J. Erdmann[49], P.A. Erland[87], M. Errenst[171], M. Escalier[66], C. Escobar[163], E. Etzion[152], G. Evans[130a,130b], H. Evans[68], L.S. Evans[95], M.O. Evans[147], A. Ezhilov[37], S. Ezzarqtouni[35a], F. Fabbri[59], L. Fabbri[23b,23a], G. Facini[96], V. Fadeyev[136], R.M. Fakhrutdinov[37], S. Falciano[75a], L.F. Falda Ulhoa Coelho[36], P.J. Falke[24], J. Faltova[133], C. Fan[162], Y. Fan[14a], Y. Fang[14a,14e], M. Fanti[71a,71b], M. Faraj[69a,69b], Z. Farazpay[97], A. Farbin[8], A. Farilla[77a], T. Farooque[107], S.M. Farrington[52], F. Fassi[35e], D. Fassouliotis[9], M. Faucci Giannelli[76a,76b], W.J. Fawcett[32], L. Fayard[66], P. Federic[133], P. Federicova[131], O.L. Fedin[37,a], G. Fedotov[37], M. Feickert[170], L. Feligioni[102], D.E. Fellers[123], C. Feng[62b], M. Feng[14b], Z. Feng[114], M.J. Fenton[160], A.B. Fenyuk[37], L. Ferencz[48], R.A.M. Ferguson[91], S.I. Fernandez Luengo[137f], M.J.V. Fernoux[102], J. Ferrando[48], A. Ferrari[161], P. Ferrari[114,113], R. Ferrari[73a], D. Ferrere[56], C. Ferretti[106], F. Fiedler[100], A. Filipčič[93], E.K. Filmer[1], F. Filthaut[113], M.C.N. Fiolhais[130a,130c,c], L. Fiorini[163], W.C. Fisher[107], T. Fitschen[101], P.M. Fitzhugh[135], I. Fleck[142], P. Fleischmann[106], T. Flick[171], L. Flores[128], M. Flores[33d,ae], L.R. Flores Castillo[64a], L. Flores Sanz De Acedo[36], F.M. Follega[78a,78b], N. Fomin[16], J.H. Foo[155], B.C. Forland[68], A. Formica[135], A.C. Forti[101], E. Fortin[36], A.W. Fortman[61], M.G. Foti[17a], L. Fountas[9,j], D. Fournier[66], H. Fox[91], P. Francavilla[74a,74b], S. Francescato[61], S. Franchellucci[56], M. Franchini[23b,23a], S. Franchino[63a], D. Francis[36], L. Franco[113], L. Franconi[48], M. Franklin[61], G. Frattari[26], A.C. Freegard[94], W.S. Freund[83b], Y.Y. Frid[152], N. Fritzsche[50], A. Froch[54], D. Froidevaux[36], J.A. Frost[126], Y. Fu[62a], M. Fujimoto[118], E. Fullana Torregrosa[163,*], K.Y. Fung[64a], E. Furtado De Simas Filho[83b], M. Furukawa[154], J. Fuster[163], A. Gabrielli[23b,23a], A. Gabrielli[155], P. Gadow[48], G. Gagliardi[57b,57a], L.G. Gagnon[17a], E.J. Gallas[126], B.J. Gallop[134], K.K. Gan[119], S. Ganguly[154], J. Gao[62a], Y. Gao[52], F.M. Garay Walls[137a,137b], B. Garcia[29], C. García[163], A. Garcia Alonso[114], A.G. Garcia Caffaro[172], J.E. García Navarro[163], M. Garcia-Sciveres[17a], G.L. Gardner[128], R.W. Gardner[39], N. Garelli[158], D. Garg[80], R.B. Garg[144,o], J.M. Gargan[52], C.A. Garner[155], S.J. Gasiorowski[139], P. Gaspar[83b], G. Gaudio[73a], V. Gautam[13], P. Gauzzi[75a,75b],

JHEP08(2025)142

I.L. Gavrilenko[37], A. Gavrilyuk[37], C. Gay[164], G. Gaycken[48], E.N. Gazis[10], A.A. Geanta[27b], C.M. Gee[136], C. Gemme[57b], M.H. Genest[60], S. Gentile[75a,75b], S. George[95], W.F. George[20], T. Geralis[46], P. Gessinger-Befurt[36], M.E. Geyik[171], M. Ghneimat[142], K. Ghorbanian[94], A. Ghosal[142], A. Ghosh[160], A. Ghosh[7], B. Giacobbe[23b], S. Giagu[75a,75b], P. Giannetti[74a], A. Giannini[62a], S.M. Gibson[95], M. Gignac[136], D.T. Gil[86b], A.K. Gilbert[86a], B.J. Gilbert[41], D. Gillberg[34], G. Gilles[114], N.E.K. Gillwald[48], L. Ginabat[127], D.M. Gingrich[2,ai], M.P. Giordani[69a,69c], P.F. Giraud[135], G. Giugliarelli[69a,69c], D. Giugni[71a], F. Giuli[36], I. Gkialas[9,j], L.K. Gladilin[37], C. Glasman[99], G.R. Gledhill[123], M. Glisic[123], I. Gnesi[43b,f], Y. Go[29,ak], M. Goblirsch-Kolb[36], B. Gocke[49], D. Godin[108], B. Gokturk[21a], S. Goldfarb[105], T. Golling[56], M.G.D. Gololo[33g], D. Golubkov[37], J.P. Gombas[107], A. Gomes[130a,130b], G. Gomes Da Silva[142], A.J. Gomez Delegido[163], R. Gonçalo[130a,130c], G. Gonella[123], L. Gonella[20], A. Gongadze[38], F. Gonnella[20], J.L. Gonski[41], R.Y. González Andana[52], S. González de la Hoz[163], S. Gonzalez Fernandez[13], R. Gonzalez Lopez[92], C. Gonzalez Renteria[17a], R. Gonzalez Suarez[161], S. Gonzalez-Sevilla[56], G.R. Gonzalvo Rodriguez[163], L. Goossens[36], P.A. Gorbounov[37], B. Gorini[36], E. Gorini[70a,70b], A. Gorišek[93], T.C. Gosart[128], A.T. Goshaw[51], M.I. Gostkin[38], S. Goswami[121], C.A. Gottardo[36], M. Gouighri[35b], V. Goumarre[48], A.G. Goussiou[139], N. Govender[33c], I. Grabowska-Bold[86a], K. Graham[34], E. Gramstad[125], S. Grancagnolo[70a,70b], M. Grandi[147], P.M. Gravila[27f], F.G. Gravili[70a,70b], H.M. Gray[17a], M. Greco[70a,70b], C. Grefe[24], I.M. Gregor[48], P. Grenier[144], C. Grieco[13], A.A. Grillo[136], K. Grimm[31], S. Grinstein[13,u], J.-F. Grivaz[66], E. Gross[169], J. Grosse-Knetter[55], C. Grud[106], J.C. Grundy[126], L. Guan[106], W. Guan[29], C. Gubbels[164], J.G.R. Guerrero Rojas[163], G. Guerrieri[69a,69b], F. Guescini[110], R. Gugel[100], J.A.M. Guhit[106], A. Guida[18], T. Guillemin[4], E. Guilloton[167,134], S. Guindon[36], F. Guo[14a,14e], J. Guo[62c], L. Guo[48], Y. Guo[106], R. Gupta[48], S. Gurbuz[24], S.S. Gurdasani[54], G. Gustavino[36], M. Guth[56], P. Gutierrez[120], L.F. Gutierrez Zagazeta[128], C. Gutschow[96], C. Gwenlan[126], C.B. Gwilliam[92], E.S. Haaland[125], A. Haas[117], M. Habedank[48], C. Haber[17a], H.K. Hadavand[8], A. Hadef[100], S. Hadzic[110], J.J. Hahn[142], E.H. Haines[96], M. Haleem[166], J. Haley[121], J.J. Hall[140], G.D. Hallewell[102], L. Halser[19], K. Hamano[165], H. Hamdaoui[35e], M. Hamer[24], G.N. Hamity[52], E.J. Hampshire[95], J. Han[62b], K. Han[62a], L. Han[14c], L. Han[62a], S. Han[17a], Y.F. Han[155], K. Hanagaki[84], M. Hance[136], D.A. Hangal[41,ad], H. Hanif[143], M.D. Hank[128], R. Hankache[101], J.B. Hansen[42], J.D. Hansen[42], P.H. Hansen[42], K. Hara[157], D. Harada[56], T. Harenberg[171], S. Harkusha[37], M.L. Harris[103], Y.T. Harris[126], J. Harrison[13], N.M. Harrison[119], P.F. Harrison[167], N.M. Hartman[110], N.M. Hartmann[109], Y. Hasegawa[141], A. Hasib[52], S. Haug[19], R. Hauser[107], C.M. Hawkes[20], R.J. Hawkings[36], Y. Hayashi[154], S. Hayashida[111], D. Hayden[107], C. Hayes[106], R.L. Hayes[114], C.P. Hays[126], J.M. Hays[94], H.S. Hayward[92], F. He[62a], M. He[14a,14e], Y. He[138], Y. He[127], N.B. Heatley[94], V. Hedberg[98], A.L. Heggelund[125], N.D. Hehir[94,*], C. Heidegger[54], K.K. Heidegger[54], W.D. Heidorn[81], J. Heilman[34], S. Heim[48], T. Heim[17a], B. Heinemann[48,af], J.G. Heinlein[128], J.J. Heinrich[123], L. Heinrich[110,ag], J. Hejbal[131], L. Helary[48], A. Held[170], S. Hellesund[16], C.M. Helling[164], S. Hellman[47a,47b], C. Helsens[36], R.C.W. Henderson[91], L. Henkelmann[32],

JHEP08(2025)142

A.M. Henriques Correia[36], H. Herde[98], Y. Hernández Jiménez[146], L.M. Herrmann[24], T. Herrmann[50], G. Herten[54], R. Hertenberger[109], L. Hervas[36], M.E. Hesping[100], N.P. Hessey[156a], H. Hibi[85], S.J. Hillier[20], J.R. Hinds[107], F. Hinterkeuser[24], M. Hirose[124], S. Hirose[157], D. Hirschbuehl[171], T.G. Hitchings[101], B. Hiti[93], J. Hobbs[146], R. Hobincu[27e], N. Hod[169], M.C. Hodgkinson[140], B.H. Hodkinson[32], A. Hoecker[36], J. Hofer[48], T. Holm[24], M. Holzbock[110], L.B.A.H. Hommels[32], B.P. Honan[101], J. Hong[62c], T.M. Hong[129], B.H. Hooberman[162], W.H. Hopkins[6], Y. Horii[111], S. Hou[149], A.S. Howard[93], J. Howarth[59], J. Hoya[6], M. Hrabovsky[122], A. Hrynevich[48], T. Hryn'ova[4], P.J. Hsu[65], S.-C. Hsu[139], Q. Hu[41], Y.F. Hu[14a,14e], S. Huang[64b], X. Huang[14c], Y. Huang[62a], Y. Huang[14a], Z. Huang[101], Z. Hubacek[132], M. Huebner[24], F. Huegging[24], T.B. Huffman[126], C.A. Hugli[48], M. Huhtinen[36], S.K. Huiberts[16], R. Hulsken[104], N. Huseynov[12], J. Huston[107], J. Huth[61], R. Hyneman[144], G. Iacobucci[56], G. Iakovidis[29], I. Ibragimov[142], L. Iconomidou-Fayard[66], P. Iengo[72a,72b], R. Iguchi[154], T. Iizawa[84], Y. Ikegami[84], N. Ilic[155], H. Imam[35a], M. Ince Lezki[56], T. Ingebretsen Carlson[47a,47b], G. Introzzi[73a,73b], M. Iodice[77a], V. Ippolito[75a,75b], R.K. Irwin[92], M. Ishino[154], W. Islam[170], C. Issever[18,48], S. Istin[21a,am], H. Ito[168], J.M. Iturbe Ponce[64a], R. Iuppa[78a,78b], A. Ivina[169], J.M. Izen[45], V. Izzo[72a], P. Jacka[131,132], P. Jackson[1], R.M. Jacobs[48], B.P. Jaeger[143], C.S. Jagfeld[109], P. Jain[54], G. Jäkel[171], K. Jakobs[54], T. Jakoubek[169], J. Jamieson[59], K.W. Janas[86a], A.E. Jaspan[92], M. Javurkova[103], F. Jeanneau[135], L. Jeanty[123], J. Jejelava[150a,ab], P. Jenni[54,g], C.E. Jessiman[34], S. Jézéquel[4], C. Jia[62b], J. Jia[146], X. Jia[61], X. Jia[14a,14e], Z. Jia[14c], Y. Jiang[62a], S. Jiggins[48], J. Jimenez Pena[13], S. Jin[14c], A. Jinaru[27b], O. Jinnouchi[138], P. Johansson[140], K.A. Johns[7], J.W. Johnson[136], D.M. Jones[32], E. Jones[48], P. Jones[32], R.W.L. Jones[91], T.J. Jones[92], R. Joshi[119], J. Jovicevic[15], X. Ju[17a], J.J. Junggeburth[36], T. Junkermann[63a], A. Juste Rozas[13,u], M.K. Juzek[87], S. Kabana[137e], A. Kaczmarska[87], M. Kado[110], H. Kagan[119], M. Kagan[144], A. Kahn[41], A. Kahn[128], C. Kahra[100], T. Kaji[168], E. Kajomovitz[151], N. Kakati[169], I. Kalaitzidou[54], C.W. Kalderon[29], A. Kamenshchikov[155], S. Kanayama[138], N.J. Kang[136], D. Kar[33g], K. Karava[126], M.J. Kareem[156b], E. Karentzos[54], I. Karkanias[153], O. Karkout[114], S.N. Karpov[38], Z.M. Karpova[38], V. Kartvelishvili[91], A.N. Karyukhin[37], E. Kasimi[153], J. Katzy[48], S. Kaur[34], K. Kawade[141], T. Kawamoto[135], E.F. Kay[36], F.I. Kaya[158], S. Kazakos[107], V.F. Kazanin[37], Y. Ke[146], J.M. Keaveney[33a], R. Keeler[165], G.V. Kehris[61], J.S. Keller[34], A.S. Kelly[96], J.J. Kempster[147], K.E. Kennedy[41], P.D. Kennedy[100], O. Kepka[131], B.P. Kerridge[167], S. Kersten[171], B.P. Kerševan[93], S. Keshri[66], L. Keszeghova[28a], S. Ketabchi Haghighat[155], M. Khandoga[127], A. Khanov[121], A.G. Kharlamov[37], T. Kharlamova[37], E.E. Khoda[139], T.J. Khoo[18], G. Khoriauli[166], J. Khubua[150b,*], Y.A.R. Khwaira[66], M. Kiehn[36], A. Kilgallon[123], D.W. Kim[47a,47b], Y.K. Kim[39], N. Kimura[96], A. Kirchhoff[55], C. Kirfel[24], F. Kirfel[24], J. Kirk[134], A.E. Kiryunin[110], C. Kitsaki[10], O. Kivernyk[24], M. Klassen[63a], C. Klein[34], L. Klein[166], M.H. Klein[106], M. Klein[92,*], S.B. Klein[56], U. Klein[92], P. Klimek[36], A. Klimentov[29], T. Klioutchnikova[36], P. Kluit[114], S. Kluth[110], E. Kneringer[79], T.M. Knight[155], A. Knue[54], R. Kobayashi[88], M. Kobel[50], S.F. Koch[126], M. Kocian[144], P. Kodyš[133], D.M. Koeck[123], P.T. Koenig[24], T. Koffas[34], M. Kolb[135], I. Koletsou[4], T. Komarek[122],

JHEP08(2025)142

K. Köneke[54], A.X.Y. Kong[1], T. Kono[118], N. Konstantinidis[96], B. Konya[98], R. Kopeliansky[68], S. Koperny[86a], K. Korcyl[87], K. Kordas[153,e], G. Koren[152], A. Korn[96], S. Korn[55], I. Korolkov[13], N. Korotkova[37], B. Kortman[114], O. Kortner[110], S. Kortner[110], W.H. Kostecka[115], V.V. Kostyukhin[142], A. Kotsokechagia[135], A. Kotwal[51], A. Koulouris[36], A. Kourkoumeli-Charalampidi[73a,73b], C. Kourkoumelis[9], E. Kourlitis[6], O. Kovanda[147], R. Kowalewski[165], W. Kozanecki[135], A.S. Kozhin[37], V.A. Kramarenko[37], G. Kramberger[93], P. Kramer[100], M.W. Krasny[127], A. Krasznahorkay[36], J.W. Kraus[171], J.A. Kremer[100], T. Kresse[50], J. Kretzschmar[92], K. Kreul[18], P. Krieger[155], S. Krishnamurthy[103], M. Krivos[133], K. Krizka[20], K. Kroeninger[49], H. Kroha[110], J. Kroll[131], J. Kroll[128], K.S. Krowpman[107], U. Kruchonak[38], H. Krüger[24], N. Krumnack[81], M.C. Kruse[51], J.A. Krzysiak[87], O. Kuchinskaia[37], S. Kuday[3a], S. Kuehn[36], R. Kuesters[54], T. Kuhl[48], V. Kukhtin[38], Y. Kulchitsky[37,a], S. Kuleshov[137d,137b], M. Kumar[33g], N. Kumari[102], A. Kupco[131], T. Kupfer[49], A. Kupich[37], O. Kuprash[54], H. Kurashige[85], L.L. Kurchaninov[156a], O. Kurdysh[66], Y.A. Kurochkin[37], A. Kurova[37], M. Kuze[138], A.K. Kvam[103], J. Kvita[122], T. Kwan[104], N.G. Kyriacou[106], L.A.O. Laatu[102], C. Lacasta[163], F. Lacava[75a,75b], H. Lacker[18], D. Lacour[127], N.N. Lad[96], E. Ladygin[38], B. Laforge[127], T. Lagouri[137e], S. Lai[55], I.K. Lakomiec[86a], N. Lalloue[60], J.E. Lambert[165], S. Lammers[68], W. Lampl[7], C. Lampoudis[153,e], A.N. Lancaster[115], E. Lançon[29], U. Landgraf[54], M.P.J. Landon[94], V.S. Lang[54], R.J. Langenberg[103], O.K.B. Langrekken[125], A.J. Lankford[160], F. Lanni[36], K. Lantzsch[24], A. Lanza[73a], A. Lapertosa[57b,57a], J.F. Laporte[135], T. Lari[71a], F. Lasagni Manghi[23b], M. Lassnig[36], V. Latonova[131], A. Laudrain[100], A. Laurier[151], S.D. Lawlor[95], Z. Lawrence[101], M. Lazzaroni[71a,71b], B. Le[101], E.M. Le Boulicaut[51], B. Leban[93], A. Lebedev[81], M. LeBlanc[36], F. Ledroit-Guillon[60], A.C.A. Lee[96], S.C. Lee[149], S. Lee[47a,47b], T.F. Lee[92], L.L. Leeuw[33c], H.P. Lefebvre[95], M. Lefebvre[165], C. Leggett[17a], G. Lehmann Miotto[36], M. Leigh[56], W.A. Leight[103], W. Leinonen[113], A. Leisos[153,t], M.A.L. Leite[83c], C.E. Leitgeb[48], R. Leitner[133], K.J.C. Leney[44], T. Lenz[24], S. Leone[74a], C. Leonidopoulos[52], A. Leopold[145], C. Leroy[108], R. Les[107], C.G. Lester[32], M. Levchenko[37], J. Levêque[4], D. Levin[106], L.J. Levinson[169], M.P. Lewicki[87], D.J. Lewis[4], A. Li[5], B. Li[62b], C. Li[62a], C-Q. Li[62c], H. Li[62a], H. Li[62b], H. Li[14c], H. Li[62b], K. Li[139], L. Li[62c], M. Li[14a,14e], Q.Y. Li[62a], S. Li[14a,14e], S. Li[62d,62c,d], T. Li[5], X. Li[104], Z. Li[126], Z. Li[104], Z. Li[92], Z. Li[14a,14e], Z. Liang[14a], M. Liberatore[48], B. Liberti[76a], K. Lie[64c], J. Lieber Marin[83b], H. Lien[68], K. Lin[107], R.E. Lindley[7], J.H. Lindon[2], A. Linss[48], E. Lipeles[128], A. Lipniacka[16], A. Lister[164], J.D. Little[4], B. Liu[14a], B.X. Liu[143], D. Liu[62d,62c], J.B. Liu[62a], J.K.K. Liu[32], K. Liu[62d,62c], M. Liu[62a], M.Y. Liu[62a], P. Liu[14a], Q. Liu[62d,139,62c], X. Liu[62a], Y. Liu[14d,14e], Y.L. Liu[106], Y.W. Liu[62a], J. Llorente Merino[143], S.L. Lloyd[94], E.M. Lobodzinska[48], P. Loch[7], S. Loffredo[76a,76b], T. Lohse[18], K. Lohwasser[140], E. Loiacono[48], M. Lokajicek[131,*], J.D. Lomas[20], J.D. Long[162], I. Longarini[160], L. Longo[70a,70b], R. Longo[162], I. Lopez Paz[67], A. Lopez Solis[48], J. Lorenz[109], N. Lorenzo Martinez[4], A.M. Lory[109], G. Löschcke Centeno[147], O. Loseva[37], X. Lou[47a,47b], X. Lou[14a,14e], A. Lounis[66], J. Love[6], P.A. Love[91], G. Lu[14a,14e], M. Lu[80], S. Lu[128], Y.J. Lu[65], H.J. Lubatti[139], C. Luci[75a,75b], F.L. Lucio Alves[14c], A. Lucotte[60], F. Luehring[68], I. Luise[146],

JHEP08(2025)142

O. Lukianchuk[66], O. Lundberg[145], B. Lund-Jensen[145,*], N.A. Luongo[123], M.S. Lutz[152], D. Lynn[29], H. Lyons[92], R. Lysak[131], E. Lytken[98], V. Lyubushkin[38], T. Lyubushkina[38], M.M. Lyukova[146], H. Ma[29], K. Ma[62a], L.L. Ma[62b], Y. Ma[121], D.M. Mac Donell[165], G. Maccarrone[53], J.C. MacDonald[100], R. Madar[40], J. Maeda[85], T. Maeno[29], M. Maerker[50], H. Maguire[140], V. Maiboroda[135], A. Maio[130a,130b,130d], K. Maj[86a], O. Majersky[48], S. Majewski[123], N. Makovec[66], V. Maksimovic[15], B. Malaescu[127], Pa. Malecki[87], V.P. Maleev[37], F. Malek[60], M. Mali[93], D. Malito[95], U. Mallik[80,*], S. Maltezos[10], S. Malyukov[38], J. Mamuzic[13], G. Mancini[53], G. Manco[73a,73b], J.P. Mandalia[94], I. Mandić[93], L. Manhaes de Andrade Filho[83a], I.M. Maniatis[169], J. Manjarres Ramos[102,ac], D.C. Mankad[169], A. Mann[109], B. Mansoulie[135], S. Manzoni[36], A. Marantis[153,t], G. Marchiori[5], M. Marcisovsky[131], C. Marcon[71a], M. Marinescu[20], M. Marjanovic[120], E.J. Marshall[91], Z. Marshall[17a], S. Marti-Garcia[163], T.A. Martin[167], V.J. Martin[52], B. Martin dit Latour[16], L. Martinelli[75a,75b], M. Martinez[13,u], P. Martinez Agullo[163], V.I. Martinez Outschoorn[103], P. Martinez Suarez[13], S. Martin-Haugh[134], V.S. Martoiu[27b], A.C. Martyniuk[96], A. Marzin[36], D. Mascione[78a,78b], L. Masetti[100], T. Mashimo[154], J. Masik[101], A.L. Maslennikov[37], L. Massa[23b], P. Massarotti[72a,72b], P. Mastrandrea[74a,74b], A. Mastroberardino[43b,43a], T. Masubuchi[154], T. Mathisen[161], J. Matousek[133], N. Matsuzawa[154], J. Maurer[27b], B. Maček[93], D.A. Maximov[37], R. Mazini[149], I. Maznas[153], M. Mazza[107], S.M. Mazza[136], E. Mazzeo[71a,71b], C. Mc Ginn[29], J.P. Mc Gowan[104], S.P. Mc Kee[106], E.F. McDonald[105], A.E. McDougall[114], J.A. Mcfayden[147], R.P. McGovern[128], G. Mchedlidze[150b], R.P. Mckenzie[33g], T.C. Mclachlan[48], D.J. Mclaughlin[96], K.D. McLean[165], S.J. McMahon[134], P.C. McNamara[105], C.M. Mcpartland[92], R.A. McPherson[165,y], S. Mehlhase[109], A. Mehta[92], D. Melini[151], B.R. Mellado Garcia[33g], A.H. Melo[55], F. Meloni[48], A.M. Mendes Jacques Da Costa[101], H.Y. Meng[155], L. Meng[91], S. Menke[110], M. Mentink[36], E. Meoni[43b,43a], C. Merlassino[126], L. Merola[72a,72b], C. Meroni[71a,71b], G. Merz[106], O. Meshkov[37], J. Metcalfe[6], A.S. Mete[6], C. Meyer[68], J-P. Meyer[135], R.P. Middleton[134], L. Mijović[52], G. Mikenberg[169], M. Mikestikova[131], M. Mikuž[93], H. Mildner[100], A. Milic[36], C.D. Milke[44], D.W. Miller[39], L.S. Miller[34], A. Milov[169], D.A. Milstead[47a,47b], T. Min[14c], A.A. Minaenko[37], I.A. Minashvili[150b], L. Mince[59], A.I. Mincer[117], B. Mindur[86a], M. Mineev[38], Y. Mino[88], L.M. Mir[13], M. Miralles Lopez[163], M. Mironova[17a], A. Mishima[154], M.C. Missio[113], T. Mitani[168], A. Mitra[167], V.A. Mitsou[163], O. Miu[155], P.S. Miyagawa[94], Y. Miyazaki[89], A. Mizukami[84], T. Mkrtchyan[63a], M. Mlinarevic[96], T. Mlinarevic[96], M. Mlynarikova[36], S. Mobius[19], K. Mochizuki[108], P. Moder[48], P. Mogg[109], A.F. Mohammed[14a,14e], S. Mohapatra[41], G. Mokgatitswane[33g], L. Moleri[169], B. Mondal[142], S. Mondal[132], K. Mönig[48], E. Monnier[102], L. Monsonis Romero[163], J. Montejo Berlingen[13,84], M. Montella[119], F. Montereali[77a,77b], F. Monticelli[90], S. Monzani[69a,69c], N. Morange[66], A.L. Moreira De Carvalho[130a], M. Moreno Llácer[163], C. Moreno Martinez[56], P. Morettini[57b], S. Morgenstern[36], M. Morii[61], M. Morinaga[154], A.K. Morley[36], F. Morodei[75a,75b], L. Morvaj[36], P. Moschovakos[36], B. Moser[36], M. Mosidze[150b], T. Moskalets[54], P. Moskvitina[113], J. Moss[31,m], E.J.W. Moyse[103], O. Mtintsilana[33g], S. Muanza[102], J. Mueller[129], D. Muenstermann[91], R. Müller[19], G.A. Mullier[161], A.J. Mullin[32], J.J. Mullin[128], D.P. Mungo[155], D. Munoz Perez[163],

JHEP08(2025)142

F.J. Munoz Sanchez[101], M. Murin[101], W.J. Murray[167,134], A. Murrone[71a,71b], J.M. Muse[120], M. Muškinja[17a], C. Mwewa[29], A.G. Myagkov[37,a], A.J. Myers[8], A.A. Myers[129], G. Myers[68], M. Myska[132], B.P. Nachman[17a], O. Nackenhorst[49], A. Nag[50], K. Nagai[126], K. Nagano[84], J.L. Nagle[29,ak], E. Nagy[102], A.M. Nairz[36], Y. Nakahama[84], K. Nakamura[84], K. Nakkalil[5], H. Nanjo[124], R. Narayan[44], E.A. Narayanan[112], I. Naryshkin[37], M. Naseri[34], S. Nasri[159], C. Nass[24], G. Navarro[22a], J. Navarro-Gonzalez[163], R. Nayak[152], A. Nayaz[18], P.Y. Nechaeva[37], F. Nechansky[48], L. Nedic[126], T.J. Neep[20], A. Negri[73a,73b], M. Negrini[23b], C. Nellist[114], C. Nelson[104], K. Nelson[106], S. Nemecek[131], M. Nessi[36,h], M.S. Neubauer[162], F. Neuhaus[100], J. Neundorf[48], R. Newhouse[164], P.R. Newman[20], C.W. Ng[129], Y.W.Y. Ng[48], B. Ngair[35e], H.D.N. Nguyen[108], R.B. Nickerson[126], R. Nicolaidou[135], J. Nielsen[136], M. Niemeyer[55], J. Niermann[55,36], N. Nikiforou[36], V. Nikolaenko[37,a], I. Nikolic-Audit[127], K. Nikolopoulos[20], P. Nilsson[29], I. Ninca[48], H.R. Nindhito[56], G. Ninio[152], A. Nisati[75a], N. Nishu[2], R. Nisius[110], J-E. Nitschke[50], E.K. Nkadimeng[33g], S.J. Noacco Rosende[90], T. Nobe[154], D.L. Noel[32], T. Nommensen[148], M.B. Norfolk[140], R.R.B. Norisam[96], B.J. Norman[34], J. Novak[93], T. Novak[48], L. Novotny[132], R. Novotny[112], L. Nozka[122], K. Ntekas[160], N.M.J. Nunes De Moura Junior[83b], E. Nurse[96], J. Ocariz[127], A. Ochi[85], I. Ochoa[130a], S. Oerdek[161], J.T. Offermann[39], A. Ogrodnik[133], A. Oh[101], C.C. Ohm[145], H. Oide[84], R. Oishi[154], M.L. Ojeda[48], Y. Okazaki[88], M.W. O'Keefe[92], Y. Okumura[154], L.F. Oleiro Seabra[130a], S.A. Olivares Pino[137d], D. Oliveira Damazio[29], D. Oliveira Goncalves[83a], J.L. Oliver[160], A. Olszewski[87], Ö.O. Öncel[54], D.C. O'Neil[143], A.P. O'Neill[19], A. Onofre[130a,130e], P.U.E. Onyisi[11], M.J. Oreglia[39], G.E. Orellana[90], D. Orestano[77a,77b], N. Orlando[13], R.S. Orr[155], V. O'Shea[59], L.M. Osojnak[128], R. Ospanov[62a], G. Otero y Garzon[30], H. Otono[89], P.S. Ott[63a], G.J. Ottino[17a], M. Ouchrif[35d], J. Ouellette[29], F. Ould-Saada[125], M. Owen[59], R.E. Owen[134], K.Y. Oyulmaz[21a], V.E. Ozcan[21a], N. Ozturk[8], S. Ozturk[82], H.A. Pacey[32], A. Pacheco Pages[13], C. Padilla Aranda[13], G. Padovano[75a,75b], S. Pagan Griso[17a], G. Palacino[68], A. Palazzo[70a,70b], S. Palestini[36], J. Pan[172], T. Pan[64a], D.K. Panchal[11], C.E. Pandini[114], J.G. Panduro Vazquez[95], H. Pang[14b], P. Pani[48], G. Panizzo[69a,69c], L. Paolozzi[56], C. Papadatos[108], S. Parajuli[44], A. Paramonov[6], C. Paraskevopoulos[10], D. Paredes Hernandez[64b], T.H. Park[155], M.A. Parker[32], F. Parodi[57b,57a], E.W. Parrish[115], V.A. Parrish[52], J.A. Parsons[41], U. Parzefall[54], B. Pascual Dias[108], L. Pascual Dominguez[152], F. Pasquali[114], E. Pasqualucci[75a], S. Passaggio[57b], F. Pastore[95], P. Pasuwan[47a,47b], P. Patel[87], U.M. Patel[51], J.R. Pater[101], T. Pauly[36], J. Pearkes[144], M. Pedersen[125], R. Pedro[130a], S.V. Peleganchuk[37], O. Penc[36], E.A. Pender[52], H. Peng[62a], K.E. Penski[109], M. Penzin[37], B.S. Peralva[83d], A.P. Pereira Peixoto[60], L. Pereira Sanchez[47a,47b], D.V. Perepelitsa[29,ak], E. Perez Codina[156a], M. Perganti[10], L. Perini[71a,71b,*], H. Pernegger[36], A. Perrevoort[113], O. Perrin[40], K. Peters[48], R.F.Y. Peters[101], B.A. Petersen[36], T.C. Petersen[42], E. Petit[102], V. Petousis[132], C. Petridou[153,e], A. Petrukhin[142], M. Pettee[17a], N.E. Pettersson[36], A. Petukhov[37], K. Petukhova[133], A. Peyaud[135], R. Pezoa[137f], L. Pezzotti[36], G. Pezzullo[172], T.M. Pham[170], T. Pham[105], P.W. Phillips[134], G. Piacquadio[146], E. Pianori[17a], F. Piazza[71a,71b], R. Piegaia[30], D. Pietreanu[27b], A.D. Pilkington[101], M. Pinamonti[69a,69c],

JHEP08(2025)142

J.L. Pinfold[2], B.C. Pinheiro Pereira[130a], A.E. Pinto Pinoargote[135], K.M. Piper[147], A. Pirttikoski[56], C. Pitman Donaldson[96], D.A. Pizzi[34], L. Pizzimento[76a,76b], M.-A. Pleier[29], V. Plesanovs[54], V. Pleskot[133], E. Plotnikova[38], G. Poddar[4], R. Poettgen[98], L. Poggioli[127], I. Pokharel[55], S. Polacek[133], G. Polesello[73a], A. Poley[143,156a], R. Polifka[132], A. Polini[23b], C.S. Pollard[167], Z.B. Pollock[119], V. Polychronakos[29], E. Pompa Pacchi[75a,75b], D. Ponomarenko[113], L. Pontecorvo[36], S. Popa[27a], G.A. Popeneciu[27d], A. Poreba[36], D.M. Portillo Quintero[156a], S. Pospisil[132], M.A. Postill[140], P. Postolache[27c], K. Potamianos[167], P.A. Potepa[86a], I.N. Potrap[38], C.J. Potter[32], H. Potti[1], T. Poulsen[48], J. Poveda[163], M.E. Pozo Astigarraga[36], A. Prades Ibanez[163], J. Pretel[54], D. Price[101], M. Primavera[70a], M.A. Principe Martin[99], R. Privara[122], T. Procter[59], M.L. Proffitt[139], N. Proklova[128], K. Prokofiev[64c], G. Proto[110], S. Protopopescu[29], J. Proudfoot[6], M. Przybycien[86a], W.W. Przygoda[86b], J.E. Puddefoot[140], D. Pudzha[37], D. Pyatiizbyantseva[37], J. Qian[106], D. Qichen[101], Y. Qin[101], T. Qiu[52], A. Quadt[55], M. Queitsch-Maitland[101], G. Quetant[56], G. Rabanal Bolanos[61], D. Rafanoharana[54], F. Ragusa[71a,71b], J.L. Rainbolt[39], J.A. Raine[56], S. Rajagopalan[29], E. Ramakoti[37], K. Ran[48,14e], N.P. Rapheeha[33g], H. Rasheed[27b], V. Raskina[127], D.F. Rassloff[63a], S. Rave[100], B. Ravina[55], I. Ravinovich[169], M. Raymond[36], A.L. Read[125], N.P. Readioff[140], D.M. Rebuzzi[73a,73b], G. Redlinger[29], A.S. Reed[110], K. Reeves[26], J.A. Reidelsturz[171], D. Reikher[152], A. Rej[142], C. Rembser[36], A. Renardi[48], M. Renda[27b], M.B. Rendel[110], F. Renner[48], A.G. Rennie[59], S. Resconi[71a], M. Ressegotti[57b,57a], S. Rettie[36], J.G. Reyes Rivera[107], B. Reynolds[119], E. Reynolds[17a], O.L. Rezanova[37], P. Reznicek[133], N. Ribaric[91], E. Ricci[78a,78b], R. Richter[110], S. Richter[47a,47b], E. Richter-Was[86b], M. Ridel[127], S. Ridouani[35d], P. Rieck[117], P. Riedler[36], M. Rijssenbeek[146], A. Rimoldi[73a,73b], M. Rimoldi[48], L. Rinaldi[23b,23a], T.T. Rinn[29], M.P. Rinnagel[109], G. Ripellino[161], I. Riu[13], P. Rivadeneira[48], J.C. Rivera Vergara[165], F. Rizatdinova[121], E. Rizvi[94], B.A. Roberts[167], B.R. Roberts[17a], S.H. Robertson[104,y], M. Robin[48], D. Robinson[32], C.M. Robles Gajardo[137f], M. Robles Manzano[100], A. Robson[59], A. Rocchi[76a,76b], C. Roda[74a,74b], S. Rodriguez Bosca[63a], Y. Rodriguez Garcia[22a], A. Rodriguez Rodriguez[54], A.M. Rodríguez Vera[156b], S. Roe[36], J.T. Roemer[160], A.R. Roepe-Gier[136], J. Roggel[171], O. Røhne[125], R.A. Rojas[103], C.P.A. Roland[68], J. Roloff[29], A. Romaniouk[37], E. Romano[73a,73b], M. Romano[23b], A.C. Romero Hernandez[162], N. Rompotis[92], L. Roos[127], S. Rosati[75a], B.J. Rosser[39], E. Rossi[126], E. Rossi[72a,72b], L.P. Rossi[57b], L. Rossini[48], R. Rosten[119], M. Rotaru[27b], B. Rottler[54], C. Rougier[102,ac], D. Rousseau[66], D. Rousso[32], A. Roy[162], S. Roy-Garand[155], A. Rozanov[102], Y. Rozen[151], X. Ruan[33g], A. Rubio Jimenez[163], A.J. Ruby[92], V.H. Ruelas Rivera[18], T.A. Ruggeri[1], A. Ruggiero[126], A. Ruiz-Martinez[163], A. Rummler[36], Z. Rurikova[54], N.A. Rusakovich[38], H.L. Russell[165], G. Russo[75a,75b], J.P. Rutherfoord[7], S. Rutherford Colmenares[32], K. Rybacki[91], M. Rybar[133], E.B. Rye[125], A. Ryzhov[44], J.A. Sabater Iglesias[56], P. Sabatini[163], L. Sabetta[75a,75b], H.F-W. Sadrozinski[136], F. Safai Tehrani[75a], B. Safarzadeh Samani[147], M. Safdari[144], S. Saha[165], M. Sahinsoy[110], M. Saimpert[135], M. Saito[154], T. Saito[154], D. Salamani[36], A. Salnikov[144], J. Salt[163], A. Salvador Salas[13], D. Salvatore[43b,43a], F. Salvatore[147], A. Salzburger[36], D. Sammel[54], D. Sampsonidis[153,e], D. Sampsonidou[123], J. Sánchez[163],

JHEP08(2025)142

A. Sanchez Pineda[4], V. Sanchez Sebastian[163], H. Sandaker[125], C.O. Sander[48], J.A. Sandesara[103], M. Sandhoff[171], C. Sandoval[22b], D.P.C. Sankey[134], T. Sano[88], A. Sansoni[53], L. Santi[75a,75b], C. Santoni[40], H. Santos[130a,130b], S.N. Santpur[17a], A. Santra[169], K.A. Saoucha[140], J.G. Saraiva[130a,130d], J. Sardain[7], O. Sasaki[84], K. Sato[157], C. Sauer[63b], F. Sauerburger[54], E. Sauvan[4], P. Savard[155,ai], R. Sawada[154], C. Sawyer[134], L. Sawyer[97], I. Sayago Galvan[163], C. Sbarra[23b], A. Sbrizzi[23b,23a], T. Scanlon[96], J. Schaarschmidt[139], P. Schacht[110], D. Schaefer[39], U. Schäfer[100], A.C. Schaffer[66,44], D. Schaile[109], R.D. Schamberger[146], C. Scharf[18], M.M. Schefer[19], V.A. Schegelsky[37], D. Scheirich[133], F. Schenck[18], M. Schernau[160], C. Scheulen[55], C. Schiavi[57b,57a], E.J. Schioppa[70a,70b], M. Schioppa[43b,43a], B. Schlag[144], K.E. Schleicher[54], S. Schlenker[36], J. Schmeing[171], M.A. Schmidt[171], K. Schmieden[100], C. Schmitt[100], S. Schmitt[48], L. Schoeffel[135], A. Schoening[63b], P.G. Scholer[54], E. Schopf[126], M. Schott[100], J. Schovancova[36], S. Schramm[56], F. Schroeder[171], T. Schroer[56], H-C. Schultz-Coulon[63a], M. Schumacher[54], B.A. Schumm[136], Ph. Schune[135], A.J. Schuy[139], H.R. Schwartz[136], A. Schwartzman[144], T.A. Schwarz[106], Ph. Schwemling[135], R. Schwienhorst[107], A. Sciandra[136], G. Sciolla[26], F. Scuri[74a], C.D. Sebastiani[92], K. Sedlaczek[115], P. Seema[18], S.C. Seidel[112], A. Seiden[136], B.D. Seidlitz[41], C. Seitz[48], J.M. Seixas[83b], G. Sekhniaidze[72a], S.J. Sekula[44], L. Selem[60], N. Semprini-Cesari[23b,23a], D. Sengupta[56], V. Senthilkumar[163], L. Serin[66], L. Serkin[69a,69b], M. Sessa[76a,76b], H. Severini[120], F. Sforza[57b,57a], A. Sfyrla[56], E. Shabalina[55], R. Shaheen[145], J.D. Shahinian[128], D. Shaked Renous[169], L.Y. Shan[14a], M. Shapiro[17a], A. Sharma[36], A.S. Sharma[164], P. Sharma[80], S. Sharma[48], P.B. Shatalov[37], K. Shaw[147], S.M. Shaw[101], A. Shcherbakova[37], Q. Shen[62c,5], P. Sherwood[96], L. Shi[96], X. Shi[14a], C.O. Shimmin[172], Y. Shimogama[168], J.D. Shinner[95], I.P.J. Shipsey[126,*], S. Shirabe[56,h], M. Shiyakova[38,w], J. Shlomi[169], M.J. Shochet[39], J. Shojaii[105], D.R. Shope[125], B. Shrestha[120], S. Shrestha[119,al], E.M. Shrif[33g], M.J. Shroff[165], P. Sicho[131], A.M. Sickles[162], E. Sideras Haddad[33g], A. Sidoti[23b], F. Siegert[50], Dj. Sijacki[15], R. Sikora[86a], F. Sili[90], J.M. Silva[20], M.V. Silva Oliveira[29], S.B. Silverstein[47a], S. Simion[66], R. Simoniello[36], E.L. Simpson[59], H. Simpson[147], L.R. Simpson[106], N.D. Simpson[98], S. Simsek[82], S. Sindhu[55], P. Sinervo[155], S. Singh[155], S. Sinha[48], S. Sinha[101], M. Sioli[23b,23a], I. Siral[36], E. Sitnikova[48], S.Yu. Sivoklokov[37,*], J. Sjölin[47a,47b], A. Skaf[55], E. Skorda[98], P. Skubic[120], M. Slawinska[87], V. Smakhtin[169], B.H. Smart[134], J. Smiesko[36], S.Yu. Smirnov[37], Y. Smirnov[37], L.N. Smirnova[37,a], O. Smirnova[98], A.C. Smith[41], E.A. Smith[39], H.A. Smith[126], J.L. Smith[92], R. Smith[144], M. Smizanska[91], K. Smolek[132], A.A. Snesarev[37], S.R. Snider[155], H.L. Snoek[114], S. Snyder[29], R. Sobie[165,y], A. Soffer[152], C.A. Solans Sanchez[36], E.Yu. Soldatov[37], U. Soldevila[163], A.A. Solodkov[37], S. Solomon[26], A. Soloshenko[38], K. Solovieva[54], O.V. Solovyanov[40], V. Solovyev[37], P. Sommer[36], A. Sonay[13], W.Y. Song[156b], J.M. Sonneveld[114], A. Sopczak[132], A.L. Sopio[96], F. Sopkova[28b], V. Sothilingam[63a], S. Sottocornola[68], R. Soualah[116b], Z. Soumaimi[35e], D. South[48], S. Spagnolo[70a,70b], M. Spalla[110], D. Sperlich[54], G. Spigo[36], M. Spina[147], S. Spinali[91], D.P. Spiteri[59], M. Spousta[133], E.J. Staats[34], A. Stabile[71a,71b], R. Stamen[63a], M. Stamenkovic[114], A. Stampekis[20], M. Standke[24], E. Stanecka[87], M.V. Stange[50], B. Stanislaus[17a], M.M. Stanitzki[48], B. Stapf[48], E.A. Starchenko[37],

JHEP08(2025)142

G.H. Stark[136], J. Stark[102,ac], D.M. Starko[156b], P. Staroba[131], P. Starovoitov[63a], S. Stärz[104], R. Staszewski[87], G. Stavropoulos[46], J. Steentoft[161], P. Steinberg[29], B. Stelzer[143,156a], H.J. Stelzer[129], O. Stelzer-Chilton[156a], H. Stenzel[58], T.J. Stevenson[147], G.A. Stewart[36], J.R. Stewart[121], M.C. Stockton[36], G. Stoicea[27b], M. Stolarski[130a], S. Stonjek[110], A. Straessner[50], J. Strandberg[145], S. Strandberg[47a,47b], M. Strauss[120], T. Strebler[102], P. Strizenec[28b], R. Ströhmer[166], D.M. Strom[123], L.R. Strom[48], R. Stroynowski[44], A. Strubig[47a,47b], S.A. Stucci[29], B. Stugu[16], J. Stupak[120], N.A. Styles[48], D. Su[144], S. Su[62a], W. Su[62d], X. Su[62a,66], K. Sugizaki[154], V.V. Sulin[37], M.J. Sullivan[92], D.M.S. Sultan[78a,78b], L. Sultanaliyeva[37], S. Sultansoy[3b], T. Sumida[88], S. Sun[106], S. Sun[170], O. Sunneborn Gudnadottir[161], N. Sur[102], M.R. Sutton[147], H. Suzuki[157], M. Svatos[131], M. Swiatlowski[156a], T. Swirski[166], I. Sykora[28a], M. Sykora[133], T. Sykora[133], D. Ta[100], K. Tackmann[48,v], A. Taffard[160], R. Tafirout[156a], J.S. Tafoya Vargas[66], E.P. Takeva[52], Y. Takubo[84], M. Talby[102], A.A. Talyshev[37], K.C. Tam[64b], N.M. Tamir[152], A. Tanaka[154], J. Tanaka[154], R. Tanaka[66], M. Tanasini[57b,57a], Z. Tao[164], S. Tapia Araya[137f], S. Tapprogge[100], A. Tarek Abouelfadl Mohamed[107], S. Tarem[151], K. Tariq[14a], G. Tarna[102,27b], G.F. Tartarelli[71a], P. Tas[133], M. Tasevsky[131], E. Tassi[43b,43a], A.C. Tate[162], G. Tateno[154], Y. Tayalati[35e,x], G.N. Taylor[105], W. Taylor[156b], H. Teagle[92], A.S. Tee[170], R. Teixeira De Lima[144], P. Teixeira-Dias[95], J.J. Teoh[155], K. Terashi[154], J. Terron[99], S. Terzo[13], M. Testa[53], R.J. Teuscher[155,y], A. Thaler[79], O. Theiner[56], N. Themistokleous[52], T. Theveneaux-Pelzer[102], O. Thielmann[171], D.W. Thomas[95], J.P. Thomas[20], E.A. Thompson[17a], P.D. Thompson[20], E. Thomson[128], Y. Tian[55], V. Tikhomirov[37,a], Yu.A. Tikhonov[37], S. Timoshenko[37], D. Timoshyn[133], E.X.L. Ting[1], P. Tipton[172], S.H. Tlou[33g], A. Tnourji[40], K. Todome[23b,23a], S. Todorova-Nova[133], S. Todt[50], M. Togawa[84], J. Tojo[89], S. Tokár[28a], K. Tokushuku[84], O. Toldaiev[68], R. Tombs[32], M. Tomoto[84,111], L. Tompkins[144,o], K.W. Topolnicki[86b], E. Torrence[123], H. Torres[102,ac], E. Torró Pastor[163], M. Toscani[30], C. Tosciri[39], M. Tost[11], D.R. Tovey[140], A. Traeet[16], I.S. Trandafir[27b], T. Trefzger[166], A. Tricoli[29], I.M. Trigger[156a], S. Trincaz-Duvoid[127], D.A. Trischuk[26], B. Trocmé[60], C. Troncon[71a], L. Truong[33c], M. Trzebinski[87], A. Trzupek[87], F. Tsai[146], M. Tsai[106], A. Tsiamis[153,e], P.V. Tsiareshka[37], S. Tsigaridas[156a], A. Tsirigotis[153,t], V. Tsiskaridze[155], E.G. Tskhadadze[150a], M. Tsopoulou[153,e], Y. Tsujikawa[88], I.I. Tsukerman[37], V. Tsulaia[17a], S. Tsuno[84], O. Tsur[151], K. Tsuri[118], D. Tsybychev[146], Y. Tu[64b], A. Tudorache[27b], V. Tudorache[27b], A.N. Tuna[36], S. Turchikhin[38], I. Turk Cakir[3a], R. Turra[71a], T. Turtuvshin[38,z], P.M. Tuts[41], S. Tzamarias[153,e], P. Tzanis[10], E. Tzovara[100], K. Uchida[154], F. Ukegawa[157], P.A. Ulloa Poblete[137c,137b], E.N. Umaka[29], G. Unal[36], M. Unal[11], A. Undrus[29], G. Unel[160], J. Urban[28b], P. Urquijo[105], G. Usai[8], R. Ushioda[138], M. Usman[108], Z. Uysal[21b], L. Vacavant[102], V. Vacek[132], B. Vachon[104], K.O.H. Vadla[125], T. Vafeiadis[36], A. Vaitkus[96], C. Valderanis[109], E. Valdes Santurio[47a,47b], M. Valente[156a], S. Valentinetti[23b,23a], A. Valero[163], E. Valiente Moreno[163], A. Vallier[102,ac], J.A. Valls Ferrer[163], D.R. Van Arneman[114], T.R. Van Daalen[139], A. Van Der Graaf[49], P. Van Gemmeren[6], M. Van Rijnbach[125,36], S. Van Stroud[96], I. Van Vulpen[114], M. Vanadia[76a,76b], W. Vandelli[36], M. Vandenbroucke[135], E.R. Vandewall[121],

JHEP08(2025)142

D. Vannicola[152], L. Vannoli[57b,57a], R. Vari[75a], E.W. Varnes[7], C. Varni[17a], T. Varol[149], D. Varouchas[66], L. Varriale[163], K.E. Varvell[148], M.E. Vasile[27b], L. Vaslin[40], G.A. Vasquez[165], F. Vazeille[40], T. Vazquez Schroeder[36], J. Veatch[31], V. Vecchio[101], M.J. Veen[103], I. Veliscek[126], L.M. Veloce[155], F. Veloso[130a,130c], S. Veneziano[75a], A. Ventura[70a,70b], A. Verbytskyi[110], M. Verducci[74a,74b], C. Vergis[24], M. Verissimo De Araujo[83b], W. Verkerke[114], J.C. Vermeulen[114], C. Vernieri[144], P.J. Verschuuren[95], M. Vessella[103], M.C. Vetterli[143,ai], A. Vgenopoulos[153,e], N. Viaux Maira[137f], T. Vickey[140], O.E. Vickey Boeriu[140], G.H.A. Viehhauser[126], L. Vigani[63b], M. Villa[23b,23a], M. Villaplana Perez[163], E.M. Villhauer[52], E. Vilucchi[53], M.G. Vincter[34], G.S. Virdee[20], A. Vishwakarma[52], A. Visibile[114], C. Vittori[36], I. Vivarelli[147], V. Vladimirov[167], E. Voevodina[110], F. Vogel[109], P. Vokac[132], J. Von Ahnen[48], E. Von Toerne[24], B. Vormwald[36], V. Vorobel[133], K. Vorobev[37], M. Vos[163], K. Voss[142], J.H. Vossebeld[92], M. Vozak[114], L. Vozdecky[94], N. Vranjes[15], M. Vranjes Milosavljevic[15], M. Vreeswijk[114], N.K. Vu[62d,62c], R. Vuillermet[36], O. Vujinovic[100], I. Vukotic[39], S. Wada[157], C. Wagner[103], J.M. Wagner[17a], W. Wagner[171], S. Wahdan[171], H. Wahlberg[90], R. Wakasa[157], M. Wakida[111], J. Walder[134], R. Walker[109], W. Walkowiak[142], A. Wall[128], T. Wamorkar[6], A.Z. Wang[170], C. Wang[100], C. Wang[62c], H. Wang[17a], J. Wang[64a], R.-J. Wang[100], R. Wang[61], R. Wang[6], S.M. Wang[149], S. Wang[62b], T. Wang[62a], W.T. Wang[80], W. Wang[14a], X. Wang[14c], X. Wang[162], X. Wang[62c], Y. Wang[62d], Y. Wang[14c], Z. Wang[106], Z. Wang[62d,51,62c], Z. Wang[106], A. Warburton[104], R.J. Ward[20], N. Warrack[59], A.T. Watson[20], H. Watson[59], M.F. Watson[20], E. Watton[59,134], G. Watts[139], B.M. Waugh[96], C. Weber[29], H.A. Weber[18], M.S. Weber[19], S.M. Weber[63a], C. Wei[62a], Y. Wei[126], A.R. Weidberg[126], E.J. Weik[117], J. Weingarten[49], M. Weirich[100], C. Weiser[54], C.J. Wells[48], T. Wenaus[29], B. Wendland[49], T. Wengler[36], N.S. Wenke[110], N. Wermes[24], M. Wessels[63a], K. Whalen[123], A.M. Wharton[91], A.S. White[61], A. White[8], M.J. White[1], D. Whiteson[160], L. Wickremasinghe[124], W. Wiedenmann[170], C. Wiel[50], M. Wielers[134], C. Wiglesworth[42], D.J. Wilbern[120], H.G. Wilkens[36], D.M. Williams[41], H.H. Williams[128], S. Williams[32], S. Willocq[103], B.J. Wilson[101], P.J. Windischhofer[39], F.I. Winkel[30], F. Winklmeier[123], B.T. Winter[54], J.K. Winter[101], M. Wittgen[144], M. Wobisch[97], Z. Wolffs[114], R. Wölker[126], J. Wollrath[160], M.W. Wolter[87], H. Wolters[130a,130c], A.F. Wongel[48], S.D. Worm[48], B.K. Wosiek[87], K.W. Woźniak[87], S. Wozniewski[55], K. Wraight[59], C. Wu[20], J. Wu[14a,14e], M. Wu[64a], M. Wu[113], S.L. Wu[170], X. Wu[56], Y. Wu[62a], Z. Wu[135], J. Wuerzinger[110], T.R. Wyatt[101], B.M. Wynne[52], S. Xella[42], L. Xia[14c], M. Xia[14b], J. Xiang[64c], X. Xiao[106], M. Xie[62a], X. Xie[62a], S. Xin[14a,14e], J. Xiong[17a], D. Xu[14a], H. Xu[62a], L. Xu[62a], R. Xu[128], T. Xu[106], Y. Xu[14b], Z. Xu[52], Z. Xu[14a], B. Yabsley[148], S. Yacoob[33a], N. Yamaguchi[89], Y. Yamaguchi[138], E. Yamashita[154], H. Yamauchi[157], T. Yamazaki[17a], Y. Yamazaki[85], J. Yan[62c], S. Yan[126], Z. Yan[25], H.J. Yang[62c,62d], H.T. Yang[62a], S. Yang[62a], T. Yang[64c], X. Yang[62a], X. Yang[14a], Y. Yang[44], Y. Yang[62a], Z. Yang[62a], W-M. Yao[17a], Y.C. Yap[48], H. Ye[14c], H. Ye[55], J. Ye[44], S. Ye[29], X. Ye[62a], Y. Yeh[96], I. Yeletskikh[38], B. Yeo[17a], M.R. Yexley[96], P. Yin[41], K. Yorita[168], S. Younas[27b], C.J.S. Young[54], C. Young[144], Y. Yu[62a], M. Yuan[106], R. Yuan[62b,k], L. Yue[96], M. Zaazoua[62a], B. Zabinski[87], E. Zaid[52], T. Zakareishvili[150b], N. Zakharchuk[34],

JHEP08(2025)142

S. Zambito[56], J.A. Zamora Saa[137d,137b], J. Zang[154], D. Zanzi[54], O. Zaplatilek[132], C. Zeitnitz[171], H. Zeng[14a], J.C. Zeng[162], D.T. Zenger Jr[26], O. Zenin[37], T. Ženiš[28a], S. Zenz[94], S. Zerradi[35a], D. Zerwas[66], M. Zhai[14a,14e], B. Zhang[14c], D.F. Zhang[140], J. Zhang[62b], J. Zhang[6], K. Zhang[14a,14e], L. Zhang[14c], P. Zhang[14a,14e], R. Zhang[170], S. Zhang[106], T. Zhang[154], X. Zhang[62c], X. Zhang[62b], Y. Zhang[62c,5], Y. Zhang[96], Z. Zhang[17a], Z. Zhang[66], H. Zhao[139], P. Zhao[51], T. Zhao[62b], Y. Zhao[136], Z. Zhao[62a], A. Zhemchugov[38], K. Zheng[162], X. Zheng[62a], Z. Zheng[144], D. Zhong[162], B. Zhou[106], H. Zhou[7], N. Zhou[62c], Y. Zhou[7], C.G. Zhu[62b], J. Zhu[106], Y. Zhu[62c], Y. Zhu[62a], X. Zhuang[14a], K. Zhukov[37], V. Zhulanov[37], N.I. Zimine[38], J. Zinsser[63b], M. Ziolkowski[142], L. Živković[15], A. Zoccoli[23b,23a], K. Zoch[56], T.G. Zorbas[140], O. Zormpa[46], W. Zou[41], L. Zwalinski[36]

[1] *Department of Physics, University of Adelaide, Adelaide; Australia*
[2] *Department of Physics, University of Alberta, Edmonton AB; Canada*
[3] [(a)] *Department of Physics, Ankara University, Ankara;* [(b)] *Division of Physics, TOBB University of Economics and Technology, Ankara; Türkiye*
[4] *LAPP, Université Savoie Mont Blanc, CNRS/IN2P3, Annecy; France*
[5] *APC, Université Paris Cité, CNRS/IN2P3, Paris; France*
[6] *High Energy Physics Division, Argonne National Laboratory, Argonne IL; United States of America*
[7] *Department of Physics, University of Arizona, Tucson AZ; United States of America*
[8] *Department of Physics, University of Texas at Arlington, Arlington TX; United States of America*
[9] *Physics Department, National and Kapodistrian University of Athens, Athens; Greece*
[10] *Physics Department, National Technical University of Athens, Zografou; Greece*
[11] *Department of Physics, University of Texas at Austin, Austin TX; United States of America*
[12] *Institute of Physics, Azerbaijan Academy of Sciences, Baku; Azerbaijan*
[13] *Institut de Física d'Altes Energies (IFAE), Barcelona Institute of Science and Technology, Barcelona; Spain*
[14] [(a)] *Institute of High Energy Physics, Chinese Academy of Sciences, Beijing;* [(b)] *Physics Department, Tsinghua University, Beijing;* [(c)] *Department of Physics, Nanjing University, Nanjing;* [(d)] *School of Science, Shenzhen Campus of Sun Yat-sen University;* [(e)] *University of Chinese Academy of Science (UCAS), Beijing; China*
[15] *Institute of Physics, University of Belgrade, Belgrade; Serbia*
[16] *Department for Physics and Technology, University of Bergen, Bergen; Norway*
[17] [(a)] *Physics Division, Lawrence Berkeley National Laboratory, Berkeley CA;* [(b)] *University of California, Berkeley CA; United States of America*
[18] *Institut für Physik, Humboldt Universität zu Berlin, Berlin; Germany*
[19] *Albert Einstein Center for Fundamental Physics and Laboratory for High Energy Physics, University of Bern, Bern; Switzerland*
[20] *School of Physics and Astronomy, University of Birmingham, Birmingham; United Kingdom*
[21] [(a)] *Department of Physics, Bogazici University, Istanbul;* [(b)] *Department of Physics Engineering, Gaziantep University, Gaziantep;* [(c)] *Department of Physics, Istanbul University, Istanbul; Türkiye*
[22] [(a)] *Facultad de Ciencias y Centro de Investigaciónes, Universidad Antonio Nariño, Bogotá;* [(b)] *Departamento de Física, Universidad Nacional de Colombia, Bogotá; Colombia*
[23] [(a)] *Dipartimento di Fisica e Astronomia A. Righi, Università di Bologna, Bologna;* [(b)] *INFN Sezione di Bologna; Italy*
[24] *Physikalisches Institut, Universität Bonn, Bonn; Germany*
[25] *Department of Physics, Boston University, Boston MA; United States of America*
[26] *Department of Physics, Brandeis University, Waltham MA; United States of America*
[27] [(a)] *Transilvania University of Brasov, Brasov;* [(b)] *Horia Hulubei National Institute of Physics and Nuclear Engineering, Bucharest;* [(c)] *Department of Physics, Alexandru Ioan Cuza University of Iasi, Iasi;* [(d)] *National Institute for Research and Development of Isotopic and Molecular Technologies, Physics Department,*

JHEP08(2025)142

Cluj-Napoca;[e] *National University of Science and Technology Politechnica, Bucharest;*[f] *West University in Timisoara, Timisoara;*[g] *Faculty of Physics, University of Bucharest, Bucharest; Romania*
[28] [a] *Faculty of Mathematics, Physics and Informatics, Comenius University, Bratislava;*[b] *Department of Subnuclear Physics, Institute of Experimental Physics of the Slovak Academy of Sciences, Kosice; Slovak Republic*
[29] *Physics Department, Brookhaven National Laboratory, Upton NY; United States of America*
[30] *Universidad de Buenos Aires, Facultad de Ciencias Exactas y Naturales, Departamento de Física, y CONICET, Instituto de Física de Buenos Aires (IFIBA), Buenos Aires; Argentina*
[31] *California State University, CA; United States of America*
[32] *Cavendish Laboratory, University of Cambridge, Cambridge; United Kingdom*
[33] [a] *Department of Physics, University of Cape Town, Cape Town;*[b] *iThemba Labs, Western Cape;*[c] *Department of Mechanical Engineering Science, University of Johannesburg, Johannesburg;*[d] *National Institute of Physics, University of the Philippines Diliman (Philippines);*[e] *University of South Africa, Department of Physics, Pretoria;*[f] *University of Zululand, KwaDlangezwa;*[g] *School of Physics, University of the Witwatersrand, Johannesburg; South Africa*
[34] *Department of Physics, Carleton University, Ottawa ON; Canada*
[35] [a] *Faculté des Sciences Ain Chock, Université Hassan II de Casablanca;*[b] *Faculté des Sciences, Université Ibn-Tofail, Kénitra;*[c] *Faculté des Sciences Semlalia, Université Cadi Ayyad, LPHEA-Marrakech;*[d] *LPMR, Faculté des Sciences, Université Mohamed Premier, Oujda;*[e] *Faculté des sciences, Université Mohammed V, Rabat;*[f] *Institute of Applied Physics, Mohammed VI Polytechnic University, Ben Guerir; Morocco*
[36] *CERN, Geneva; Switzerland*
[37] *Affiliated with an institute covered by a cooperation agreement with CERN*
[38] *Affiliated with an international laboratory covered by a cooperation agreement with CERN*
[39] *Enrico Fermi Institute, University of Chicago, Chicago IL; United States of America*
[40] *LPC, Université Clermont Auvergne, CNRS/IN2P3, Clermont-Ferrand; France*
[41] *Nevis Laboratory, Columbia University, Irvington NY; United States of America*
[42] *Niels Bohr Institute, University of Copenhagen, Copenhagen; Denmark*
[43] [a] *Dipartimento di Fisica, Università della Calabria, Rende;*[b] *INFN Gruppo Collegato di Cosenza, Laboratori Nazionali di Frascati; Italy*
[44] *Physics Department, Southern Methodist University, Dallas TX; United States of America*
[45] *Physics Department, University of Texas at Dallas, Richardson TX; United States of America*
[46] *National Centre for Scientific Research "Demokritos", Agia Paraskevi; Greece*
[47] [a] *Department of Physics, Stockholm University;*[b] *Oskar Klein Centre, Stockholm; Sweden*
[48] *Deutsches Elektronen-Synchrotron DESY, Hamburg and Zeuthen; Germany*
[49] *Fakultät Physik, Technische Universität Dortmund, Dortmund; Germany*
[50] *Institut für Kern- und Teilchenphysik, Technische Universität Dresden, Dresden; Germany*
[51] *Department of Physics, Duke University, Durham NC; United States of America*
[52] *SUPA — School of Physics and Astronomy, University of Edinburgh, Edinburgh; United Kingdom*
[53] *INFN e Laboratori Nazionali di Frascati, Frascati; Italy*
[54] *Physikalisches Institut, Albert-Ludwigs-Universität Freiburg, Freiburg; Germany*
[55] *II. Physikalisches Institut, Georg-August-Universität Göttingen, Göttingen; Germany*
[56] *Département de Physique Nucléaire et Corpusculaire, Université de Genève, Genève; Switzerland*
[57] [a] *Dipartimento di Fisica, Università di Genova, Genova;*[b] *INFN Sezione di Genova; Italy*
[58] *II. Physikalisches Institut, Justus-Liebig-Universität Giessen, Giessen; Germany*
[59] *SUPA — School of Physics and Astronomy, University of Glasgow, Glasgow; United Kingdom*
[60] *LPSC, Université Grenoble Alpes, CNRS/IN2P3, Grenoble INP, Grenoble; France*
[61] *Laboratory for Particle Physics and Cosmology, Harvard University, Cambridge MA; United States of America*
[62] [a] *Department of Modern Physics and State Key Laboratory of Particle Detection and Electronics, University of Science and Technology of China, Hefei;*[b] *Institute of Frontier and Interdisciplinary Science and Key Laboratory of Particle Physics and Particle Irradiation (MOE), Shandong University, Qingdao;*[c] *State Key Laboratory of Dark Matter Physics, School of Physics and Astronomy, Shanghai Jiao Tong University, Key Laboratory for Particle Astrophysics and Cosmology (MOE), SKLPPC,*

JHEP08(2025)142

Shanghai;[(d)] *State Key Laboratory of Dark Matter Physics, Tsung-Dao Lee Institute, Shanghai Jiao Tong University, Shanghai; China*
[63] [(a)] *Kirchhoff-Institut für Physik, Ruprecht-Karls-Universität Heidelberg, Heidelberg;*[(b)] *Physikalisches Institut, Ruprecht-Karls-Universität Heidelberg, Heidelberg; Germany*
[64] [(a)] *Department of Physics, Chinese University of Hong Kong, Shatin, N.T., Hong Kong;*[(b)] *Department of Physics, University of Hong Kong, Hong Kong;*[(c)] *Department of Physics and Institute for Advanced Study, Hong Kong University of Science and Technology, Clear Water Bay, Kowloon, Hong Kong; China*
[65] *Department of Physics, National Tsing Hua University, Hsinchu; Taiwan*
[66] *IJCLab, Université Paris-Saclay, CNRS/IN2P3, 91405, Orsay; France*
[67] *Centro Nacional de Microelectrónica (IMB-CNM-CSIC), Barcelona; Spain*
[68] *Department of Physics, Indiana University, Bloomington IN; United States of America*
[69] [(a)] *INFN Gruppo Collegato di Udine, Sezione di Trieste, Udine;*[(b)] *ICTP, Trieste;*[(c)] *Dipartimento Politecnico di Ingegneria e Architettura, Università di Udine, Udine; Italy*
[70] [(a)] *INFN Sezione di Lecce;*[(b)] *Dipartimento di Matematica e Fisica, Università del Salento, Lecce; Italy*
[71] [(a)] *INFN Sezione di Milano;*[(b)] *Dipartimento di Fisica, Università di Milano, Milano; Italy*
[72] [(a)] *INFN Sezione di Napoli;*[(b)] *Dipartimento di Fisica, Università di Napoli, Napoli; Italy*
[73] [(a)] *INFN Sezione di Pavia;*[(b)] *Dipartimento di Fisica, Università di Pavia, Pavia; Italy*
[74] [(a)] *INFN Sezione di Pisa;*[(b)] *Dipartimento di Fisica E. Fermi, Università di Pisa, Pisa; Italy*
[75] [(a)] *INFN Sezione di Roma;*[(b)] *Dipartimento di Fisica, Sapienza Università di Roma, Roma; Italy*
[76] [(a)] *INFN Sezione di Roma Tor Vergata;*[(b)] *Dipartimento di Fisica, Università di Roma Tor Vergata, Roma; Italy*
[77] [(a)] *INFN Sezione di Roma Tre;*[(b)] *Dipartimento di Matematica e Fisica, Università Roma Tre, Roma; Italy*
[78] [(a)] *INFN-TIFPA;*[(b)] *Università degli Studi di Trento, Trento; Italy*
[79] *Universität Innsbruck, Department of Astro and Particle Physics, Innsbruck; Austria*
[80] *University of Iowa, Iowa City IA; United States of America*
[81] *Department of Physics and Astronomy, Iowa State University, Ames IA; United States of America*
[82] *Istinye University, Sariyer, Istanbul; Türkiye*
[83] [(a)] *Departamento de Engenharia Elétrica, Universidade Federal de Juiz de Fora (UFJF), Juiz de Fora;*[(b)] *Universidade Federal do Rio De Janeiro COPPE/EE/IF, Rio de Janeiro;*[(c)] *Instituto de Física, Universidade de São Paulo, São Paulo;*[(d)] *Rio de Janeiro State University, Rio de Janeiro; Brazil*
[84] *KEK, High Energy Accelerator Research Organization, Tsukuba; Japan*
[85] *Graduate School of Science, Kobe University, Kobe; Japan*
[86] [(a)] *AGH University of Krakow, Faculty of Physics and Applied Computer Science, Krakow;*[(b)] *Marian Smoluchowski Institute of Physics, Jagiellonian University, Krakow; Poland*
[87] *Institute of Nuclear Physics Polish Academy of Sciences, Krakow; Poland*
[88] *Faculty of Science, Kyoto University, Kyoto; Japan*
[89] *Research Center for Advanced Particle Physics and Department of Physics, Kyushu University, Fukuoka; Japan*
[90] *Instituto de Física La Plata, Universidad Nacional de La Plata and CONICET, La Plata; Argentina*
[91] *Physics Department, Lancaster University, Lancaster; United Kingdom*
[92] *Oliver Lodge Laboratory, University of Liverpool, Liverpool; United Kingdom*
[93] *Department of Experimental Particle Physics, Jožef Stefan Institute and Department of Physics, University of Ljubljana, Ljubljana; Slovenia*
[94] *Department of Physics and Astronomy, Queen Mary University of London, London; United Kingdom*
[95] *Department of Physics, Royal Holloway University of London, Egham; United Kingdom*
[96] *Department of Physics and Astronomy, University College London, London; United Kingdom*
[97] *Louisiana Tech University, Ruston LA; United States of America*
[98] *Fysiska institutionen, Lunds universitet, Lund; Sweden*
[99] *Departamento de Física Teorica C-15 and CIAFF, Universidad Autónoma de Madrid, Madrid; Spain*
[100] *Institut für Physik, Universität Mainz, Mainz; Germany*
[101] *School of Physics and Astronomy, University of Manchester, Manchester; United Kingdom*
[102] *CPPM, Aix-Marseille Université, CNRS/IN2P3, Marseille; France*
[103] *Department of Physics, University of Massachusetts, Amherst MA; United States of America*

JHEP08(2025)142

[104] Department of Physics, McGill University, Montreal QC; Canada
[105] School of Physics, University of Melbourne, Victoria; Australia
[106] Department of Physics, University of Michigan, Ann Arbor MI; United States of America
[107] Department of Physics and Astronomy, Michigan State University, East Lansing MI; United States of America
[108] Group of Particle Physics, University of Montreal, Montreal QC; Canada
[109] Fakultät für Physik, Ludwig-Maximilians-Universität München, München; Germany
[110] Max-Planck-Institut für Physik (Werner-Heisenberg-Institut), München; Germany
[111] Graduate School of Science and Kobayashi-Maskawa Institute, Nagoya University, Nagoya; Japan
[112] Department of Physics and Astronomy, University of New Mexico, Albuquerque NM; United States of America
[113] Institute for Mathematics, Astrophysics and Particle Physics, Radboud University/Nikhef, Nijmegen; Netherlands
[114] Nikhef National Institute for Subatomic Physics and University of Amsterdam, Amsterdam; Netherlands
[115] Department of Physics, Northern Illinois University, DeKalb IL; United States of America
[116] [(a)] New York University Abu Dhabi, Abu Dhabi;[(b)] University of Sharjah, Sharjah; United Arab Emirates
[117] Department of Physics, New York University, New York NY; United States of America
[118] Ochanomizu University, Otsuka, Bunkyo-ku, Tokyo; Japan
[119] Ohio State University, Columbus OH; United States of America
[120] Homer L. Dodge Department of Physics and Astronomy, University of Oklahoma, Norman OK; United States of America
[121] Department of Physics, Oklahoma State University, Stillwater OK; United States of America
[122] Palacký University, Joint Laboratory of Optics, Olomouc; Czech Republic
[123] Institute for Fundamental Science, University of Oregon, Eugene, OR; United States of America
[124] Graduate School of Science, University of Osaka, Osaka; Japan
[125] Department of Physics, University of Oslo, Oslo; Norway
[126] Department of Physics, Oxford University, Oxford; United Kingdom
[127] LPNHE, Sorbonne Université, Université Paris Cité, CNRS/IN2P3, Paris; France
[128] Department of Physics, University of Pennsylvania, Philadelphia PA; United States of America
[129] Department of Physics and Astronomy, University of Pittsburgh, Pittsburgh PA; United States of America
[130] [(a)] Laboratório de Instrumentação e Física Experimental de Partículas — LIP, Lisboa;[(b)] Departamento de Física, Faculdade de Ciências, Universidade de Lisboa, Lisboa;[(c)] Departamento de Física, Universidade de Coimbra, Coimbra;[(d)] Centro de Física Nuclear da Universidade de Lisboa, Lisboa;[(e)] Departamento de Física, Escola de Ciências, Universidade do Minho, Braga;[(f)] Departamento de Física Teórica y del Cosmos, Universidad de Granada, Granada (Spain);[(g)] Departamento de Física, Instituto Superior Técnico, Universidade de Lisboa, Lisboa; Portugal
[131] Institute of Physics of the Czech Academy of Sciences, Prague; Czech Republic
[132] Czech Technical University in Prague, Prague; Czech Republic
[133] Charles University, Faculty of Mathematics and Physics, Prague; Czech Republic
[134] Particle Physics Department, Rutherford Appleton Laboratory, Didcot; United Kingdom
[135] IRFU, CEA, Université Paris-Saclay, Gif-sur-Yvette; France
[136] Santa Cruz Institute for Particle Physics, University of California Santa Cruz, Santa Cruz CA; United States of America
[137] [(a)] Departamento de Física, Pontificia Universidad Católica de Chile, Santiago;[(b)] Millennium Institute for Subatomic physics at high energy frontier (SAPHIR), Santiago;[(c)] Instituto de Investigación Multidisciplinario en Ciencia y Tecnología, y Departamento de Física, Universidad de La Serena;[(d)] Universidad Andres Bello, Department of Physics, Santiago;[(e)] Instituto de Alta Investigación, Universidad de Tarapacá, Arica;[(f)] Departamento de Física, Universidad Técnica Federico Santa María, Valparaíso; Chile
[138] Department of Physics, Institute of Science, Tokyo; Japan
[139] Department of Physics, University of Washington, Seattle WA; United States of America
[140] Department of Physics and Astronomy, University of Sheffield, Sheffield; United Kingdom
[141] Department of Physics, Shinshu University, Nagano; Japan

JHEP08(2025)142

[142] Department Physik, Universität Siegen, Siegen; Germany
[143] Department of Physics, Simon Fraser University, Burnaby BC; Canada
[144] SLAC National Accelerator Laboratory, Stanford CA; United States of America
[145] Department of Physics, Royal Institute of Technology, Stockholm; Sweden
[146] Departments of Physics and Astronomy, Stony Brook University, Stony Brook NY; United States of America
[147] Department of Physics and Astronomy, University of Sussex, Brighton; United Kingdom
[148] School of Physics, University of Sydney, Sydney; Australia
[149] Institute of Physics, Academia Sinica, Taipei; Taiwan
[150] [(a)] E. Andronikashvili Institute of Physics, Iv. Javakhishvili Tbilisi State University, Tbilisi;[(b)] High Energy Physics Institute, Tbilisi State University, Tbilisi;[(c)] University of Georgia, Tbilisi; Georgia
[151] Department of Physics, Technion, Israel Institute of Technology, Haifa; Israel
[152] Raymond and Beverly Sackler School of Physics and Astronomy, Tel Aviv University, Tel Aviv; Israel
[153] Department of Physics, Aristotle University of Thessaloniki, Thessaloniki; Greece
[154] International Center for Elementary Particle Physics and Department of Physics, University of Tokyo, Tokyo; Japan
[155] Department of Physics, University of Toronto, Toronto ON; Canada
[156] [(a)] TRIUMF, Vancouver BC;[(b)] Department of Physics and Astronomy, York University, Toronto ON; Canada
[157] Division of Physics and Tomonaga Center for the History of the Universe, Faculty of Pure and Applied Sciences, University of Tsukuba, Tsukuba; Japan
[158] Department of Physics and Astronomy, Tufts University, Medford MA; United States of America
[159] United Arab Emirates University, Al Ain; United Arab Emirates
[160] Department of Physics and Astronomy, University of California Irvine, Irvine CA; United States of America
[161] Department of Physics and Astronomy, University of Uppsala, Uppsala; Sweden
[162] Department of Physics, University of Illinois, Urbana IL; United States of America
[163] Instituto de Física Corpuscular (IFIC), Centro Mixto Universidad de Valencia — CSIC, Valencia; Spain
[164] Department of Physics, University of British Columbia, Vancouver BC; Canada
[165] Department of Physics and Astronomy, University of Victoria, Victoria BC; Canada
[166] Fakultät für Physik und Astronomie, Julius-Maximilians-Universität Würzburg, Würzburg; Germany
[167] Department of Physics, University of Warwick, Coventry; United Kingdom
[168] Waseda University, Tokyo; Japan
[169] Department of Particle Physics and Astrophysics, Weizmann Institute of Science, Rehovot; Israel
[170] Department of Physics, University of Wisconsin, Madison WI; United States of America
[171] Fakultät für Mathematik und Naturwissenschaften, Fachgruppe Physik, Bergische Universität Wuppertal, Wuppertal; Germany
[172] Department of Physics, Yale University, New Haven CT; United States of America

[a] Also Affiliated with an institute covered by a cooperation agreement with CERN
[b] Also at An-Najah National University, Nablus; Palestine
[c] Also at Borough of Manhattan Community College, City University of New York, New York NY; United States of America
[d] Also at Center for High Energy Physics, Peking University; China
[e] Also at Center for Interdisciplinary Research and Innovation (CIRI-AUTH), Thessaloniki; Greece
[f] Also at Centro Studi e Ricerche Enrico Fermi; Italy
[g] Also at CERN, Geneva; Switzerland
[h] Also at Département de Physique Nucléaire et Corpusculaire, Université de Genève, Genève; Switzerland
[i] Also at Departament de Fisica de la Universitat Autonoma de Barcelona, Barcelona; Spain
[j] Also at Department of Financial and Management Engineering, University of the Aegean, Chios; Greece
[k] Also at Department of Physics and Astronomy, Michigan State University, East Lansing MI; United States of America
[l] Also at Department of Physics, Ben Gurion University of the Negev, Beer Sheva; Israel
[m] Also at Department of Physics, California State University, Sacramento; United States of America

JHEP08(2025)142

[n] Also at Department of Physics, King's College London, London; United Kingdom
[o] Also at Department of Physics, Stanford University, Stanford CA; United States of America
[p] Also at Department of Physics, University of Fribourg, Fribourg; Switzerland
[q] Also at Department of Physics, University of Thessaly; Greece
[r] Also at Department of Physics, Westmont College, Santa Barbara; United States of America
[s] Also at Faculty of Physics, Sofia University, 'St. Kliment Ohridski', Sofia; Bulgaria
[t] Also at Hellenic Open University, Patras; Greece
[u] Also at Institucio Catalana de Recerca i Estudis Avancats, ICREA, Barcelona; Spain
[v] Also at Institut für Experimentalphysik, Universität Hamburg, Hamburg; Germany
[w] Also at Institute for Nuclear Research and Nuclear Energy (INRNE) of the Bulgarian Academy of Sciences, Sofia; Bulgaria
[x] Also at Institute of Applied Physics, Mohammed VI Polytechnic University, Ben Guerir; Morocco
[y] Also at Institute of Particle Physics (IPP); Canada
[z] Also at Institute of Physics and Technology, Mongolian Academy of Sciences, Ulaanbaatar; Mongolia
[aa] Also at Institute of Physics, Azerbaijan Academy of Sciences, Baku; Azerbaijan
[ab] Also at Institute of Theoretical Physics, Ilia State University, Tbilisi; Georgia
[ac] Also at L2IT, Université de Toulouse, CNRS/IN2P3, UPS, Toulouse; France
[ad] Also at Lawrence Livermore National Laboratory, Livermore; United States of America
[ae] Also at National Institute of Physics, University of the Philippines Diliman (Philippines); Philippines
[af] Also at Physikalisches Institut, Albert-Ludwigs-Universität Freiburg, Freiburg; Germany
[ag] Also at Technical University of Munich, Munich; Germany
[ah] Also at The Collaborative Innovation Center of Quantum Matter (CICQM), Beijing; China
[ai] Also at TRIUMF, Vancouver BC; Canada
[aj] Also at Università di Napoli Parthenope, Napoli; Italy
[ak] Also at University of Colorado Boulder, Department of Physics, Colorado; United States of America
[al] Also at Washington College, Chestertown, MD; United States of America
[am] Also at Yeditepe University, Physics Department, Istanbul; Türkiye
[*] Deceased

JHEP08(2025)142